BRITISH ANTARCTIC SURVEY

BAS GEOMAP SERIES
Geological and Geomorphological Maps and Supplementary Text

SHEET 6-A and 6-B

Geology and geomorphology of Deception Island

MAPS AT SCALE 1:25 000

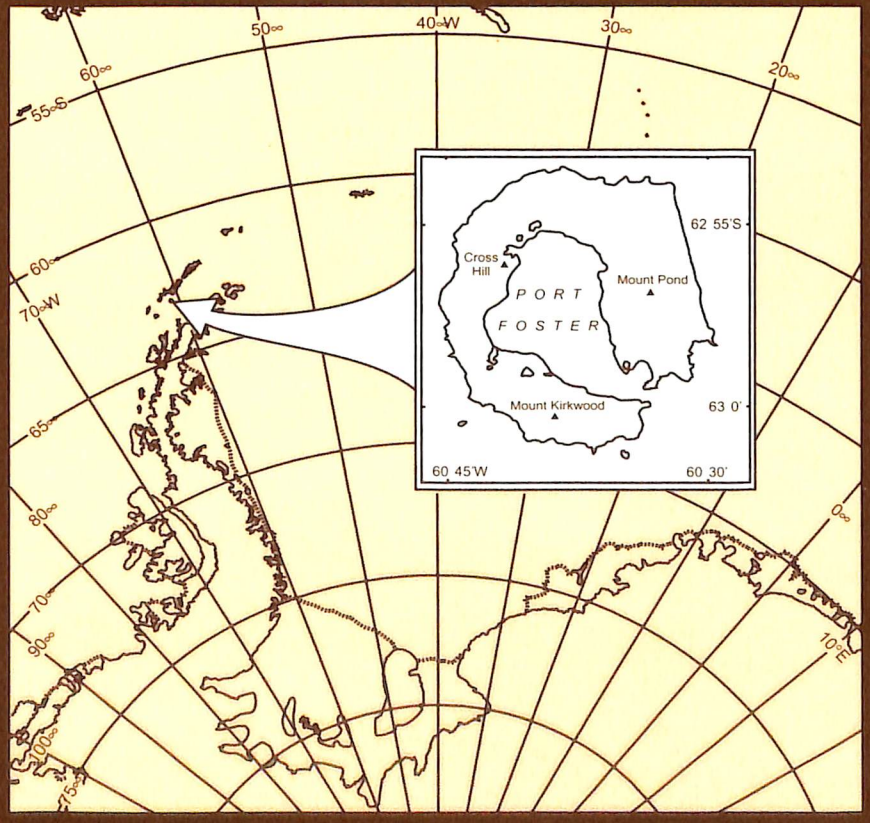

CAMBRIDGE
PUBLISHED BY THE BRITISH ANTARCTIC SURVEY
NATURAL ENVIRONMENT RESEARCH COUNCIL
2002

BAS GEOMAP Series

SHEETS 6-A AND 6-B

Geology and geomorphology of Deception Island

MAPS AT SCALE 1:25 000

GEOLOGICAL MAP COMPILED BY J.L. SMELLIE and J. LÓPEZ-MARTÍNEZ
GEOMORPHOLOGICAL MAP COMPILED BY J. LÓPEZ-MARTÍNEZ, E. SERRANO, J. REY and J.L. SMELLIE

TEXT BY J.L. SMELLIE , J. LÓPEZ-MARTÍNEZ, R.K. HEADLAND, F. HERNÁNDEZ-CIFUENTES, A. MAESTRO, I.L. MILLAR, J. REY, E. SERRANO, L. SOMOZA and J.W. THOMSON

EDITED BY J. LÓPEZ-MARTÍNEZ, J.L. SMELLIE, J.W. THOMSON and M.R.A. THOMSON

COLLABORATIVE PUBLICATION BY BRITISH ANTARCTIC SURVEY AND PROGRAMA ESPAÑOL DE INVESTIGACIÓN EN LA ANTÁRTIDA

Supplied with topographic map compiled by Servicio Geográfico del Ejército and Universidad Autónoma de Madrid, by courtesy of Centro Geográfico del Ejército, Spain

CAMBRIDGE

PUBLISHED BY THE BRITISH ANTARCTIC SURVEY
NATURAL ENVIRONMENT RESEARCH COUNCIL
2002

BRITISH ANTARCTIC SURVEY
Natural Environment Research Council

Director: Professor C.G. Rapley
Head of Geological Sciences Division: Dr J.A. Crame
BAS GEOMAP Series Editor: J.W. Thomson
Text design: J.W. Thomson

Bibliographical reference:

SMELLIE, J.L., LÓPEZ-MARTÍNEZ, J. and others. 2002. *Geology and geomorphology of Deception Island*, 78 pp., with accompanying maps. BAS GEOMAP Series, Sheets 6-A and 6-B, 1:25 000. Cambridge, British Antarctic Survey.

Published by the British Antarctic Survey, High Cross, Madingley Road, Cambridge CB3 0ET, UK

ISSN 0951-8886

Text printed in England by Burlington Press.

GEOLOGY AND GEOMORPHOLOGY OF DECEPTION ISLAND SUPPLEMENTARY TEXT

J.L. SMELLIE, J. LÓPEZ-MARTÍNEZ, R.K. HEADLAND, F. HERNÁNDEZ-CIFUENTES, A. MAESTRO, I.L. MILLAR, J. REY, E. SERRANO, L. SOMOZA *and* J.W. THOMSON

Abstract

Deception Island is an active volcano in Antarctica. It is also one of the few places in the world where scientific and tourist vessels can sail directly into the centre of a restless caldera, and it has had a longer history of human interest, exploration and occupation than any other region of Antarctica. It was one of the first parts of Antarctica to be discovered, and the protection of its fine natural harbour was used during early 19th Century intensive sealing activities, then for early 20th Century whale exploitation. It was also used as a base for the first aeroplane explorations and aerial surveys in Antarctica. After 1944, the island became a site for scientific studies, a role that it still serves today. Yet, despite the long history of economic and scientific interest, Deception Island is also one of only two active volcanoes in the Antarctic region (south of 60°S) at which eruptions have been observed. It was responsible for numerous ash layers dispersed across the South Shetland Islands, Bransfield Strait and Scotia Sea, and Deception Island ash has even been recorded in an ice core at the South Pole, *c.* 3000 km distant. Deception Island ash layers are an important scientific resource that is beginning to be used to create a regional tephrostratigraphy. This will be of immense importance for correlating marine, lacustrine and ice core data, and for Quaternary climatic research generally. Prior to the spate of short-lived eruptions between 1967 and 1970, there were no detailed investigations of the history of the Deception Island volcano, its eruptive products, behaviour, hazards and morphological development, presumably because of the lack of recent historical eruptive activity at the volcano and its situation in a sparsely populated remote area. However, the potential impact on human activities represented by eruptions has increased significantly in recent years: more than 10 000 people (mainly tourists) now visit the island in each short austral summer, and 17 international scientific stations are situated within a 150 km radius, including two on the island itself. Since the mid-1980s, numerous modern investigations have been conducted on the island, mainly by scientists from Britain, Spain and Argentina. In this BAS GEOMAP, we have produced, for the first time in a single source, 1:25 000-scale topographic, geological and geomorphological maps accompanied by a text describing the history of investigations, geology, geomorphology, marine geology and geophysics, and volcanic hazards, and appendices containing chronological lists of all known eruptions, selected expeditions and historical events, geochemical and isotopic analyses, and a gazetteer. With this unique resource, we are able to describe the eruptive record of the Deception Island volcano and its history of erosive modification under a harsh Antarctic maritime climate, extending over the past few tens of thousands of years, at least. Although the volcano erupted only during two short periods in the 20th Century, it contains a restless caldera that is actively deforming. It is therefore likely that it will erupt again in the future. This report is the best guide to understanding future eruptions of Deception Island and predicting their likely physical impact on the region. It will thus be an important tool in the formulation of plans for mitigating the effects of those eruptions.

AUTHORS' AND EDITORS' AFFILIATIONS

R.K. HEADLAND	Scott Polar Research Institute, University of Cambridge, Lensfield Road, Cambridge CB2 1ER, UK
F. HERNÁNDEZ-CIFUENTES	Centro Geográfico del Ejército, Darío Gazapo 8, 28024 Madrid Spain.
J. LÓPEZ-MARTÍNEZ	Departamento de Geología y Geoquímica, Universidad Autónoma de Madrid, 28049 Madrid, Spain
A. MAESTRO	División de Geología Marina, IGME (Geological Survey of Spain), Ríos Rosas 23, 28003 Madrid, Spain
I.L. MILLAR	British Antarctic Survey, c/o NERC Isotope Geoscience Laboratory, Kingsley Dunham Centre, Keyworth, Nottingham NG12 5GG, UK
J. REY	Estudios Geológicos Marinos, Edificio Stella Maris, Puerto de Málaga, 29001 Málaga, Spain
E. SERRANO	Departamento de Geografía, Universidad de Valladolid, 47011 Valladolid, Spain
L. SOMOZA	División de Geología Marina, IGME (Geological Survey of Spain), Ríos Rosas 23, 28003 Madrid, Spain
J.L. SMELLIE	Geological Sciences Division, British Antarctic Survey, Cambridge CB3 0ET, UK
J.W. THOMSON	Mapping and Geographic Information Centre, British Antarctic Survey Cambridge CB3 0ET, UK
M.R.A.THOMSON	Formerly Geological Sciences Division, British Antarctic Survey, Cambridge CB3 0ET, UK

CONTENTS

PREFACE

BAS GEOMAP Sheet 6 is a collaborative venture between British and Spanish geoscientists of the British Antarctic Survey and the Spanish Antarctic Programme.

The two new maps (geological and geomorphological), presented here as BAS GEOMAP 6-A and 6-B, use as their base the 1:25 000 topographic map of Deception Island prepared by Servicio Geográfico del Ejército and Universidad Autónoma de Madrid, published in 1994. The topographic map is also included in this publication.

Joint compilation of the geological and geomorphological maps has enabled the production of the most up-to-date summary that takes into account extensive databases and a diverse body of opinions.

Thus the geological and geomorphological maps constitute the most complete overview of the physical and geological aspects of this important island, the most active volcano in West Antarctica and one of the most visited areas in Antarctica.

The maps in the present booklet were printed in Spain, under the auspices of projects ANT94-0666, ANT98-0225 and REN2001-0654, Universidad Autónoma de Madrid and thanks to the co-operation of the Centro Geográfico del Ejército (the former Servicio Geográfico del Ejército); the booklet was printed in the UK by the British Antarctic Survey.

We hope that this publication will be useful for the scientists working on Antarctic geology and for the many visitors to Deception Island, as well as providing an authoritative earth sciences basis for the future management and conservation of this important Antarctic site.

J.L. Smellie, British Antarctic Survey
J. López-Martínez, Universidad Autónoma de Madrid

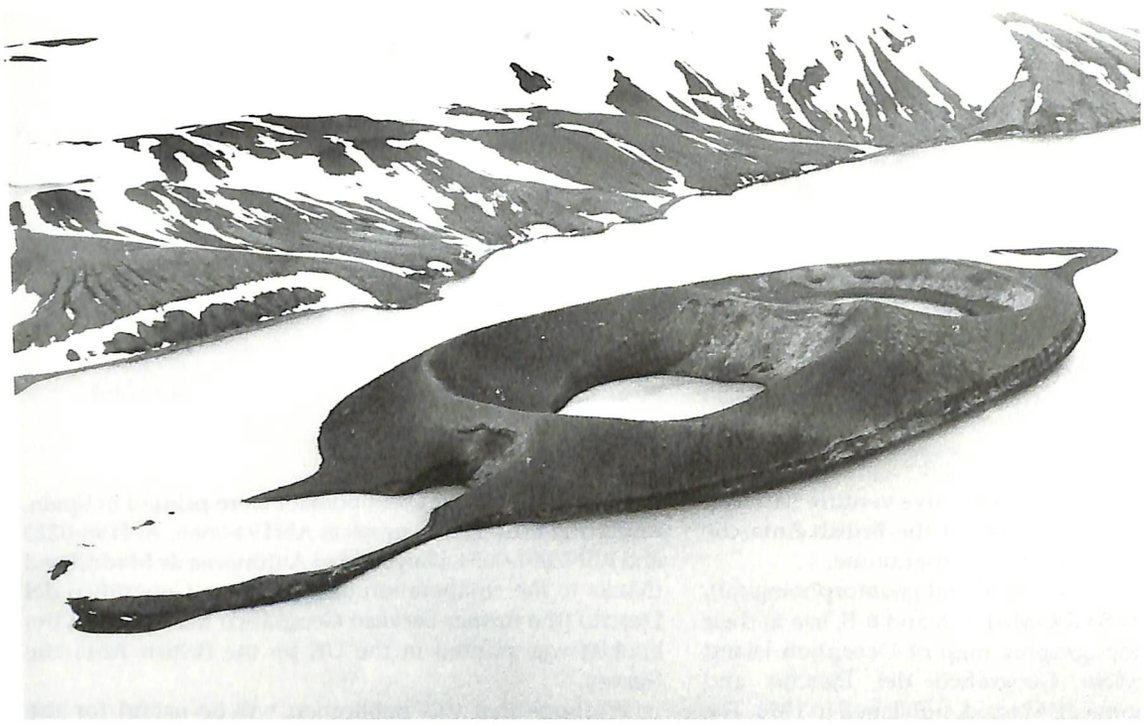

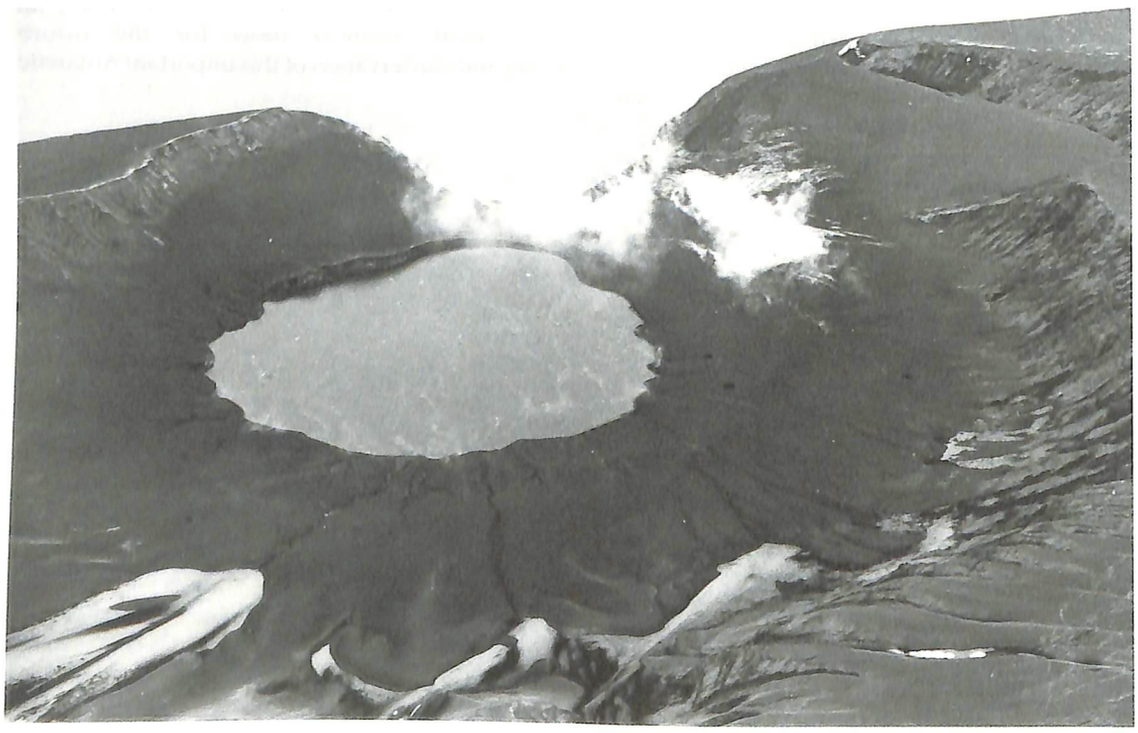

Frontispiece. Views of two volcanic centres on Deception Island formed during eruptions on 4 December 1967. The upper photograph shows several co-eruptive, small coalesced pyroclastic cones of the small compound Surtseyan centre that formed a new island in Telefon Bay (view looking north-north-west). The lower photograph is a view looking south-west into the so-called land centre, situated about 2.5 km east-north-east of the new island; two phreatomagmatic vents were simultaneously active in this crater, located beneath the small maar-like lake and in the shallow coastal indentation beyond. Unlike the eruptions in Telefon Bay, eruptions at the land centre seem to have been particularly violent due to interaction of the rising magma and groundwater (rather than surface water), and the two vents excavated and enlarged the pre-existing large tuff cone at that site. Both the new island and the land centre were ephemeral features. They were modified significantly by eruptions on 13 December 1970. The later eruptions removed large parts of the NW flanks of the new island, the craters were largely infilled, and the island itself was joined to the adjacent coast by new land created by 1970 tephra. Elsewhere, a line of vents cut across the northern margins of the land centre. They constructed several prominent small pyroclastic cones across the steep slopes in the foreground shown in that photograph; the coastal indentation has also subsequently become infilled and straightened. Both photographs were probably taken between 4 December 1968 and 10 January 1969 (photographs provided by PE Baker, now held in British Antarctic Survey archives).

1 Introduction

by J.L. Smellie and J. López-Martínez

BAS GEOMAP 6 describes the geology and geomorphology of Deception Island, South Shetland Islands. It integrates the results from scientific programmes carried out independently by the British Antarctic Survey (BAS) and the Programa Antártico Español. BAS GEOMAP 6 has four parts: three maps, each at 1:25 000 scale, depicting the topography, geology and geomorphology, and this booklet. The maps contain information in their legends and marginalia, and the booklet summarizes our knowledge of the geology and geomorphology of Deception Island. The geological and geomorphological maps (BAS GEOMAP Sheets 6-A and 6-B, respectively) have been co-ordinated and common elements (e.g craters, lava flow outcrops, glaciers and moraines) have the same symbols on both. Together, the maps and booklet constitute the most complete available account of the island, and they will serve as a reference framework for current and future research studies of this significant volcano.

Location and geography

Deception Island is located between latitudes 62°53′30″S and 63°01′20″S, and longitudes 60°29′20″W and 60°45′10″W. It is situated in Bransfield Strait, about 25 km south of Livingston Island (South Shetland Islands) and 100 km north of the Antarctic Peninsula (Fig. 1.1).

Deception Island measures 15 km in maximum diameter, rising to 539 m at Mount Pond, the highest point, and 452 m at Mount Kirkwood, both summits being covered by ice. The island is roughly circular and horseshoe-shaped. It encloses a large bay (Port Foster), 7–10 km in diameter, which is flooded by the sea. Access to Port Foster is gained via a shallow silled entrance only 500 m wide, called Neptunes Bellows (Fig. 1.2).

The ice-free area of Deception Island is *c.* 47 km^2, a figure only exceeded in the South Shetland Islands by Byers Peninsula, Livingston Island (*c.* 60 km^2 of ice-free ground). About 57% of Deception Island is covered by glaciers and partially ice-cored moraines, and areas of glacial ice covered by pyroclasts. The glaciers are up to 100 m thick. Although the extent of permanent ice has not changed greatly since 1956, when full aerial photographic cover was obtained for the first time, it is estimated that the glacier surfaces have lowered by at least 40 m since that time. An almost complete ring of hills encircles the sunken interior of Port Foster. The hills form a prominent annular escarpment facing Port Foster, and have relatively steep outer slopes, which fall away to a broad gently undulating plain on the north-west side (Kendall Terrace). Tuff cones and craters are conspicuous surrounding Port Foster, and several contain lakes.

The bathymetry of Port Foster indicates that it is dominated by a deep flat-floored basin fringed by a

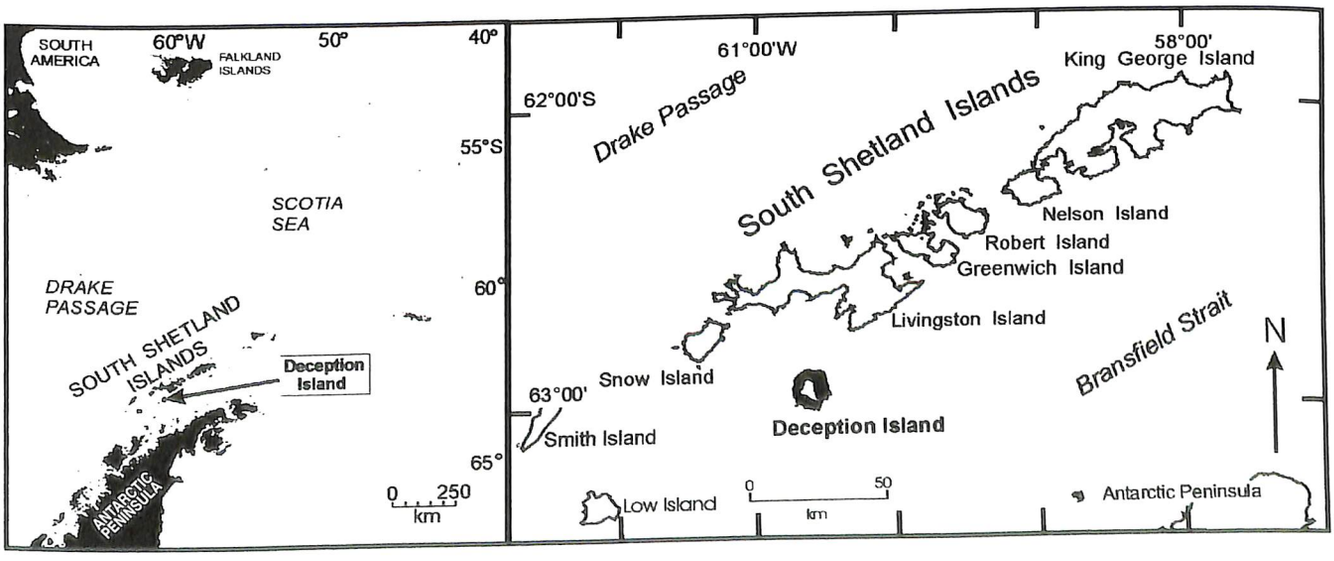

Fig. 1.1. Sketch maps showing the location of Deception Island.

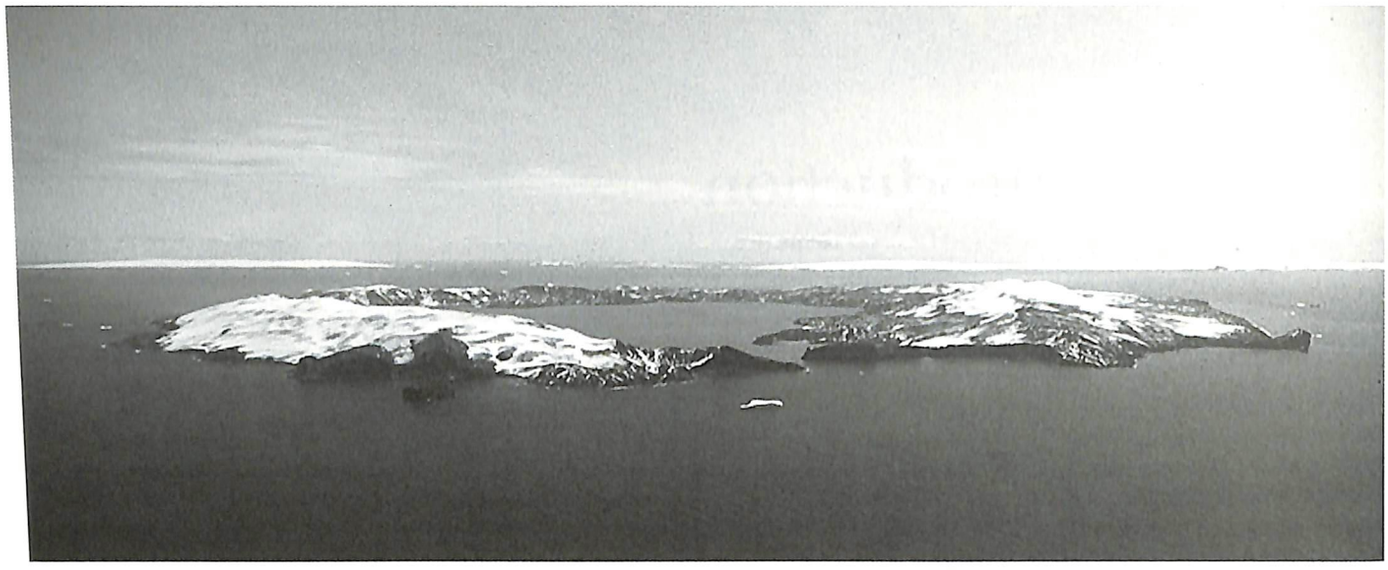

Fig. 1.2. Oblique aerial view of Deception Island from the south. Note the narrow entrance (Neptunes Bellows) leading to the large inner bay (Port Foster), and ice-covered ridges at Mount Pond (539 m; right) and Mount Kirkwood (452 m; left).

shallow coastal shelf up to 500 m wide and narrow sandy-gravelly beaches almost everywhere, except along the snout of the Mount Pond glacier. It also contains several small submarine cones and domes. The basin has a flat floor < 170 m deep and steep bordering slopes; other basins are substantially smaller and shallower, with uneven floors and depths mainly < 120 m (Rey and others, 1992; Cooper and others, 1998; Chapter 5 and see BAS GEOMAP Sheet 6-B, back pocket). By contrast, the outer coast of the island is almost entirely ringed by rock and ice cliffs 30–70 m high (exceptionally 150 m, at South Point) and beaches are rare. A spectacular linear ice cliff with a narrow sandy-gravelly beach forms the eastern coastline, known as the Costa Recta, between Baily Head and Macaroni Point.

Geological setting

Bransfield Strait is situated at the south-western end of the Scotia arc, a structure linking South America and the Antarctic Peninsula. It is a late Neogene basin or structural trough developed in mainly Mesozoic—Cenozoic continental magmatic arc crust now exposed in the Antarctic Peninsula and South Shetland Islands. It formed in an area influenced by movements of the Antarctic, Pacific and Scotia plates (Galindo-Zaldívar and others, 1996; Fig.1.3), in association with very slow subduction at the South Shetland Trench (Larter, 1991; Lawver and others, 1995). It is not a normal back-arc basin as it is not associated with an active volcanic arc and it is perhaps better described as a marginal marine basin (Barker and Austin, 1994; González-Casado and others, 2000). The opening of Bransfield Strait is probably related to some combination of:

(1) rollback and passive subduction of the former Phoenix Plate along the South Shetland Trench (e.g. Lawver and others, 1995), which commenced after spreading in Drake Passage ceased about 4 m.y. ago (Barker, 1982), and

(2) strike-slip tectonism (e.g. Lawver and others, 1996; González-Casado and others, 2000).

Numerous multichannel surveys by British, Polish, Brazilian, Spanish, Italian, German and American scientists have made it one of the most intensively studied regions of the Antarctic. There is evidence for crustal thinning, a neovolcanic zone characterised by an almost continuous low axial volcanic ridge and several axial and off-axis seamounts and islands, including Deception Island (Lawver and others, 1996; Gràcia and others, 1997). Together, they resemble a nascent spreading centre, and a primary locus for extension. Conversely, earthquake and multichannel seismic evidence for diffuse extension, and an absence of unequivocal oceanic crust (Keller and others, 1992, 2002), are more compatible with a model of distributed extension in a continental setting (Barker and Austin, 1994, 1998). North-east to south-west propagation of the Bransfield Strait rift has also been suggested (Barker and Austin, 1998) but lacks supporting systematic along-axis geochemical variations (Keller and others, 2002).

Deception Island itself is a shield volcano with a submerged basal diameter of *c.* 30 km (Smellie, 1989, 1990). It is one of a series of volcanic edifices, most of them submarine, which occur along or close to the axis of a spreading ridge trending 59°N between Deception and Bridgeman islands (Grad and others, 1992; Gràcia and others, 1996, 1997). Deception Island is the most active volcanic centre in West Antarctica (e.g. González-Ferrán and Katsui, 1970; Baker and others, 1975; Baker, 1990). Its activity is recorded not only on the island itself but also in numerous tephra layers in ice and lake sediments on neighbouring islands and in marine sediments (summarized in Smellie, 1999; Pallàs and others, 2001). The island is seismically active, and numerous low magnitude volcano-tectonic and volcanic tremors have been recorded, with focal depths generally less than 10 km (e.g. Ortiz and others, 1992; Vila and others, 1992*a*; Ibañez and others 1997*a*,*b*; Alguacil and others, 1999).

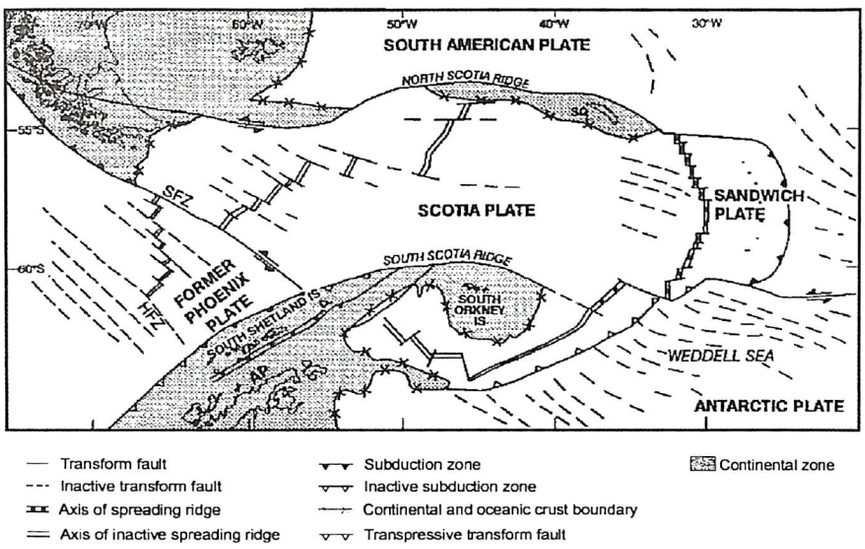

Fig. 1.3. Sketch map showing the regional plate tectonic setting of the Scotia arc and South Shetland Islands (after Galindo Zaldívar and others, 1996).

History of investigations

A complete chronological list of expeditions to Deception Island is presented in Appendix 1. Only the more important expeditions and events are described below.

Discovery and first commercial period (sealing): The first authenticated sighting of Deception Island was of its east coast, by William Smith and Edward Bransfield from the brig *Williams*, on 29 January 1820, during Smith's fourth voyage to the South Shetland Islands and in which Bransfield observed and charted the mainland of Antarctica for the first time (Campbell, 2000). Smith's other voyages took place in February, May and October 1819, although land was not sighted during the May voyage due to ice and poor weather. Port Foster, also briefly called Yankee Harbour and Port Dunbar, was probably first entered by American sealer Nathaniel Palmer in *Hero* late in 1820, although Bertrand (cited in Killingbeck, 1977, p. 11) suggested that the British sealer Macfarlane may alternatively have been first. Palmer is also credited with naming Deception Island. Sealing was the major occupation in the region during the years from late-1819 to 1824, after which sealing stocks were essentially exhausted in the South Shetland Islands. Although Deception Island was never an important source of seals, Port Foster was the operational base for a relatively large American sealing fleet from Stonington commanded by Captain Pendleton. Killingbeck (1977) also recorded that Pendleton observed the Antarctic mainland from the slopes of Deception Island, and so instructed Palmer on his sealing and exploratory voyage in *Hero* in November 1820. In January 1821, a historic meeting occurred between the Russian Admiral Bellingshausen and Palmer, probably close to Deception Island (? near Neptunes Bellows, Killingbeck, 1977), but Bellingshausen did not enter Port Foster. Bellingshausen named the island Yaroslav (Hattersley-Smith, 1991).

Sealing captain Robert Fildes made the first description of the island based on observations made in 1820-21 and, in 1829, published a chart of Port Foster, which was the first published chart for any part of Antarctica (Killingbeck, 1977).

First scientific period: The first truly scientific expedition in Antarctica was that led by Captain Foster, in *Chanticleer*, in January–March 1829. The expedition made its base at Pendulum Cove, on the north-east side of Port Foster, and obtained magnetic and gravitational field measurements, constructed the first topographic map of the island, described the island (including temperature measurements), and conducted a hydrographic survey. The topographic map, made by Lt Kendall, is remarkably accurate, and its features were used by Roobol (1980) to describe topographic changes caused by eruptions after 1829. Kendall's descriptions leave little doubt of the hardships encountered in those early days on the island: "It was.....cheerless work. The fogs were so frequent that, for the first ten days, we saw neither sun nor star; and it was withal so raw and cold, that I do not recollect having suffered more at any time in the arctic regions even at the lowest range of the thermometer" (Kendall, 1931). Kendall recorded how the ship's company ate (reluctantly) upwards of 7000 penguins during their two-month stay. He also described how the remains of earlier sealing activities, including wooden casks, metal hoops, smoke-blackened buildings and several half-buried timbers of a large ship, were found in a cove on the north-east side of Port Foster (probably the former cove (now infilled) situated *c.* 3 km north-west of Pendulum Cove). On a hill immediately above the cove, Kendall discovered a shallow grave with a rotten wooden coffin containing the body of an "English-looking" sailor remarkable for its excellent preservation. The final departure of *Chanticleer* from Port Foster took seven days owing to high winds and poor holding of anchors, illustrating the difficulties of sailing safely through the narrow entrance in poor weather (Killingbeck, 1977); Neptunes Bellows (or Billows) is thought to be named after "the gusts that blow in and out as if they came from a trumpet or funnell [sic]" (Fildes,

1821, cited by Hattersley-Smith, 1991).

Following the *Chanticleer* expedition, despite visits by several exploratory, scientific and commercial expeditions (Appendix 1), there was little significant advance in knowledge of Deception Island until the early 20th Century. However, two sets of interesting observations are recorded from that period. During a short visit by Lt. Johnson in March 1839, on the *Sea Gull*, immense quantities of steam were observed rising from a locality now called Crater Lake (Dana, cited in Roobol, 1980). The description leaves little doubt that it records the aftermath of a recent effusive eruption from the flanks of Mount Kirkwood, with the steam generated at the front of a conspicuous lava that entered Crater Lake at its south-east side (Pallàs and others, 2001). The sealer WH Smiley also observed that, in February 1842, "the whole south side of Deception Island appeared as if on fire. He counted thirteen volcanoes in action" (Wilkes, 1845). This is the first observation of an eruption observed on Deception Island.

The French Antarctic Expedition of 1908–1910, led by J-B Charcot in *Pourquoi-Pas*, produced topographic maps and soundings, including marked positions of fumaroles (Bongrain, 1912, cited by Roobol, 1980). Among the several minor differences with the map drawn by Kendall, the most notable feature is a new crater at Kroner Lake, which must have erupted between 1829 and 1908. Roobol (1973) suggested a pre-1912 age based on whale bone detritus in the area dating from 1912, but the map by Charcot clearly suggests that eruptions at Kroner Lake took place prior to 1908.

Later commercial period (whaling): The whaling period on Deception Island began in 1905, in which, by virtue of its well-known natural harbour, the whale catchers used the broad beach at Whalers Bay to haul out their catch for flensing ashore. A cemetery at Whalers Bay was begun in 1908. By 1912–13, there were 12 factory ships and 27 catchers based at Deception Island. The value of the industry peaked that year and the total catch briefly exceeded that of the South Georgia whaling stations. It is also the season in which W Moyes, the British Stipendary Magistrate, reported 3000 rotting whale carcasses in Whalers Bay area. At its peak, about 200 people were occupied on Deception Island in the summer (Yoder, 1929). After 1924, the revenue from whaling licences and taxes obtained by the Falklands Islands Government were made available for the launching and maintenance of the *Discovery* expeditions, which frequently used the island as a shelter and base for their activities (Killingbeck, 1977). Whaling revenue from Deception Island also amounted to 25% of the entire revenue for the Falkland Islands throughout the 1914–19 period. A Norwegian shore station for flensing whales operated from 1912 until the arrival of pelagic whaling ships resulted in the station closure by the end of the 1930–31 season. Thus, within a span of 25 years, Deception Island witnessed the rise and fall of the Antarctic's greatest commercial industry (Killingbeck, 1977). As a footnote, Salvesens of Leith were granted, in addition to a whaling licence, a mineral licence for the South Shetland Islands and Graham Land. Salvesen employed D Ferguson to undertake a geological study of the region in 1913–14, which produced a short report of Deception Island (Ferguson, 1921).

Aerial expeditions: H Wilkins used Deception Island to launch two aerial exploring surveys in 1928 and 1929, with the first flight in Antarctica taking place on 16 November 1928 from a small ash runway on the north side of Whalers Bay. Wilkins also inaugurated the first seaplane flight from Port Foster in 1929, although Port Foster was frequently unsuitable for amphibious air operations. Lincoln Ellsworth used Deception Island in October 1934 and again one year later to assemble his plane (the *Polar Star*), but he moved to Dundee Island (Weddell Sea) for his successful flight to the Bay of Whales, which was the first aerial crossing of Antarctica. Port Foster was used again in 1949 for the assembly of a seaplane to relieve a party of men marooned at Stonington Island.

In 1955–57, Hunting Aero Surveys Ltd were employed by the Falkland Islands Dependencies Survey (FIDS, later British Antarctic Survey) to photograph the South Shetland Islands and northern Graham Land, provide ground control and obtain airborne magnetic observations (Falkland Islands and Dependencies Aerial Survey Expedition (FIDASE); Gavin-Robinson, 1958; Mott, 1958). From 1960, FIDS extended the ash runway at Whalers Bay, and light aircraft were regularly used to resupply sledging parties in the Antarctic Peninsula, provide sea-ice information for shipping, and to undertake radio-echo soundings of the ice sheet, until the runway was partly destroyed during eruptions in 1967–70. Argentina also used seaplanes from their station on Deception Island from 1948, and planes flew from Argentina to Deception Island to drop mail. Finally, Chile operated seaplanes from Pendulum Cove in 1956. The first commercial tourist flight in Antarctica took place from near Punta Arenas in 1957, and overflew Deception Island.

Modern scientific era and third commercial period (tourism): Apart from visits by the Norwegian Antarctic Expedition (1927–28), and British Graham Land Expedition (1934–37; see Holtedahl, 1929; Tyrrell, 1945), the next important event occurred in 1942, when the British Naval vessel, *Queen of Bermuda*, destroyed supplies of coal and oil at Whalers Bay. This wartime naval action began a major period of British interest on the island, initially called *Operation Tabarin*, which resulted in the construction of a scientific station and its continuous occupation from 1944 until eruptions on the island in 1967. After World War II, the station was transferred to the FIDS. Argentine and Chilean stations were also built in December 1947 and February 1955, respectively. The construction of these three stations signalled the beginning of an era of essentially continuous scientific exploration of Deception Island. Following eruptions in 1967, 1969 and 1970, all three stations were either destroyed or abandoned, although the eruptions generated a flurry of international interest (e.g. Baker and others, 1969, 1975). There were few expeditions to Deception Island during the next 15 years but, from 1986, Britain, Argentina and Spain recommenced major scientific investigations, with Britain deploying occasional field parties and Argentina re-occupying its station regularly until the late 1990s. Spain constructed a new station on the island in 1989, from which scientific investigations have been supported during each subsequent austral summer. Spanish and Argentine scientists have monitored the island seismically for two and

a half months during each summer since January 1987. The Argentine station was redesignated as a volcanological observatory. Other countries, notably Poland, Brazil and Korea, also deployed scientists for short periods during the 1980s and 1990s. Spain published a new detailed topographic map of the island in 1994 (Servicio Geográfico del Ejército and Universidad Autónoma de Madrid, 1994; see back pocket and also Chapter 2), superseding that published by Britain in 1960 (Directorate of Overseas Surveys, 1960).

The first commercial cruise in Antarctica took place in January 1966, with the arrival in Deception Island of the tour ship *Lapata*. Tourist activities occurred during each austral summer thereafter, together with visits from private yachts, and the number of people to visit the island has increased steadily ever since (Figure 1.4). It is estimated that more than 10 000 tourists have visited Deception Island each year since 1999 (www.iaato.org). This represents the most significant commercial development in the region since its discovery in 1819. The site of the former whaling station, including FIDASE huts and the unoccupied British scientific station, became the first museum to be created in Antarctica (Muñoz, 1996). At present, the Antarctic Treaty System is considering designating Deception Island as an Antarctic Specially Managed Area (ASMA) under the procedures of the Protocol on Environmental protection and the Committee for Environmental Protection (CEP) (Downie and Smellie, 2001).

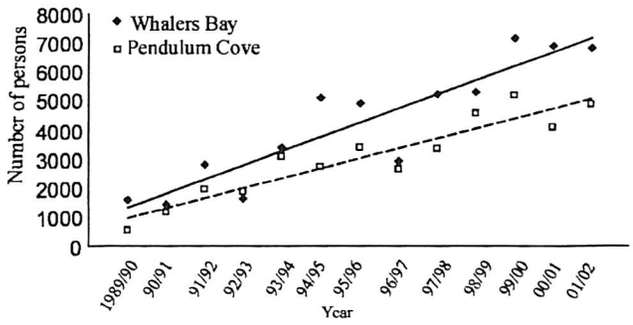

Fig. 1.4. Diagram illustrating the rapid rise in the numbers of tourists visiting Deception Island between 1989 and 2001 (information from www.iaato.org).

The topographic map

The thematic maps in this volume were prepared using the most recent topographic map as a base. The topographic map (see back pocket and Chapter 2) was published in 1994 by the Servicio Geográfico del Ejército (SGE) with the co-operation of the Universidad Autónoma de Madrid (UAM) (Servicio Geográfico del Ejército and Universidad Autónoma de Madrid, 1994). It is at 1:25 000 scale and has a contour interval of 10 m. The map was prepared using GPS observations obtained by SGE and the Real Observatorio de la Armada (ROA) and field surveys of geographical and geomorphological features by SGE and UAM during Spanish Antarctic expeditions in 1991–92 and 1992–93. The map also includes bathymetric data collected by the Instituto Hidrográfico de la Marina (IHM) and the Instituto Español de Oceanografía (IEO) during Antarctic expeditions in 1988–89, 1989–90 and 1990–91.

The geological map

Geological features were shown on maps and sketches accompanying early papers (e.g. Holtedahl, 1929; Tyrrell, 1945; Olsacher, 1956), but because of their small scale those figures and maps only gave a limited and partial view of the geological diversity of Deception Island. The first detailed island-wide geological survey was conducted by Hawkes in the 1957–58 season and resulted in published 1:25 000-scale colour geological and topographic maps and an accompanying report (Hawkes, 1961). The 1967–1970 eruptions and their products were comprehensively described by Baker and others (1975) in much greater detail than any other aspects of the island. Reports on the eruptions were also published by other geologists but are much less comprehensive (e.g. González-Ferrán and Katsui, 1970). Revisions of the geology of the island were published by Birkenmajer (1992, 1995*a*), based on three short visits in 1984–85, 1987–88 and 1990–91. Finally, the entire island was geologically re-examined during three austral summers (1986–87, 1987–88, 1993–94) by Smellie (1988, 1989, 2001*b*). The results of the lithostratigraphical investigation by Smellie (2001*b*) are the most comprehensive and modern to date, and the map and geological sections in this report are based mainly on that work.

The BAS GEOMAP Sheet 6-A (see back pocket) is the most detailed and modern geological map of Deception Island available. It was compiled at 1:25 000 scale using, as a base, the topographic map of the island at the same scale (Servicio Geográfico del Ejército and Universidad Autónoma de Madrid, 1994; see back pocket). Some details of the original topographic map were corrected on the geological and geomorphological maps as a result of more recent work, and they should be considered the most accurate maps available.

On the geological map, all the major geological formations are distinguished, mapped across the entire island and constrained within a two-fold geological history divided into pre- and post-caldera periods. Although superficial deposits, such as beaches, alluvium and scree, are distinguished (collectively), a mapping practice adopted was to ignore thin veneers of such deposits where they are < *c.* 0.5 m thick, and to map the much thicker and thus volumetrically more important deposits underneath. Thus, the extensive outcrops of "scree" mapped by Hawkes (1961) are depicted in BAS GEOMAP Sheet 6-A mainly as tephra of the late post-caldera Pendulum Cove Formation, although most of the latter outcrops have suffered post-eruptive erosion, mainly by wind-deflation, and are covered by a stony "armour" (Smellie, 2001*b*). The distribution of moraines is also indicated and those deposits are used as an approximate stratigraphical datum used to separate the post-caldera formations, although the moraines are likely to be diachronous. The geological map also shows a few selected faults (also depicted on the geomorphological map), which have ground truth, principally geological and geomorphological expression (e.g. aligned cinder cones on Kendall Terrace).

All of the volcanic products on Deception Island are subsumed within the Deception Island Volcanic Complex. It includes two groups (Mount Pond and Port Foster), which are separated by an important episode of caldera collapse. Each group contains three formations, and a small number of members are defined. The exposed pre-caldera products consist of palagonitized scoria, hyaloclastite breccia and peperite, representing eruptions from multiple centres during the shoaling and emergence of the early volcanic edifice (Fumarole Bay Formation); and a subaerial lava-shield succession (Basaltic Shield Formation). These formations are draped by deposits of multiple, dense pyroclastic currents (flows and surges; Outer Coast Tuff Formation; formerly Yellow Tuff Formation of Martí and Baraldo, 1990). The eruption of the Outer Coast Tuff Formation was voluminous (possibly 30 km^3) and immediately preceded the collapse of the Port Foster caldera. It is thus regarded as the caldera-forming eruption.

The morphology of the caldera rim fault, comprising several essentially linear sections, suggests a combination of regional and volcanotectonic controls on its origin. Early studies on the island postulated that the caldera formed by subsidence along one or more concentric faults (e.g. Hawkes, 1961; González-Ferrán and Katsui, 1970; Baker and others, 1975). However, recent geophysical and marine seismic investigations have not confirmed a concentric intra-caldera structure, dominated by ring faults. In particular, present-day seismic epicentres are distributed in a prominent SW–NE-orientated zone that extends right across the island, cross-cutting the caldera and suggesting a strong regional tectonic influence (Vila and others, 1992*a*; Rey and others, 1995; Martí and others, 1996; González-Casado and others, 1999; *cf.* Smellie, 1989). The presence of radial faults, postulated by some authors, has not been proven (e.g. Hawkes, 1961; Birkenmajer, 1992).

All post-caldera activity consisted of small-scale eruptions (< 0.05 km^3; Roobol, 1982), varying from phreatomagmatic (including a sub-glacial pyroclastic fissure eruption of likely sub-Plinian type in 1969; Baily Head and Pendulum Cove formations) to magmatic (mainly Strombolian/Hawaiian; Stonethrow Ridge Formation) reflecting a strong local hydrological control (Baker and others, 1975). Some eruptions in the early post-caldera period occurred on the outer flanks of the volcano, but all later eruptions were from multiple centres confined within the caldera.

The geomorphological map

Geomorphological features of Deception Island were previously described using figures and sketch maps in numerous published papers. However, most of the published illustrations show the entire island at a small scale (<1:100 000) or are views of selected small areas (e.g. González-Ferrán and Katsui, 1970; Igarzabal, 1974, 1977; Smellie, 1989; Smellie and others, 1997; Birkenmajer, 1992, 1995*a,b*; Criado and others, 1992; Risso and others, 1992). In addition, the geomorphological features were mostly depicted on geological maps; they included the main morphostructural elements, such as craters, lava flows, fractures and prominent scarps. Submarine geomorphological features were also depicted only as small-scale sketches (e.g. Kowalewski and others, 1990; Rey and others, 1992).

Prior to this volume, a large-scale topographically correct and geomorphologically comprehensive map of the entire island did not exist. The BAS GEOMAP Sheet 6-B (back pocket) shows, for the first time, a complete view of the morphostructural features, glacier extent, and landforms and deposits related to glacial, periglacial, nival, fluvial, aeolian and marine processes. These are represented on the map using different colours for each genetic group identified.

Primary volcanic landforms and effects of the present day glaciation are the most conspicuous geomorphological features. The distribution of craters, fractures with morphological expression, principal scarps on the island, and the submerged part of the caldera show a dominant control by NE-, NW- or NNW-trending structures. Areas of heated ground and fumarolic activity are also shown and are more complete than in previous publications (e.g. López-Martínez and others, 1996). They are confined mainly to the caldera, particularly around the shores of Port Foster, but fumarolic activity is also present on the slopes north and south of Mount Pond and on the western outer slopes of Stonethrow Ridge.

The subaerial drainage network (including seasonal streams, lakes and seasonal flooded depressions) and extent of present-day glaciers on the island are depicted on the geomorphological map in much greater detail than previously shown on the published topographic map (Servicio Geográfico del Ejército and Universidad Autónoma de Madrid, 1994). Areas of debris-covered and debris-free glacier ice, and ice-free and ice-cored moraines, are also distinguished. Evidence of periglacial activity is common and periglacial processes are facilitated by the high porosity of many of the volcanic rocks. Fluvial processes related to snow and ice ablation also exerted an important morphogenetic influence on the island and controlled much of the sediment redistribution. Permafrost is present at low elevations (*c.* 2.5 m a.s.l.) on the island and depths to the active layer vary between 60 and 100 cm (López-Martínez and others, 1996; Serrano and others, 2002).

The map also shows the morphological features and distribution of sedimentary deposits within the flooded caldera. The latter range from proximal gravel to distal sandy mud. Seismic reflection profiles (sparker, geopulse and 3.5 kHz subbottom profiler) indicate that the northern deep basin in the flooded caldera is enclosed by steep bordering slopes displaying evidence for multiple slope instability and slumping (Rey and others, 1992; Chapter 5). The caldera also contains several submerged volcanic cones, mainly in the southern parts of Port Foster. A variety of features is present on the slopes, including slump scars and related deposits, prograding sediment wedges, furrows and channels. Above these slopes, there is an inner coastal shelf up to 500 m wide. The outer coast of the island is almost entirely ringed by rock and ice cliffs caused by continuing erosional retreat. This contrasts with processes acting on the inner coast around Port Foster, which are dominantly depositional.

2 Topographic maps

by J.W. Thomson and F. Hernández-Cifuentes

Introduction

Deception Island, a horseshoe-shaped island which is a breached and drowned volcanic crater, has provided a natural harbour to shipping since it was discovered by sealers in 1820. The island was visited frequently by expeditionary ships during the nineteenth and early part of the twentieth centuries (Hattersley-Smith, 1991, p. 182–183) and many of the expeditions surveyed or prepared hydrographic charts of its coastal waters. Its location close to the northern end of the Antarctic Peninsula made it a suitable base for the first airborne survey of the peninsula in December 1928 (Wilkins, 1929), and for the Canso flying boats used during the Falkland Islands and Dependencies Aerial Survey Expedition (FIDASE) of 1955–57 (Mott, 1986).

Despite its attraction as the safest harbour in the South Shetland Islands (Fanning, 1833), the island is an active volcano and its shape has changed several times since the first charts were prepared in the 1820s.

Historical maps and charts: An early survey of Deception Island by H. Foster and E.N. Kendall in 1829 recorded the overall shape of the island on a map at 1:145 920 scale (Kendall, 1831). Further charts prepared by a succession of subsequent visitors give contemporary evidence of the dynamic nature of the island: W.H. Smiley, a sealer, suggested in 1842 that the shape of the island was undergoing change and Mossman (1905) noted several changes in the configuration of the island around Pendulum Cove. The French Antarctic Expedition, 1908–10, improved on the early surveys and produced a hydrographic chart in 1912 which featured hill-shaded land features and emphasized the rim of mountains encircling the central harbour (see reproduction of chart in Wilkins, 1929).

The first 'modern' topographic map of Deception Island, published by the Directorate of Colonial Surveys in 1955, was drawn from a survey by R.R. Kenney and N.A. Leppard in 1953–54 and based on a triangulation by the then Hydrographic Department of the Admiralty, 1948–49. The map, published at a scale of 1:50 000 (Directorate of Colonial Surveys, 1955), distinguished clearly between areas of rock and those of permanent snow.

The overall shape of the island shown on the 1955 map was confirmed a few years later when a new topographic map at 1:25 000 scale (Directorate of Overseas Surveys, 1960) was constructed from vertical aerial photography acquired by the FIDASE in December 1956. The new map used the same astronomical fix and triangulation as the 1:50 000 scale map, with further control from triangulation acquired by FIDASE. Neither of the British topographic maps showed any bathymetric detail. The 1960 map benefitted from the application of hill-shading and it is a fine example of a relief map. Within a few years, however, this elegant map became obsolete when Deception Island was subjected in December 1967 to the first of three volcanic eruptions. The inner coast of the island, especially in the north-western part of Port Foster, in Telefon Bay, changed radically. A new small island was formed, which became incorporated into the main island during subsequent eruptions in 1970 (Baker and others, 1975, figs 14 and 29). The Argentine Servicio de Hidrografía acquired 1:28 000 scale aerial photography of the whole island in January1968 and partial cover of it in August 1970, immediately after the last eruption. Brecher (1975, figs 1-3) used the 1956, 1968 and 1970 photographs to compile a series of 1:10 000 scale maps of the volcanically active areas of Deception Island. The 1994 Spanish map, published at 1:25 000 scale, shows the post-1970 topography of the entire island.

Compilation of the 1994 topographic map

A modern survey of Deception Island, using GPS receivers, was undertaken by the Spanish Servicio Geográfico del Ejército (SGE) and Real Observatorio de la Armada during 1991–92 and 1992–93. The area subjected to the most change during the 1967 and 1970 eruptions was mapped in detail on the ground during this period (mainly by SGE and Universidad Autónoma de Madrid in 1992–93); the new map (Servicio Geográfico del Ejército and Universidad Autónoma de Madrid, 1994) was constructed using a combination of the 1991–93 survey data and earlier, pre-eruption aerial photography. The 1994 map also incorporated bathymetric data for Port Foster, a useful feature which had not been shown on the earlier topographic maps. The bathymetric data were collected by the Instituto Hidrográfico de la Marina and the Instituto Español de Oceanografía between 1988 and 1991. Data sources used in the preparation of the 1994 map are shown below and the processes involved are summarized in Table 2.1.

Table 2.1. Summary of processes involved during the preparation of the 1994 topographic map of Deception Island

Phase	*Task*
Preliminary study	Appraisal of existing maps, aerial photographs and co-ordinates of control points
Field work on Deception Island	Reconnaissance of terrain and positioning of triangulation flags GPS observation of ground control points for stereoplotting Points radiation using EDM Trigonometric levelling Preliminary calculation of co-ordinates
Calculation of geodetic stations and ground control points	Definitive calculation of co-ordinates
Photogrammetric stereo-plotting	Triangulation from aerial photographs and stereoplotting, digital files obtained
Creation and review of the map	Digitization of data obtained by survey Addition of toponymy and marginalia
Finalization	Editing film positives and printing

Data sources:

(a) Topographic maps and marine charts of Deception Island at 1:25 000 scale or smaller (Directorate of Overseas Surveys, 1960; Hydrographic Office, 1987).

(b) Vertical aerial photographs obtained in December 1956 by the Falkland Islands and Dependencies Aerial Survey Expedition.

(c) Geodetic survey by Servicio Geográfico del Ejército and Real Observatorio de la Armada during 1991–92 and 1992–93.

(d) Bathymetric data collected in 1988–89, 1989–90 and 1990–91 by Instituto Hidrográfico de la Marina and Instituto Español de Oceanografía.

(e) Maps of topographic features prepared on the ground by Universidad Autónoma de Madrid in 1992–93.

Equipment:

(a) Geodetic and topographic data were acquired in the field using GPS Trimble 4000 SLD and 4000 ST receivers and Wild T-2 theodolite (accurate to centesimal seconds) and a DI-20 electronic distance meter (EDM) (accurate to distances of rms = 5 ± 1 mm/km).

(b) Photogrammetric interpretation: Matra Traster T-1 analytical stereoplotter and Wild A-10 analogue stereoplotter.

(c) Map compilation: Intergraph TD-100 workstation and Calcom digitizing table.

(d) Map editing and printing: Raster Scitex Response 250 and Roland Rekor II offset printer.

Field work:

Phase 1 - Ground control observations. The network of geodetic stations and control points used is shown in Fig. 2.1. The co-ordinates of 22 points were measured using a theodolite and electronic distance meter (Table 2.2), and GPS observations were made at all the other points (Table 2.3). A static 4000 SLD receiver, located at the 'Deception' control point, was used in conjunction with a roving GPS receiver (ST model); only the L1 frequency of the two available was used. One hundred measurements, in two sessions of 50, were obtained for each control point, connecting to a minimum of four satellites, with 15° elevation above the horizon.

The height differences between the ellipsoid and the geoid were solved by levelling geodetic control points to mean sea level and averaging the result. Table 2.4 shows that the difference between altitude measured relative to mean sea level and the values obtained by GPS is about 13 m.

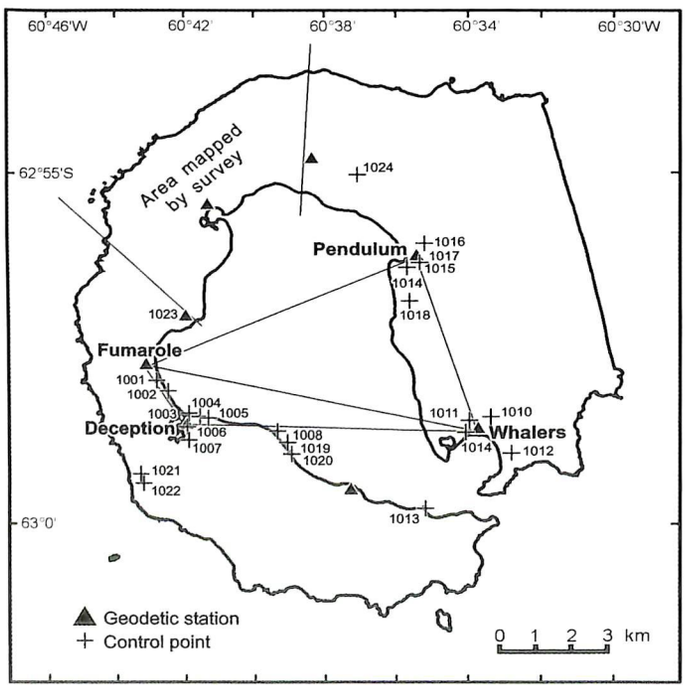

Fig. 2.1. Location of geodetic stations and ground control points on Deception Island.

Table 2.2. Final co-ordinates of the ground control points obtained by theodolite

Point	*X*	*Y*	*Z*
Baliza	618541.497	3014505.039	105.773
Bandera	620707.315	3013031.984	34.446
Muratura	616741.959	3017840.085	124.427
Crater	617819.245	3020532.617	61.139
Arista	619805.798	3021412.711	91.346
1001	615812.295	3016421.616	18.184
1002	616124.808	3015732.400	20.811
1003	616602.083	3015117.269	13.582
1004	616653.137	3015094.551	14.664
1005	616668.932	3015062.723	16.312
1006	616648.372	3015020.707	17.825
1007	616536.784	3014924.861	18.417
1008	618554.317	3014493.321	105.483
1009	623435.102	3014493.205	14.881
1010	623525.848	3014470.197	14.586
1011	623395.988	3014556.829	19.650
1012	624016.227	3013986.703	13.269
1013	622221.297	3012545.985	20.258
1014	621923.698	3018869.462	107.218
1015	622176.747	3019199.773	22.433
1016	622189.424	3019233.516	24.336
1017	622156.093	3019228.038	20.667

Table 2.3. Final co-ordinates of the geodetic stations and ground control points obtained by GPS

Point	*X*	*Y*	*Height (in m)*
Deception	616668.573	3015072.739	15.96
Fumarole	615793.877	3016629.362	16.66
Pendulum	622165.599	3019220.725	20.50
Whalers	623426.708	3014566.972	19.70
1018	621779.062	3018275.990	19.548
1019	619019.683	3014173.956	12.990
1020	619051.691	3014120.649	13.427
1021	615281.762	3013625.325	61.913
1022	615493.951	3013404.219	75.669

Table 2.4. Height difference (in metres) between the ellipsoid and geoid

Point	*Mean sea level*	*GPS*	*Difference*
Deception	2.547	15.96	13.413
Fumarole	3.885	16.66	12.775
Pendulum	9.313	22.50	13.187
Whalers	6.989	19.70	12.711

Phase 2 - Field mapping. The area around Telefon Bay, where the topography had changed significantly after the 1967–70 volcanic eruptions, was the focus of fieldwork in 1992–93.

The co-ordinates collected at a large number of points were plotted and contours interpolated from the elevation data. Two control points (Muratura and Arista), located in Phase 1 and observable on the existing aerial photographs, provided accurate reference points for the work. They form a network with the points listed in Table 2.5. A common area was mapped by stereoplotting and by ground survey methods. Features mapped on the ground included coastline, crater rims, lake shores, valleys and theoretical contours; these were plotted and linked to the stereoplot of the same area.

Table 2.5. Co-ordinates of the control points used for the positioning of the area mapped by survey

Geodetic control points	*X*	*Y*	*Z*
Muratura	616741.959	3017840.085	124.427
Arista	619805.798	3021412.711	91.346
81	619338.318	3021866.221	45.528
82	619072.440	3021866.221	45.677
83	618409.774	3021194.459	24.822
84	618064.820	3021155.954	24.748
85	617395.595	3020649.075	27.650
86	616924.648	3020772.129	60.932
87	617652.015	3020252.947	44.727

Accuracy of the topographic map

The methods used and the precision of the topographic map are appropriate for the time of its preparation and publication in the early 1990s. The root mean square accuracies (rms) in the location of the control points are less than 1.5 cm, as shown in the error ellipses and distribution of rms residuals (Figs 2.2 and 2.3).

During the preparation of the geomorphological map (BAS GEOMAP 6B, back pocket), several elements of the map were improved, for example, the extent of glaciers and positions of drainage channels. The representation of these elements on the geomorphological map is more accurate than on the topographic map published in 1994.

Place names

Because Deception Island has been visited by many expeditions from different nations since its discovery, it has a variety of place names in different languages for several of its features. When the 1994 topographic map was in preparation, there was no agreed international convention for selecting Antarctic place names for use on maps and in other publications. There was, however, a general interest in avoiding the introduction of further synonyms to the map. Thus those features which had no equivalent name in Spanish were shown in English, rather than translating them into Spanish. Although the majority of the place names are in Spanish, the selection shown on the 1994 map include those of Argentine, British, Chilean, and Spanish origin. The names of Spanish origin introduced on the map are officially approved names only (López-Martínez and Hernández-Cifuentes, 1997).

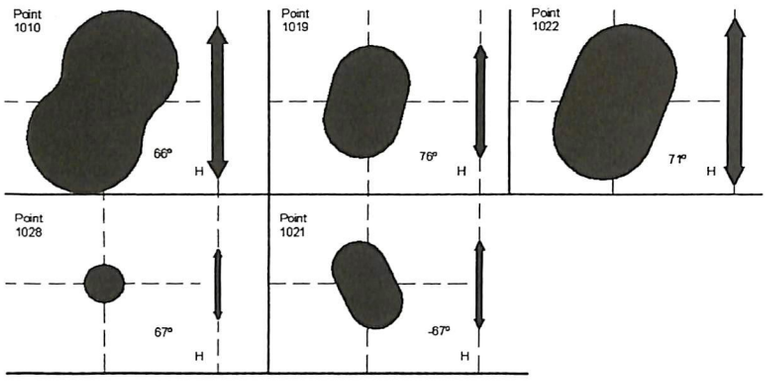

Fig. 2.2. Error ellipses in the positioning of different control points. Scale bar graduation = 0.01 m.

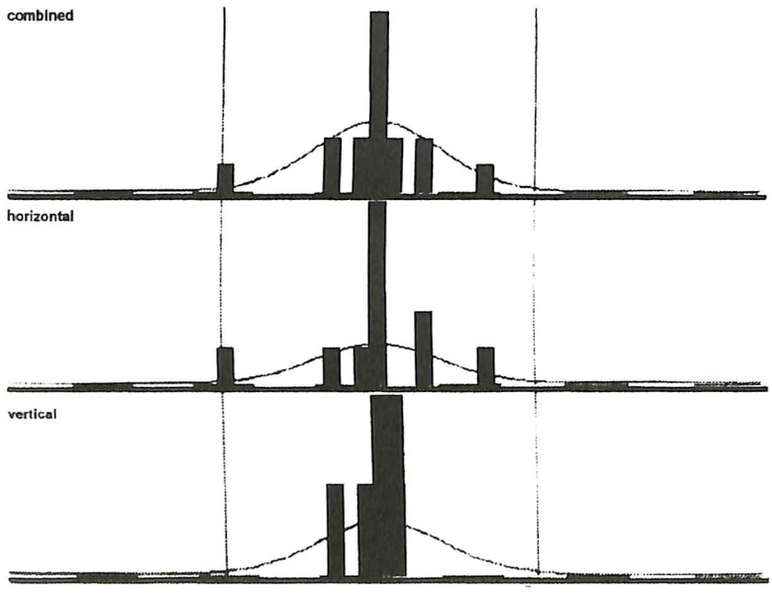

Fig. 2.3. Distribution of standardized residuals in the positioning of the geodetic control points. Horizontal axis, deviation from the central value (see Fig. 2.2), scale graduations = 1 τ; vertical axis, relative number of observations

During the production of the map an international project, undertaken by the Scientific Committee on Antarctic Research's Working Group on Geodesy and Geographic Information, began to collate all the lists of formally approved names for Antarctic features. The aim of the project was to prepare a *Composite Gazetteer of Antarctica* (CGA) that could be used to identify which features had already been named and thus avoid further duplication of names in the future.

Selecting the names based on their inclusion in the CGA (Scientific Committee on Antarctic Research, 1998, 2000, 2002), and using the principle of historical precedence, has given rise to the different set of names shown on the geological and geomorphological maps of Deception Island compared with those used on the 1994 topographic map. A gazetteer of place names referred to in this publication, and all those features within the map area that have been named officially in current gazetteers by the relevant authorities of Argentina, Chile, Poland, Spain and the UK, is given in Appendix 2.

3 Geology

by J.L. Smellie

Deception Island is a large active Quaternary volcano with a restless caldera about 10 km in diameter that is flooded by the sea (Roobol, 1973, 1980, 1982; Baker and others, 1975; Cooper and others, 1998). It is also situated close to a nascent spreading centre yet, atypically for marginal basin systems, is exposed above sea level. Deception Island thus represents a rare opportunity for following the progress of volcanism associated with an active caldera in a rifted ensialic marginal basin setting (Baker and others, 1975; Smellie, 2001*b*). The island is only occupied for about two months each year and there is no year-round volcano-monitoring programme, despite hosting visits by several thousand tourists and scientists during each short austral summer. Knowledge of the geology and, thus, eruptive history of the island is our best guide to how the volcano may erupt in the future.

Age

Chronological age control is very poor on Deception Island. Moreover, despite a maximum thickness of 1.5–2 km for the entire volcanic succession suggested by geophysical studies (Grad and others, 1992, fig. 10), at least 80% of the volcano is submerged and is unavailable for study. The presence of Eocene nannofosils in a single 'clast in agglomerate' (Birkenmajer and Dudziak, 1991) indicates a maximum (and highly unlikely) early Tertiary age. The only other fossils recovered from the island so far comprise an age-undiagnostic *Laternula* species (a type of burrowing clam) collected within volcanic breccias on the north-east side of Whalers Bay (Smellie, 2001*b*). All of the subaerial rock formations have a normal polarity, indicating that they formed within the present chron (i.e. < 750 Ka; Valencio and others, 1979). Isotopic dating yielded an imprecise K-Ar whole-rock age of 150 Ka ± 50 Ka (Keller and others, 1992), likely to be unreliable (too old; see Smellie, 2001*b*), whilst C^{14} dating of organic remains associated with Deception-sourced marine and lacustrine tephras in the region range back to 36 Ka (Matthies and others, 1990; Björk and others, 1991; Moreton, 1999). Numerous eruptions dating back to about 1780 have been dated by ice-layer stratigraphy, and a few eruptions have been witnessed (Orheim, 1972*a*, 1972*b*; Roobol, 1973, 1980; Baker and others, 1975; Pallàs and others, 2001). Thus, it can only be asserted confidently that Deception Island is likely to be < 750 Ka in age, and none of the volcanic units can be correlated based on chronological age alone.

Stratigraphy

Despite its long history of exploration and scientific studies (Chapter 1; Appendix 1), few geologists have spent more than a few weeks studying the island and only four substantive stratigraphical studies of Deception Island have been published: Hawkes (1961), Baker and others (1975), Birkenmajer (1992, 1995*a*) and Smellie (2001*b*). Hawkes (1961) used a mixture of chronostratigraphical and lithostratigraphical divisions, whilst Baker and others (1975) used an informal system of rock names (also Smellie, 1988, 1989). Neither Hawkes (1961) nor Baker and others (1975) defined formations, and the description by Baker and others was focused principally on a volcanological study of the products of the 1967–1970 eruptions. Martí and Baraldo (1990) revised part of Hawkes' stratigraphy, grouping all the pre-caldera units within two new formations (Basaltic Shield and Yellow Tuff formations). Birkenmajer (1992) created a complicated stratigraphy that was proposed as a lithostratigraphical standard for the island. However, more detailed mapping does not agree with many of the correlations described by Birkenmajer (1992) and it is not recommended. The comprehensive lithostratigraphy of Smellie (2001*b*) is the most recently published and most detailed. It is used as the basis for the following descriptions.

All of the lithified and unlithified volcanic rocks on Deception Island are grouped together within the *Deception Island Volcanic Complex*. A fundamental division into pre- and post-caldera groups is based on the recognition of a single major caldera-forming event, which was immediately preceded by a large-volume cataclysmic eruption. Each group is divided into three formations (Table 3.1).

Port Foster Group

The Port Foster Group includes all the pre-caldera volcanic formations on the island. Principal exposures include South Point, near Entrance Point and the spectacular outer coast cliffs between Punta de la Descubierta and Macaroni Point. It is also well seen in inner caldera wall sections at Stonethrow Ridge, Cathedral Crags and south of Collins Point (Figs 3.1 and 3.2). Other exposures are small and scattered. The group is divided into the Fumarole Bay, Basaltic Shield and Outer Coast Tuff formations.

Table 3.1. Lithostratigraphy of Deception Island. Excludes un-named alluvial, beach, scree and moraine deposits. After Smellie (2001*b*), modified

DECEPTION ISLAND VOLCANIC COMPLEX			
Mount Pond Group Post-caldera deposits, the products of phreatomagmatic (Baily Head (early) and Pendulum Cove (late) formations) and magmatic (Stonethrow Ridge Formation) eruptions	**Pendulum Cove Formation** Predominantly tuff cone and maar deposits; deposits typically grey and loose or friable; primary landforms well preserved; centres occur in geographically well defined clusters within caldera although teprha deposits generally blanket the island	**Telefon Bay cones***	Deposits of 1967 and 1970 eruptions
		Kroner Lake cones	Three eruptive centres; mainly 19th century
		Crimson Hill cones	At least two large centres; pre-1829
		Cross Hill cones	Multiple centres, pre-1829; includes White Ash Member
		Vapour Col cones	Several large centres, pre-1829
		Crater Lake cones	Multiple co-eruptive centres; probably pre-1829
		Collins Point cones	Two centres; includes dacite lava(s)
	Baily Head Formation Indurated, grey to khaki hydrovolcanic t ephra; primary landforms not preserved; centres not restricted to caldera		Degraded, mainly indurated tuff cone deposits
	Stonethrow Ridge Formation Mainly fissure-erupted, post-caldera Strombolian scoria and lavas (many clastogenic); subdivision mainly based on known or inferred relationship to moraine deposits	**Mount Kirkwood Member**	Includes products of 1838/9, 1842 and 1969 eruptions
		Kendall Terrace Member	At least partly older than Baily Head Formation
PRINCIPAL CALDERA COLLAPSE			
Port Foster Group Pre-caldera deposits, mainly hydrovolcanic tephra, typically indurated and bright yellow; also lavas and Strombolian scoria	**Outer Coast Tuff Formation** Indurated yellow lapilli-tuffs; particularly conspicuous in outer coast cliffs		Multiple thick pyroclastic current deposits
	Basaltic Shield Formation Simple and compound sheet lava flows; Strombolian scoria		
	Fumarole Bay Formation Indurated yellow hydrovolcanic (?) tephra; minor syn-eruption intrusions	**Stratified lapilli tuff member**	Thin-bedded, surge-like deposits
		Scoria member	Massive palagonitized scoria deposits
		Lava lobe member	Mainly massive hyaloclastite breccia and peperite

* Note: cone clusters are not stratigraphical units. See text for details.

a

b

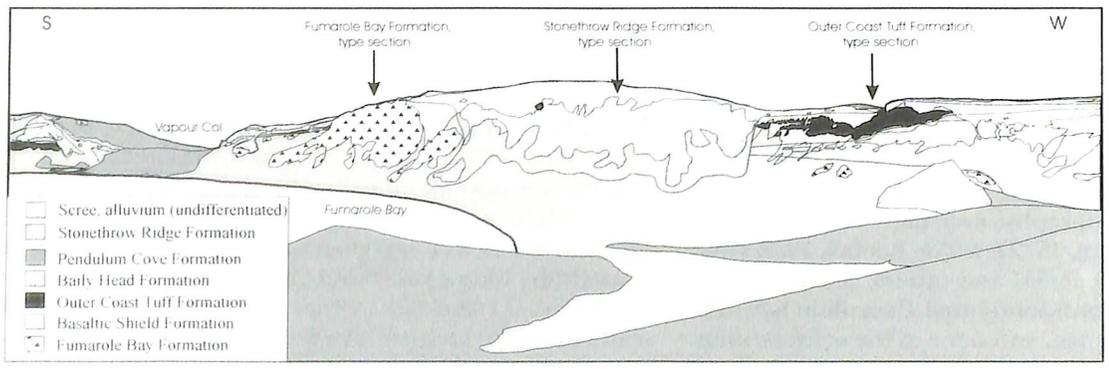

Fig. 3.1. Panoramic view (a) and geological features (b) of central and southern Stonethrow Ridge, looking south-west from Wensleydale Beacon. The ridge is one of the most important outcrops on the island, containing the type sections of three formations and unambiguous field relationships.

A

B

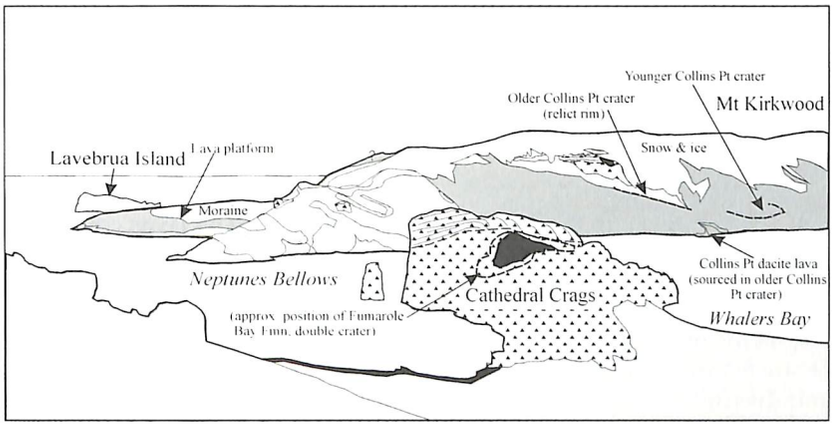

Fig. 3.2. Photographic view (A) and geological features (B) of southern part of the island, looking south-west along Cathedral Crags to Entrance Point. See Fig. 3.1 for explanation of ornaments used.

Fumarole Bay Formation: The Fumarole Bay Formation is divided into (from base to top) lava lobe, scoria and stratified lapilli tuff members. The lava lobe member is exposed at southern Stonethrow Ridge, South Point (inaccessible) and the outer coast near Entrance Point. The scoria member forms most of Cathedral Crags and also crops out at southern Stonethrow Ridge, the caldera wall south of Collins Point and near Entrance Point. The stratified lapilli tuff member is best seen at Cathedral Crags and southern Stonethrow Ridge, but outcrops also occur south of Collins Point and at South Point. A type section for the Fumarole Bay Formation is defined at the prominent khaki-yellow crags overlooking Fumarole Bay, at southern Stonethrow Ridge, where it attains a maximum thickness exceeding 200 m (Fig. 3.1).

The *lava lobe member* is mainly composed of hyaloclastite breccia and lava. Monomict breccia, typically poor in fine tuff matrix, dominates the member. It is massive, khaki coloured and formed of porphyritic poorly- to non-vesicular blocky vitric lapilli and fine-grained blocks up to 1 m in diameter. Faint discontinuous stratification is rarely present. The breccia contains numerous irregular amoeboid, lobate and pillow-like masses of grey-brown porphyritic lava up to 6 m thick and 10–50 m in length that locally form up to 80% of the basal parts of outcrops. The poorly vesicular lava has thick glassy margins, is typically blocky jointed with local jigsaw breccia, and it breaks up marginally into glassy hyaloclastite breccia (Fig. 3.3). Thin lava "stringers" emanate from a few lobes and pillows (Smellie, 2001*b*, fig. 6). At South Point, lava pods and lenses are intruded by two upward-flaring columnar intrusions extending a few tens of metres up the cliffs, with gradational upper terminations. Scarce bombs occur in the higher parts of the lithofacies.

Massive, monomict fine vitric lapillistone and coarse vitric lapilli tuff of the *scoria member* gradationally overlie the lava lobe member. The scoria member is apparently absent in the sequence at South Point, where the lava lobe member is conformably overlain by the stratified lapilli tuff member, although in places an intervening unusual 10 m-thick unit of very coarse blocky breccia (blocks several metres in diameter) intervenes. By contrast with the lava lobe member, the scoria member and succeeding stratified lapilli tuff member are essentially aphyric. Although predominantly yellow (due to palagonite-altered lapilli rims), the scoria member is dark grey locally (e.g. below

Fig. 3.3. Close view of isolated strongly jointed lava pillows and hyaloclastite breccia in lava lobe member outcrop 500 m south-south-west of Entrance Point. Minor current coeval activity is suggested by the presence of faint stratification in the overlying finer deposits. The hammer is 55 cm in length.

Fig. 3.4. Folded and faulted megaclast of stratified lapilli tuff within the southern margin of the scoria member outcrop at the type locality for the Fumarole Bay Formation. The megaclast shown is about 10 m high.

Neptunes Window and northerly exposures at the type locality). Fine tuff is absent and the deposits consist mainly of fine sideromelane lapilli and coarse tuff with a wide range of vesicularity (to highly vesicular) and blocky shapes with planar faces. Many clasts are fragments of bombs. Traces of cm- to dm-scale stratification are faintly present in a few places. Finely vesicular bombs (usually < 30 cm in diameter, but ranging up to 2 m) are common and conspicuous, with flattened cowpat and spindle shapes, that locally form bomb-dominated beds. Strongly folded and faulted intraformational megaclasts (up to a few tens of metres across), composed of thinly stratified lapilli tuff, are locally conspicuous (Fig. 3.4).

The contact between the scoria member and the overlying *stratified lapilli tuff member* is gradational and well exposed at Cathedral Crags, although it may be locally erosive in the type section. The member consists of well-stratified (mainly alignment bedding (*cf.* Fisher and Schmincke, 1984), rarely cross stratified) yellow fine vitric lapillistone and vitric lapilli tuff in beds up to a few dm thick and with a high proportion of coarse tuff matrix. The juvenile sideromelane varies from blocky and sliver-shaped, to rarely spinose. Vesicularity is extremely variable, mainly poor to moderate, rarely highly vesicular, and accretionary and armoured lapilli are locally common. Bombs are rare. In the Cathedral Crags outcrop, radial bedding directions suggest the former presence of at least two co-eruptive centres (Fig. 3.2).

Basaltic Shield Formation: This formation (defined originally by Martí and Baraldo (1990), but modified by Smellie (2001b)) is well exposed in northern Stonethrow Ridge, the type section (Fig. 3.5), but it also crops out in a tiny bay on the outer coast to the north-west, and in the caldera wall west of Cross Hill. It is up to 110 m thick and dominated by lavas, particularly in basal exposures, but includes abundant scoria in higher sections. The lavas commonly show conspicuous platy jointing, and most have grey to maroon scoriaceous surfaces. The thickest lava (at least 25 m) is a pahoehoe flow, with buff-coloured, trough cross-laminated sandy ash in inter-'pillow' spaces toward the top of the unit. Pyroclastic deposits in the basal part of the sequence are thin beds of massive to crudely stratified dark brown fine lapillistone with coarse tuff matrix, and thinly laminated tuff, whereas dark grey and bright red scoria with abundant bombs are dominant higher up.

Outer Coast Tuff Formation: The 'Outer Coast Tuff' of Hawkes (1961) was subsumed as the lower of two members within a newly-defined 'Yellow Tuff Formation' by Martí and Baraldo (1990). The upper member in the new formation comprised numerous scattered outcrops of stratified lapilli tuffs, to which Smellie (2001*b*) ascribed a *post*-caldera age and origin unrelated to the lower member. With the removal of the upper member from the Yellow Tuff Formation, the original terminology of Hawkes (1961) was reinstated and formally defined, with formation status, by Smellie (2001*b*).

The Outer Coast Tuff Formation is exposed almost continuously on the western and northern outer coast cliffs for a distance of 16 km. Inland exposures are patchy and confined to the caldera wall, particularly at Vapour Col and south of Collins Point (Figs 3.2 and 3.6). The formation is 50–70 m thick in most outcrops, but may reach 90 m on the outer coast west of Fumarole Bay. It has a conspicuous and characteristic yellow colouration due to pervasive palagonitization. The formation is formed of vitric lapilli tuff that is crudely organized into several thick (individually up to 30 m) multistorey bedsets, which can be traced laterally several km (Fig. 3.7). The bedsets fade out laterally, probably by amalgamation but the palagonite alteration masks many features. Coarse columnar jointing

Fig. 3.5. Northern Stonethrow Ridge, looking west. The section is composed mainly of lavas of the Basaltic Shield Formation, overlain by a thin wedge of Outer Coast Tuff Formation and capped by Stonethrow Ridge Formation scoria and clastogenic lavas.

A

B

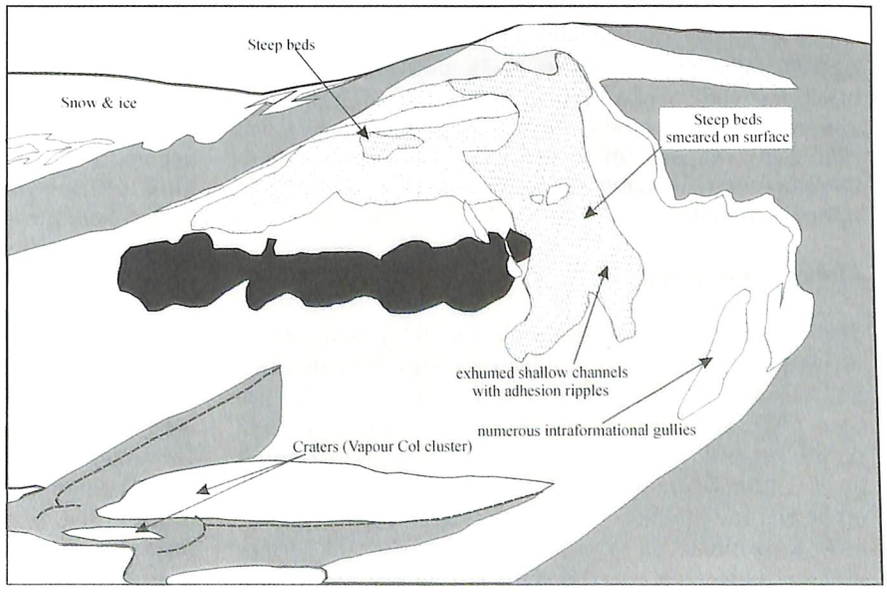

Fig. 3.6. Photographic view (A) and geological features (B) of southern Vapour Col, looking south. Steep tephra beds indicated are part of Baily Head Formation tuff cone. See Fig. 3.1 for explanation of other ornaments used.

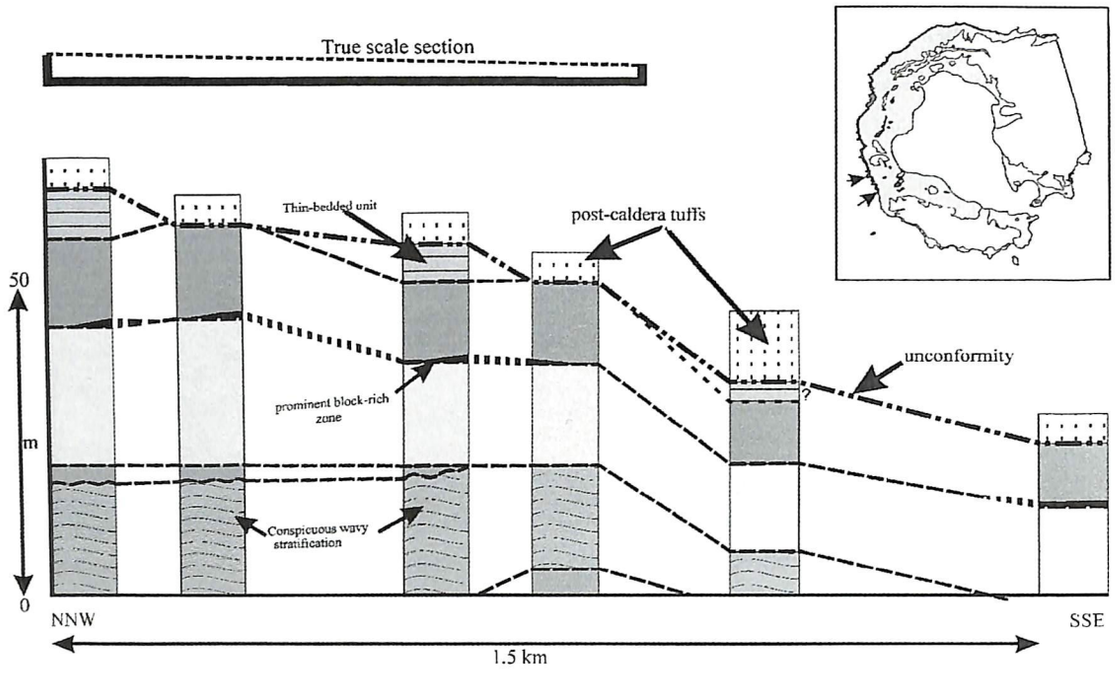

Fig. 3.7. Geological sketch section of the outer coast cliffs south-west of Vapour Col, showing correlation of thick multistorey bedsets (flow units) in the Outer Coast Tuff Formation.

is developed at two localities (Fig. 3.8; *cf.* Smellie, 1988, 1989). Each bedset is composed of multiple beds, usually < 3 m thick, of massive lapilli tuff, rarely with reverse-graded bases and normal graded tops and usually with gradational bases, several of which are marked by lenses richer in coarse juvenile lapilli and accessory blocks; these weather as prominent notches. Amalgamation is common. A second bedding type comprises multiple thin beds, faintly to prominently wavy-planar stratified in a cm to dm scale, and showing frequent erosional scour surfaces (Fig. 3.9).

The juvenile lapilli and ash-sized sideromelane clasts are blocky to rarely cuspate, commonly showing signs of abrasion and fine ash armour, and occasionally occurring as bombs. They have a wide compositional range, mainly basalt to basaltic andesite, but including a small proportion of white dacite pumice lacking flattening and welding, and dense glassy dacite blocks. Some pumice shows magma-comingling textures. Accessory clasts are common and include holocrystalline basaltic and andesite lavas, red and black tachylitic scoria, yellow lapilli tuff, dolerite and gabbroid, usually < 50 cm in diameter, but up to 1.5 m (Fig. 3.10). Coarse silt to very fine sand-size matrix is abundant, cemented by zeolite (Martí and Baraldo, 1990) or minor carbonate.

Mount Pond Group

The Mount Pond Group encompasses all the post-caldera formations on the island, of which there are three defined: Baily Head and Pendulum Cove formations, which are pyroclastic and formed during explosive hydrovolcanic eruptions, and the Stonethrow Ridge Formation, formed by a combination of weakly energetic magmatic (dry) eruptions and effusion. The post-caldera outcrops are the most widespread on the island and dominate the surface geology. However, apart from thick accumulations within the caldera, the post-caldera products form a relatively thin skin on top of the pre-caldera formations. Differences in preservation state of the original volcanic structures, and relationship to glacial moraines on the island suggest that the Baily Head Formation is older than the Pendulum Cove Formation, and the two formations were erupted in ill-defined 'early' and 'late' post-caldera times, respectively. Eruptions of the Stonethrow Ridge Formation occurred at intervals throughout the post-caldera period and overlapped in timing with both the Baily Head and Pendulum Cove formations.

Stonethrow Ridge Formation: This formation crops out exclusively along the summit ridge and outer coast of the island, except where it has spilled over the inner face of the caldera walls. A type section is defined at central southern Stonethrow Ridge, where thin lavas and scoria cascade over the caldera wall (Fig. 3.1). A distinction is made between an early Kendall Terrace Member and a later Mount Kirkwood Member. The two members are lithologically indistinguishable but are separated by an intervening glacial period, which deposited numerous grey and red (often scoria-rich) moraines on the island. The Mount Kirkwood Member is the best-dated unit on the island, and includes the products of several well-dated historical eruptions, in 1839–42 and 1969, which erupted from fissures through the Mount Kirkwood and Mount Pond glaciers (*cf.* Baker and others, 1975; Smellie, 2001*b*, 2002).

The formation has a maximum thickness of about 100 m and is formed mainly of red and black coarse scoria, maroon agglutinate and grey lavas (Fig. 3.11). The lavas are usually << 10 m thick but locally reach 45 m, are platy jointed and mainly clastogenic. Exceptions include a lava draping the northern caldera wall, which is a chaotic mixture of pahoehoe toes, lava tubes and block lava. Block lava with crude concentric pressure ridges (ogives) also

▲ **Fig. 3.8.** View of north-western outer coast cliffs, looking north-east towards Livingston Island (background). Crude columnar jointing is conspicuous in the cliffs, which are formed of Outer Coast Tuff Formation pyroclastic current deposits. The cliffs are about 60 m high.

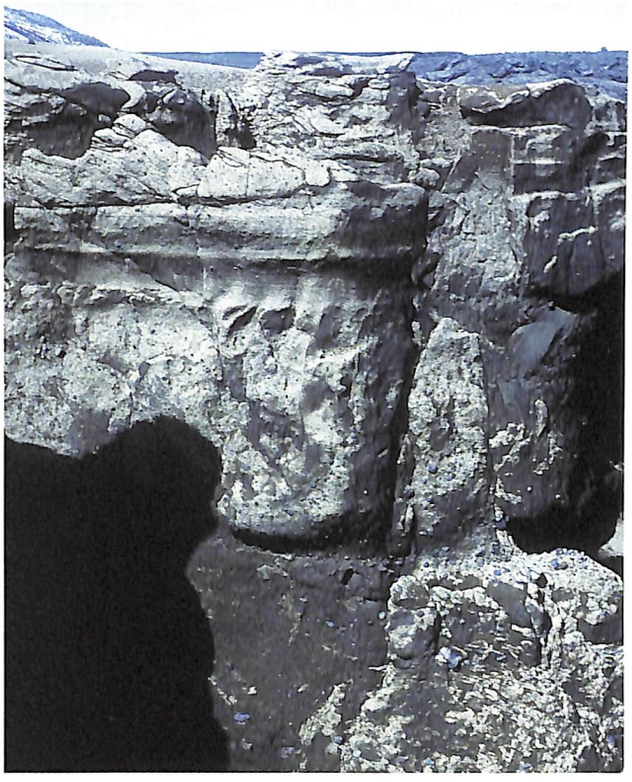

Fig. 3.9. View of thinly stratified, surge-like unit about 1 m thick interbedded with thicker massive pyroclastic flow deposits in the Outer Coast Tuff Formation, north-west outer coast cliffs.

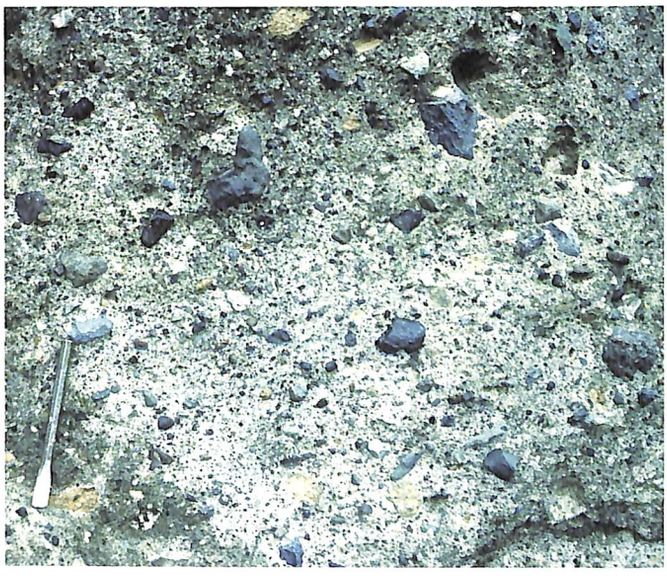

Fig. 3.10. Close view of massive pyroclastic flow deposit typical of most of the Outer Coast Tuff Formation. Note abundance of lithic clasts and fine matrix. Dacite obsidian and pumice are also present. Telefon Ridge about 1 km north-west of Cross Hill. Chisel is 20 cm in length.

Fig. 3.11. Close view of reddened coarse scoria and ragged bombs flattened by impact. Stonethrow Ridge Formation, on Telefon Ridge, about 3 km north-north-east of Cross Hill. Lens cap is 6 cm in diameter.

flowed from a cinder cone on the north-west flank of Mount Kirkwood and entered Crater Lake, where it formed several small inconspicuous littoral cones up to 20 m wide and 5 m high. Eruptions were focused in several fissures, now marked in places by lines of small cinder cones. Sections through former fissures are exposed, mainly in places where collapse recession of the caldera walls has occurred. There, feeder dykes filled by agglomerate and lava can be traced up into scoria (Fig. 3.12). An unusual massive deposit, on the outer coast 2.5 km west of Macaroni Point, is formed of heteromict coarse blocks of multi-coloured scoria breccia and lava up to 2 m in diameter, and megaclasts (6–8 m thick by 10–20 m long) of yellow stratified lapilli tuff derived from the adjacent Fumarole Bay Formation outcrop, which it steeply cross-cuts. The deposit is invaded by numerous pillows, pods and irregular apophyses of lava, which are chilled and locally change progressively into breccia around their margins. It is overlain by undisturbed planar-stratified scoria and a 40 m-thick grey lava with scoria lenses.

Fig. 3.12. View of interior of Stonethrow Ridge Formation feeder dyke exposed in the caldera wall west of Cross Hill. The dyke cuts across thinly stratified Outer Coast Tuff Formation. It has prominent thick chilled margins of crystalline basalt whereas the interior is filled by indurated agglomerate. Map case is 30 cm in length.

Fig. 3.13. View of Baily Head, looking north-east; Livingston and Greenwich islands are in the background. Baily Head and Sewing-Machine Needles (stacks to right) are remnants of an early post-caldera tuff cone, the type locality for the Baily Head Formation.

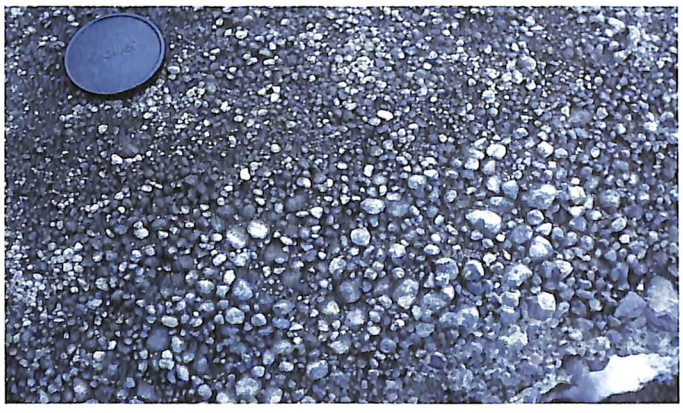

Fig. 3.14. Close view of well rounded ash-coated lapilli in relict tuff cone outcrop below the caldera wall west of Wensleydale Beacon. The lens cap is 6 cm in diameter.

Baily Head Formation: This formation encompasses several geographically isolated and usually small outcrops widely distributed on the island. It is distinguished from the lithologically very similar Pendulum Cove Formation by an absence of preserved primary landforms (cones and craters), the occurrence of several original eruptive centres outside of the caldera (Pendulum Cove Formation centres are exclusively found within the caldera; see below), and generally greater lithification. A type section is defined at Baily Head, a degraded tuff cone situated on the outer coast at its easternmost point, which also has the maximum thickness recorded for the formation (180 m; Fig. 3.13). The formation is formed of poorly to moderately lithified grey to khaki vitric lapillistones and lapilli tuffs in which armoured lapilli are common (Fig. 3.14). Stratification is well developed, mainly planar but including large cross beds, some of which are likely antidune bedforms (Fig. 3.15; Smellie, 2001*b*, fig. 10). Directional bomb-impact structures are common and, together with radial and cross bedding orientations, the locations of former vents can usually be determined. Although co-eruptive un-conformities (of minor time significance) are uncommon in the formation, they are spectacularly well exposed in an inner crater wall outcrop on the south side of Vapour Col (Fig. 3.6). They consist of numerous gullies, up to 2 m deep and 4 m wide, with V-shaped or flat bases and steep to overhanging sides, in places plastered by younger beds (Fig. 3.16 and 3.17).

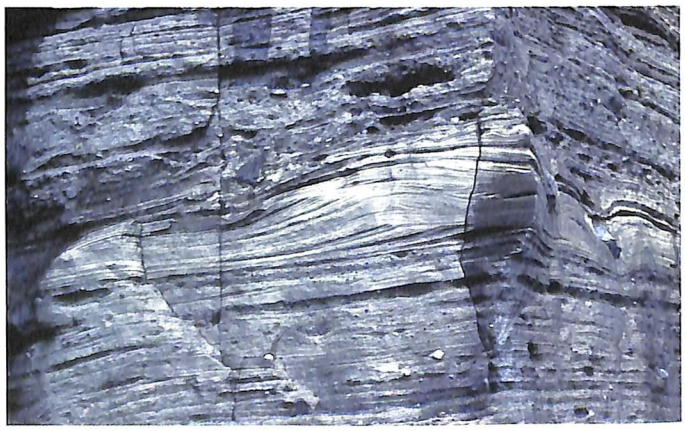

Fig. 3.15. Likely antidune bedforms in tuff cone deposits, east side of Vapour Col. Bomb impact structures seen at right. Section shown is about 5 m high.

The gullies flare upward to become shallow and saucer-shaped. Adhesion ripples are also present in an exhumed gully nearby (Smellie, 1989). An inner crater-wall slip plane is exposed on the east side of Vapour Col, but was misinterpreted by Martí and Baraldo (1990, fig. 5) as an important stratigraphical unconformity separating pre- and post-caldera deposits.

Fig. 3.16. Syn-eruptive unconformities in tuff cone deposits, south side of Vapour Col. The gullies have narrow V-shaped or flat bases and flare upward to shallow saucer-shaped upper parts. The hammer is 55 cm in length.

Pendulum Cove Formation: The Pendulum Cove Formation has a very wide outcrop. It corresponds largely to the area mapped by Hawkes (1961) as 'scree' because post-eruptive erosion of the outcrop, particularly wind-deflation, has resulted in a superficial stony 'armour' practically everywhere. A thin tephra cover is present on the outer flanks of the island whereas numerous substantial tuff cones occur in a narrow zone 1.5 km-wide around the shores of Port Foster within the caldera. Several maars are also included (e.g. Kroner Lake, Crater Lake and several facing Telefon Bay), and the formation tentatively contains a few unsampled submarine cones in Port Foster (British Antarctic Survey, 1987; Rey and others, 1992). The centres are relatively well preserved and apparently younger than glacial moraines on the island. Although only a single member is defined (White Ash Member), the volcanic cones are divided into several clusters, defined by a combination of geographical distribution, similar petrology and/or comparable degree of dissection (Smellie, 2001*b*; Fig. 3.18).

The tuff cone outcrops are up to 160 m thick, whereas maar tephra thicknesses and outcrops away from tuff cone centres are much less (typically << 10 m). There are two principal lithofacies. The tuff cones are formed mainly of poorly to unlithified grey stratified vitric lapillistones, lapilli tuffs and ashes. Beds are on a cm to dm scale, continuous over only a few tens of metres, and comprise alternating lapilli-rich and lapilli-poor layers and thin lapilli trails, with indistinct bed surfaces (Smellie, 2001*b*, fig. 13). Lapilli-dominated beds are relatively well sorted and grain supported. A few lapilli tuffs are vesiculated. The juvenile sideromelane lapilli and ash grains are incipiently to moderately vesicular (rarely highly vesicular), blocky and commonly show significant abrasion effects, sometimes enhanced by fine ash rims (armoured lapilli; *cf.* Fig. 3.14). Accessory lapilli are minor (< 1–2%). Bombs and blocks are common and most lack impact structures. Asymmetrical dune and antidune bedforms are present but are always minor. Other tuff cone lithofacies are uncommon and include:

1) monomict tuff breccia with weakly sintered bomb beds (within basal parts of some tuff cones; e.g. 1967 "New Island", Collins Point), well-sorted scoria; and thin dacite lavas; and

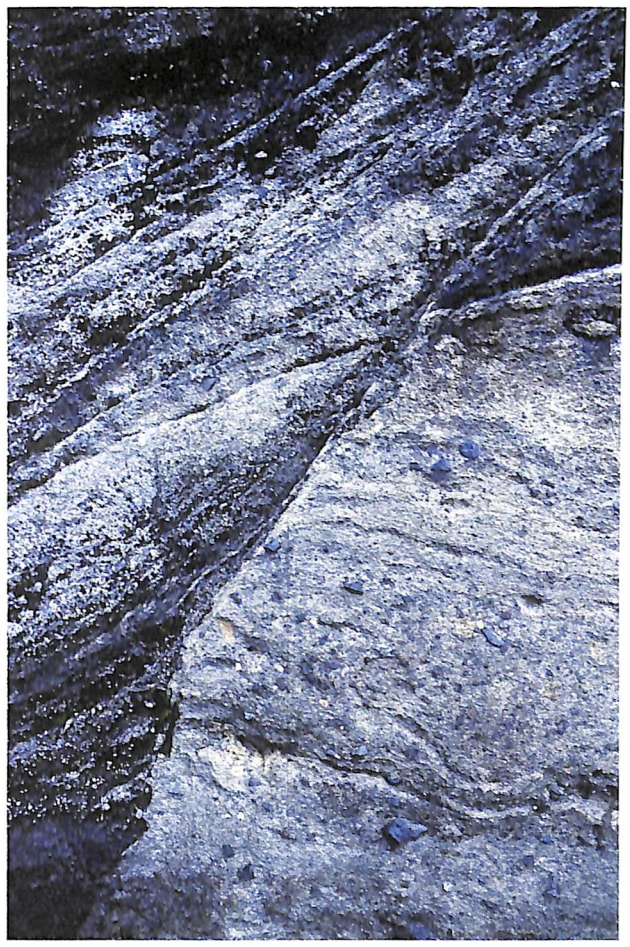

Fig. 3.17. Steep syn-eruptive erosional surface draped by thinly stratified younger tephra layers from same eruption, south side of Vapour Col. The view is about 50 cm in height.

2) topographically-confined, massive fine vitric lapilli tuff beds (on the ring plains surrounding tuff cones; Fig. 3.19).

By contrast, the maar centres are constructed of stratified lapilli tuffs with abundant accessory clasts (Fig. 3.20). They are poorly exposed generally but differ from the lapilli tuffs in the tuff cones in the more crudely defined planar stratification, thinner deposits, absence of dune or antidune bedforms, abundant fine to medium ash matrix and ash beds, and (in particular) a conspicuous abundance of lithic accessory clasts (10–40%). Rounded and armoured lapilli are also absent.

Intra-formational unconformities resemble those in the Baily Head Formation and are similarly uncommon. Faulting comprises two types: inner crater-wall slip planes, and steep cross-cutting fault planes sometimes associated with slumped strata.

The White Ash Member comprises two beds of normally-graded, stratified white dacite ash (Fig. 3.21). The beds are up to 1 m thick each and thin in a south-westerly direction. Tube-pumice lapilli are abundant in the coarser basal parts and occur as fine lapilli layers higher up. Angular blocks of pumice and obsidian, up to 2.5 m in length and probably related to the White Ash Member eruption, are strewn on the high south-west flanks of Cross

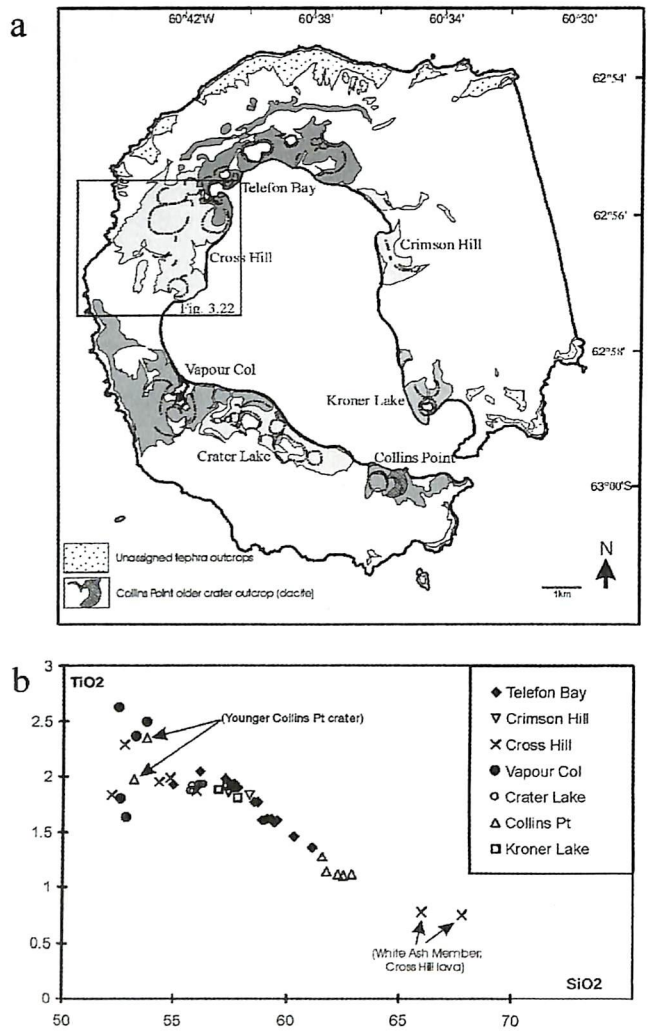

Fig. 3.18. a) Sketch map showing the geographical distribution of tuff cone clusters around Port Foster, and unassigned Pendulum Cove Formation tephra outcrops on the outer coast. b) Diagram of TiO_2 *versus* SiO_2, illustrating the geochemical coherence of most of the tuff cone clusters. This, together with field evidence within each cone cluster, strongly suggests co-eruption of most of the tuff cones within each group, and magma fed from several separate small high-level magma chambers distributed probably at shallow depths around the margins of Port Foster. The Telefon Bay cluster is unusual in showing a continuous wide range of compositions; all but one of the tuff cones was formed in 1967 or 1970, but the group includes a much older tuff cone at the site of the 1967 land centre which is known to be pre-19th century in age (Appendix 3). Clusters at Collins Point and Cross Hill are bimodal and their component tuff cones may be unrelated in time.

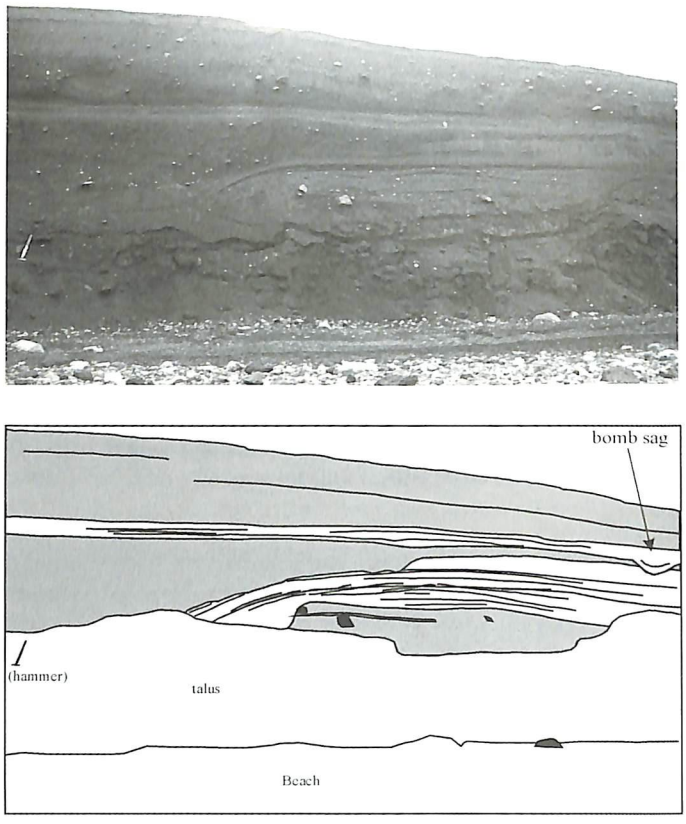

Fig. 3.19. Photograph (a) and sketch (b) of temporary outcrop of distal tuff cone lapilli and ash beds related to the Vapour Col cluster, about 1 km north-west of Crater Lake, showing alternation of planar stratified and massive beds. The massive beds (dark grey in (b)) are topographically confined and thin over topographic highs (to right in view). The hammer is 55 cm in length.

Hill (the presumed eruptive source) and an adjacent crater, and are associated with platy slabs of a lava similar in appearance to that exposed within the Cross Hill crater (Fig. 3.22).

Physical volcanology

Pre-caldera period: Nothing is known about the submarine, inaccessible part of Deception Island, which represents about 80% of the history of the volcano. By analogy with better-exposed subaqueous volcanoes, it is likely to consist mainly of pillow lava, hyaloclastite breccia and likely mass flow (slumped) deposits, capped by tephra from explosive hydrovolcanic eruptions during shoaling and subaerial emergence (e.g. Staudigel and Schmincke, 1984; Schmincke and Bednarz, 1990; Skilling, 1994; Smellie, 2000). On Deception Island, the oldest formation exposed (Fumarole Bay Formation) probably represents a period of shoaling and subaerial emergence of the volcano, which has not been documented before. The coarseness of most of the deposits (including very large bombs), combined with quaquaversal bedding orientations (at Cathedral Crags), suggests that the outcrops are vent-proximal and that several centres are represented (Cathedral Crags, eastern Mount Kirkwood ridge, southern Stonethrow Ridge and probably Goddard Hill). The Fumarole Bay Formation is dominated basally by hyaloclastite breccia associated with lava pillows with thick glassy margins and jigsaw-fit breccia, which are all features characteristic of a subaqueous eruptive environment. Higher deposits are pyroclastic, dominated initially by coarse vitric scoria with numerous bombs (scoria member), and then stratified lapilli tuffs.

A water-rich environment for the scoria member is suggested by the presence of abundant vitric pyroclasts, palagonite alteration, wide range of sideromelane vesicularity and dominant blocky clast shapes, although many clast shapes were clearly derived by impact-fragmentation of bombs. In many respects, the scoria

Fig. 3.20. Planar stratified lapilli ashes typical of the maar centres; unit forms a cap on the northernmost centre on the 1967 former new island, about 1.5 km north-north-east of Cross Hill. The deposits are characteristically rich in lithic accessory clasts. The hammer is 55 cm in length.

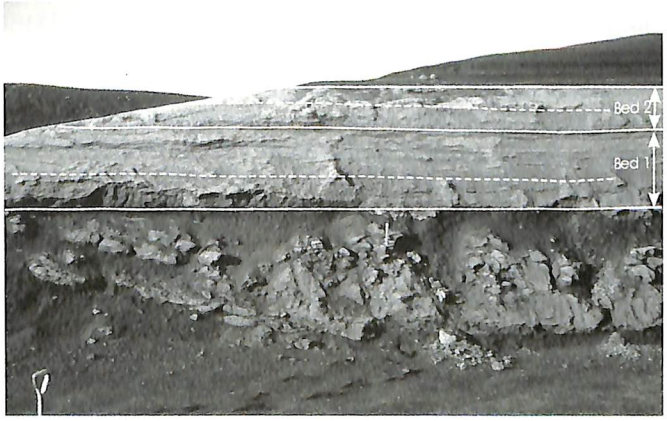

Fig. 3.21. Close view of twin beds of planar stratified dacite ash of the White Ash Member, in the valley between Cross Hill and Wensleydale Beacon. Each bed shows a prominent division into a lower unit rich in small pumice lapilli and an upper ash unit. The hammer (centre of photograph) is 35 cm long.

member is similar to Strombolian tephra (abundant scoria and bombs, lack of fine ash particles; *cf.* Baraldo and Rapalini, 2000), but the unusual combination of characteristics is hard to reconcile with a fully subaerial setting. This conflict was tentatively reconciled by Smellie

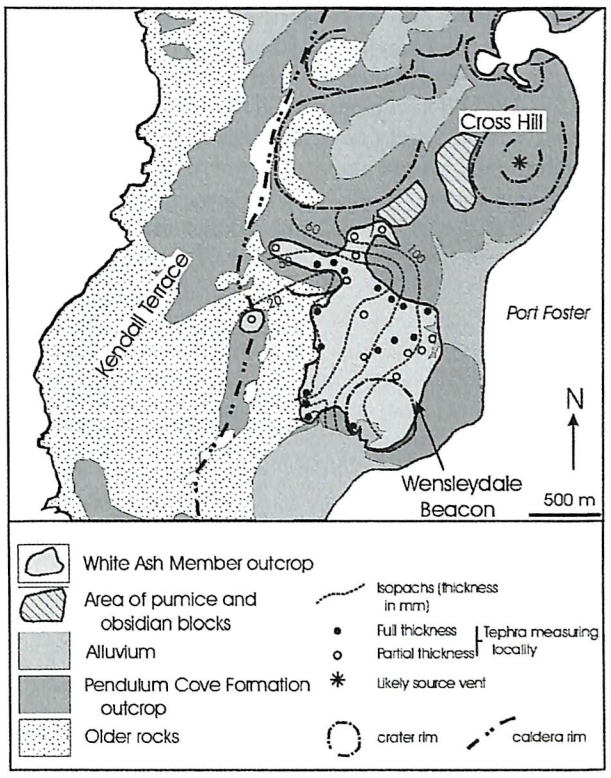

Fig. 3.22. Geological sketch map showing isopachs and outcrop of the White Ash Member (see Figure 3.18 for map location). Maximum tephra thicknesses suggest two outcrop lobes, diverging to the west-south-west and south-south-west relative to Cross Hill, the likely location of the source vent. Although separated in outcrop, the area of abundant dacite pumice and obsidian blocks is thought to form part of the same eruption.

(2001*b*), who noted a greater overall resemblance to deposits formed during subaqueous fire fountaining (*cf.* Mueller and White, 1992; McPhie and others, 1993). A high eruption velocity would cause clastic- (rather than effusive-) dominated behaviour of the magma, and thus fountaining (Smith and Batiza, 1989). Although the physical characteristics of subaqueous fire fountains are poorly understood, it is possible that the eruption columns may be encased partly in a protective steam shroud over the vent (or perhaps within the uppermost part of the vent), leading to production of fluidal bombs and scoria with "normal" Strombolian characteristics (Kokelaar, 1983; Kokelaar and Busby, 1992). Smith and Batiza (1989) and Mueller and White (1992) suggested that efficient mixing and heat exchange may occur between magma and water in subaqueous lava fountains, changing the clast fragmentation process from magmatic to hydrovolcanic. Rapid tephra fallout of the dense tephra columns would lead to transport down the volcano flanks, probably as gravity flows (Batiza and others, 1984; Smith and Batiza, 1989; Kokelaar and Busby, 1992; White, 2000). If water depths were shallow, as seems likely, mixing of still-hot pyroclasts with ambient water may also have caused additional fragmentation by some combination of contact-surface or bulk steam explosivity and/or cooling-contraction granulation (Kokelaar, 1986). It is unclear what effect steam explosivity may have on transport processes in a gravity flow, although it may have acted to induce or enhance any turbulence.

The density, flow characteristics and flow behaviour of these postulated gravity flows cannot be tightly constrained from available evidence. Momentum needed to carry the material would have been gained from the heights obtained from the lava fountains themselves (possibly extending a few hundred metres above the vent) and transport down steep cone flanks. However, the absence of fine ash matrix suggests that particle support was predominantly by grain collisions and dispersive pressures, and transport within grain flows (and, therefore, on steep slopes) seems likely. The clast shapes may also have been influenced by grain jostling and collisions. Absence of clast rounding is explained by the short transport distances involved, since the deposits are vent-proximal and likely preserved on the cone flanks. Run-out would possibly be enhanced by particle support derived from abundant steam whilst the flow was hot and in a high-concentration state. Finally, although a submarine setting is most likely, there is no intrinsic reason why the water may not be meltwater within subglacial vault(s), if eruptions took place beneath a substantial ice cover, although evidence for coeval ice has not been found.

The gradationally overlying stratified lapilli tuff member has characteristics of tephra formed during explosive hydrovolcanic eruptions. Eruption conditions must have been substantially different to those of the scoria member, and presence of interbeds with abundant accessory clasts indicates that, at times, explosions occurred at much deeper levels (sufficient to rework underlying bedrock). The change to a well-stratified, fine ash-rich lithofacies probably indicates a more pulsed and violent explosive style of eruption, possibly due to a change in the water:magma ratio as the vent became emergent. However, there is no clear difference from high-density gravity flows of tephra formed in some subaqueous eruptions (e.g. Mueller and White, 1992; Smellie and Hole, 1997; Smellie, 2001*a*), although the stratification is somewhat better developed and possibly more similar to subaerial hydrovolcanic sequences.

The succeeding Basaltic Shield Formation is radically different from the Fumarole Bay Formation. It represents a period of eruptions that were fully subaerial and characterised by lava effusion and relatively low energy Strombolian and Hawaiian pyroclastic eruptions. Together, they constructed a small lava-dominated shield edifice that had an original basal diameter of about 6–8 km (based on extrapolation of mapped outcrops). The location of the original vent(s) is unknown but they must have been within Port Foster, possibly east of Wensleydale Beacon. More than one vent is indicated by the distribution of volcaniclastic lithofacies in the succession: the lower clastic layers are distal airfall deposits of magmatic eruptions and sieve deposits of small streams, whereas coarse scoria and clastogenic lavas dominate upper parts of the sequence. The latter were formed from Hawaiian and Strombolian eruptions from a flank vent situated comparatively close to Stonethrow Ridge.

The widespread distribution of Outer Coast Tuff Formation outcrops indicates that it was formerly distributed thickly over the entire island and was draped unconformably on the Fumarole Bay and Basaltic Shield formations. A locus for the eruptive vent is impossible to define but, from crudely outward-radiating bedding dips, it lay presumably in Port Foster, and multiple vents are not precluded. The Outer Coast Tuff Formation was interpreted as airfall tephra by Baker and others (1975) but that interpretation conflicts with the massive, poorly-sorted fine ash-rich nature of most of the deposits. They probably formed mainly from pyroclastic flows, whereas the subordinate wavy-stratified beds resemble pyroclastic surge deposits (Smellie, 1988, 1989, 2001*b*; Martí and Baraldo, 1990). However, these are end members in a continuous spectrum of density currents (Druitt, 1998) and they are probably better described as deposits of pyroclastic currents that varied in their degree of inflation and fluidisation. The presence of airfall beds mentioned by Martí and Baraldo (1990) is unconfirmed, as is the presence of welded textures and inference of abundant pumice reported by those authors. The paucity of pumice and dominance of microvesicular basaltic sideromelane indicates that the deposits are not ignimbrites (*s.s.*) but could possibly be described as scoria flow deposits, although the proportion of ash matrix may be too high (*cf.* Cas and Wright, 1987; Druitt, 1998). The abundant fine ash matrix and sideromelane characterised by low vesicularities and blocky shapes suggest that fragmentation mechanisms were hydrovolcanic. The common occurrence of armoured lapilli also suggests that the eruption was wet.

Caldera-forming eruption and caldera collapse: Exposures in Stonethrow Ridge clearly show lapilli tuffs of the Outer Coast Tuff Formation draping the Basaltic Shield Formation. Elsewhere (e.g. south of Collins Point, Cathedral Crags), it overlies Fumarole Bay formation outcrops, and a similar relationship can reasonably be inferred by extrapolating patchy exposures at southern Stonethrow Ridge. Martí and Baraldo (1990) postulated that emplacement of the Outer Coast Tuff Formation (their Yellow Tuff Formation, lower member) was followed by eruptions in several tuff cones. Their interpretation implies that an unspecified period of time elapsed after the main eruption of their 'lower member' and before collapse of the caldera. Thus, a causal relationship between eruption and caldera formation was regarded as unlikely. Present-day seismicity also shows no geographical association with arcuate fractures and a presumed caldera ring fault, and the epicentres are aligned in a broad NE–SW-trending zone that crosses the entire island (Vila and others, 1992*b*). Circumferential faults and associated vent rings are rare features of calderas, and the unique presence of two annular rings of intra-caldera vents at Deception Island was highlighted by Walker (1984) in his review of caldera development.

In the model of Martí and Baraldo (1990; see also Martí and others, 1996), Port Foster is viewed as a depression created by passive collapse along orthogonal faults imposed by regional tectonics. Its formation was thought to be unrelated to an eruption. However, outcrops in the caldera wall suggest that the Outer Coast Tuff Formation is the youngest formation present that is cut by the caldera fault, indicating that it represents products of the final eruption to have occurred prior to (or possibly during) formation of the caldera. Conversely, the tuff cone outcrops included in the upper member of their Yellow Tuff Formation by Martí and Baraldo (1990) drape the caldera and are of early post-caldera age (Smellie, 2001*b*).

It is thus suggested that the association in timing, in combination with the calculated large erupted volume (see below), strongly suggest a genetic relationship between the eruption of the Outer Coast Tuff Formation and formation of the Deception Island caldera. Several authors have postulated an important influence of regional tectonics on faults and fractures on the island (Fig. 3.23), although the positions of several structures vary between publications (*cf.* Smellie, 1988, 1989; Rey and others, 1995; Martí and others, 1996). Several sections of the caldera rim fault are strikingly linear and probably reflect that tectonic influence. However, it is likely that caldera collapse following a large-scale eruption would have exploited any pre-existing faults, and it is suggested that the caldera is fundamentally volcano-tectonic and not simply a passive response to regional tectonics.

As noted above, the caldera-forming eruption was hydrovolcanic and created a large volume of tephra emplaced by a variety of pyroclastic density currents. On the basis of alteration mineralogy, Martí and Baraldo (1990) postulated that the erupting magma may have interacted with seawater, resulting in relatively low, non-convecting columns. This interpretation is consistent with the absence of a Plinian fall layer at the base of the formation, and with the abundance of accessory lithic fragments in the eruption mixture, which would both load and cool the jet, tending to favour its collapse (Legros and others, 2000). Because of the large volume of erupted magma (below), a large amount of water is also implicated, which is only likely to have been seawater.

Juvenile clasts in the deposits are extremely variable in composition and they follow two fractionation trends (see below). In this, the Outer Coast Tuff Formation is the most compositionally distinctive eruptive unit on the island. The presence of two compositional trends suggests that two discrete magmas interacted, causing convective destabilisation of the magma chamber feeding Deception Island eruptions. The interaction may have acted as an eruption trigger by causing explosive devolatilisation (*cf.* Smellie and others, 1992; Folch and Martí, 1998; and see below). Simple mass balance calculations, which assume that the volume of erupted magma corresponds approximately to the volume of the present caldera, suggest that the caldera-forming eruption ejected about 30 km^3 of magma (Smellie, 2001*b*). If a thickness of about 70 m was maintained throughout the resulting deposit (as it is on the island), that would be sufficient to extend the island by at least 6 km in all directions beyond its present margins.

Post-caldera period: In early post-caldera times, areally extensive eruptions took place on the outer island slopes (especially Kendall Terrace and Mount Kirkwood) and along the caldera rim, forming the Kendall Terrace Member of the Stonethrow Ridge Formation. Eruptions were pyroclastic (Hawaiian and Strombolian) and effusive, constructing numerous small cinder cones and conspicuous lava delta platforms. The latter are particularly prominent on the outer coast between Punta Descubierta and South East Point and presumably overlie thick hyaloclastite breccia foreset beds (*cf.* Jones and Nelson, 1970). Although the style of eruptions and resulting lithologies are closely similar to those forming the pre-caldera Basaltic Shield Formation, they did not construct a substantive shield

Fig. 3.23. View looking south from Macaroni Point to Baily Head, showing the remarkably linear coastline backed by ice cliffs. Although invariably interpreted as a fault-controlled feature, its origin is enigmatic: the coastline lacks seismic activity and it is backed by glaciers moving at different speeds, which should deform and rapidly distort the coastline with time. Moreover, no major faults cut the two prominent rock headlands at its north and south terminations.

structure. By contrast, the unusual heterogeneous polymict breccia on the north coast, west of Macaroni Point, was probably formed during collapse and avalanching of scoria and lava along a fault plane, or (perhaps more likely) as a gravity slide down a slump scar. The abundant evidence for chilling and brecciation of cogenetic lava indicates that the deposit was wet, possibly by emplacement into seawater (when sea level was higher than today?).

Also in the early post-caldera period, tuff cone activity was widespread on the volcano, from numerous centres distributed both within and outside of the caldera (Baily Head Formation). The scarcity of lithic fragments in the tephras suggests that the associated explosivity probably took place very near the surface or above the vent (*cf.* Batiza and others, 1984), when the magma interacted with abundant water close to or at the ground surface. The abundance of armoured lapilli, tephra adhering to steep surfaces, and scarce adhesion ripples (Smellie, 1989) are also consistent with cool wet surges, containing condensed water droplets. All of the mapped outcrops occur close to or at present sea level, and it seems likely that the cones were constructed in shallow seawater. As some of those

occur around the shores of Port Foster, it is likely that Port Foster was flooded by the sea soon after caldera collapse. For the caldera to be flooded implies that large-scale sector collapse of the pre-caldera edifice, sufficient for seaways to be created into the island interior, probably occurred during or soon after the caldera-forming event. Seismic evidence for large-scale flank collapse exists south-east of Neptunes Bellows (Acosta and others, 1992), and the sub-ice morphology east of Mount Pond is also suggestive of a major slope collapse (Smellie, 2001*b*). Although the age(s) of those two collapse events is uncertain, the slope scar east of Mount Pond is draped by early post-caldera tephras, indicating an early post-caldera or greater age.

Hydroclastic eruptions, in tuff cones and maars, and effusive and magmatic pyroclastic activity, from cinder cones along fissures, extended the volcanic activity to historical times, as recently as 1970, in the late post-caldera Pendulum Cove Formation and Mount Kirkwood Member of the Stonethrow Ridge Formation. The younger age of those eruptions, compared with early post-caldera activity, is indicated by the generally much better-preserved primary landforms associated with the centres, and a younger age than glacial moraines on the island. By contrast with the earlier activity, the late post-caldera hydroclastic centres are all situated within the caldera, mainly around the shores of Port Foster, but also including unsampled submarine pyroclastic cones detected within Port Foster itself (British Antarctic Survey, 1987; Rey and others, 1992). The contrast between hydroclastic activity at lower elevations, and essentially dry magmatic activity at higher elevations, is a reflection of the local hydrology (Baker and others, 1975). Furthermore, the differences in lithofacies characteristics between the tuff cones and maars probably reflect magmatic interaction with shallow seawater (tuff cones) and groundwater (maars). The maars also contain only thin deposits, implying that eruptions were very short-lived compared to the tuff cones. Uncommon scoria beds and lavas in the tuff cones (e.g. at Cross Hill and Collins Point) implies that, at times, the vents dried out sufficiently to permit drier, magmatic eruptions and rare effusion.

The characteristics of the dominant deposits suggest deposition from suspension and by traction sedimentation from turbulent pyroclastic currents ('surges'). The currents fluctuated in velocity and particle concentration, with more rapid suspension fallout forming the thicker layers, and slower fallout and greater grain segregation yielding thinner stratification characterised by lapilli trails and lenses. Relatively cool, wet currents, with condensed water, is suggested by ash rims to fragments, scarce vesiculated beds, adhesion ripples and beds smearing steep surfaces. The common clast rounding is attributed to repeated entrainment and collision of particles in fluctuating eruption columns until 'escape' and deposition on the cone flanks and ring plain. Beds of tuff breccia in tuff cones, with weakly sintered bomb beds (e.g. basal part of the 1967 island centre), are interpreted as deposits of high-concentration particle dispersions derived from collapsing, dense, low-energy eruption columns rich in condensed water. The topographically confined massive beds found only on the tuff cone ring plains are deposits of highly-concentrated pyroclastic flows. An alternation, in some places, between massive and stratified lapilli tuffs (e.g. stream bank exposures in the valley between Cross Hill and Wensleydale Beacon; also Fig. 3.19) may be cogenetic. It suggests rapid particle fallout from suspension in the 'body' of a high-density turbulent current to yield the massive beds (a kind of density underflow). The overlying stratified units would then represent deposition from a turbulent low-concentration 'tail' dominated by traction sedimentation.

Interpretation of the White Ash Member is uncertain. The abundant pumice suggests magmatic explosivity, but the fine stratification, abundant ash and shape of the isopachs (suggesting two diverging lobes; Fig. 3.22) are more consistent with pyroclastic currents and hydroclastic eruptions. However, the isopachs show no evidence for confinement by the pre-existing topography, which they should if deposition occurred from pyroclastic currents. The eruptive source for the White Ash Member was probably the Cross Hill crater.

Caldera resurgence: Eruptions and signs of seafloor inflation within Port Foster are evidence for a restless caldera (Cooper and others, 1998). Baker and others (1975) observed that, after the 1969 eruption from fissures crossing the Mount Pond glacier, bridges of unbroken ice were preserved across two of the fissures. The observation suggested that the eruptive fissures were not associated with caldera fault displacements. Empirically, this implies that magmatic and lithostatic stresses are finely balanced. Between 1967 and 1970, excess magmatic pressures were released in several small-volume eruptions around the caldera margins. Temporary ground inflation, increased tremor activity and raised water temperatures were also recorded during December 1991–January 1992 in the Vapour Col area and were interpreted as an indication of resurgent activity (Ortiz Ramis and others, 1992). However, an eruption did not occur and the area rapidly returned to normal background activity.

Seismic refraction studies of the seafloor within Port Foster have provided a relatively clear picture of the shallow structure (< 300 m below sea floor) within the central part of the caldera (Fig. 3.24 and Chapter 5; Kowalewski and others, 1990; Rey and others, 1990). Whilst there are discrepancies in details of the seismic interpretations (*cf.* Rey and others, 1990, 1995, 1997), the surface of the seismically isotropic basal unit (A) of presumed pre-caldera sequences (probably pyroclastic) appears to be a tilted and slab-like feature, dipping gently down to the south-west and overlain by two major post-caldera sediment units (B, C). Each of the sediment units, B and C, is subdivided further into several sub-units separated by minor unconformities. The lower of these units (B) forms a large-scale monoclinal antiform that verges to the north-east, and which may be associated with a WNW–ESE-striking normal fault. The fault, which may be slightly arcuate (concave to the north-east), is interpreted as a fundamental structure involved in the development of the caldera. Bedding within units B and C dips to the south-west at angles which diminish progressively upward in the younger beds, onlapping older sub-units in a north-easterly direction. They also contain numerous small-displacement normal faults, mainly orientated NE–SW and NW–SE reflecting a regional tectonic influence of the Bransfield Strait marginal basin

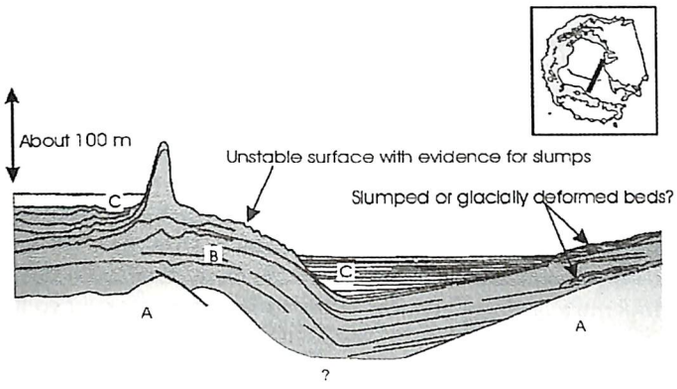

Fig. 3.24. Simplified schematic composite section across Port Foster, showing the structure of the caldera basin sequences (modified after Kowalewski and others, 1990, and Rey and others, 1990). Seismic unit A, presumed to be pre-caldera lithofacies, is overstepped by post-caldera stratified unit B, itself deformed by a prominent monoclinal structure downstepping to the north-east. The youngest post-caldera stratified unit C is also overstepped on to unit B. The overstepping relationships suggest repeated differential post-caldera uplift episodes affecting the north-east side of the caldera basin, as was postulated by Cooper and others (1998).

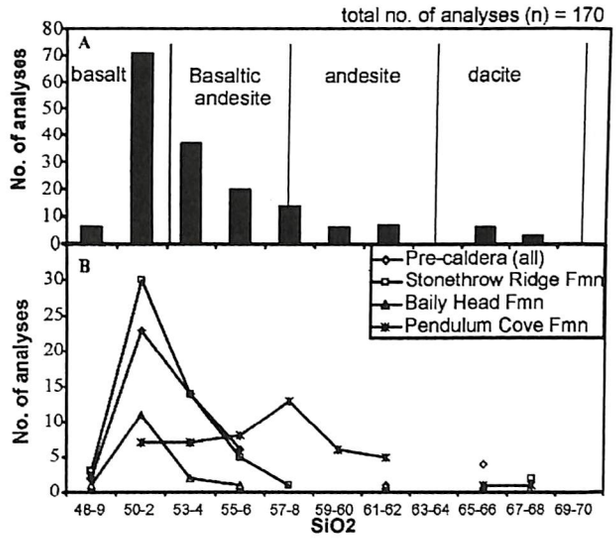

Fig. 3.25. Diagrams illustrating (A) the total range of compositions in magmas on Deception Island, and (B) compositional ranges broken down by stratigraphy. Basaltic magma was erupted abundantly during all periods represented, but the late post-caldera tuff cones of the Pendulum Cove Formation show a shift to predominantly more evolved compositions compared with the other stratigraphical groups.

(Martí and others, 1996). Several of those faults are associated with hydrothermal mounds that were formed at different times throughout the history of the Port Foster basin (Rey and others, 1997).

Normal faulting affects the monocline. Moreover, north-eastern parts of older sediment units (B and possibly lower parts of C) crop out at higher elevations than younger sediment units to the south-west. Together, these observations suggest either that subsidence of the basin along the monocline occurred at greater rates than local sedimentation, or that subsidence in the south-western part of the basin was accompanied by uplift in the north-east. Support for the latter is provided by a study of the evolving bathymetry of Port Foster. That study identified an area on the north-eastern side of the basin which has undergone uplift rates as high as 0.3–0.5 $m.a^{-1}$ over the past 50 years, and which is coincident with a zone of relatively high heat-flow underlain by a high-level magmatic intrusion (Cooper and others, 1998). Thus, the pre-caldera sequence beneath Port Foster may be regarded as a giant 'slab' which, after the initial catastrophic collapse, rotated about an ill-defined NW–SE-orientated axis, subsiding in the south-west and rising in the north-east. The presence of planar unconformities separating sequence C sub-units suggests that the rotation of the caldera roof was not continual but occurred in sequential *steps* in the overall progressive development of the caldera. The recent rapid uplift of part of the caldera, associated geographically with a hot magmatic intrusion, suggests that resurgence of the caldera is currently taking place.

Geochemistry

Although several papers discuss the geochemistry of Deception Island, most are based on analyses of very few samples, and often include major oxides only (Gourdon, 1914; Barth and Holmsen, 1939; Tyrrell, 1945; Hawkes, 1961; González-Ferrán and Katsui, 1970; Baker and others, 1975; Weaver and others, 1979; Smellie, 1990; Keller and others, 1992; Peccerillo and others, 1991; Smellie and others, 1992; de Rosa and others, 1995). This summary incorporates the principal results of those published investigations, but is supplemented by a large unpublished data set of about 175 analysed samples from Deception Island compiled by the author; representative analyses from that data set are given in Appendix 4. However, there has been no comprehensive study of the geochemistry in relation to the very detailed stratigraphy that is now known and fuller examination of the petrology and magmagenesis on the island awaits a future investigation.

Major and trace elements: In contrast to other Quaternary volcanoes in Bransfield Strait, which are all basaltic to basaltic andesitic except for a single small submarine centre with extrusive rhyolite (Keller and others, 1992, 2002), Deception Island contains a wide range of magmatic compositions extending from basalt to dacite (Fig. 3.25). Reports of rhyodacite on the island should probably be discounted: the rhyodacite sample analysed by Baker and others (1975) and re-analysed by Weaver and others (1979) was collected loose on a beach within Port Foster (personal communication from John Roobol) and it bears a greater compositional resemblance to pumice erupted at Protector Shoal, South Sandwich Islands (*cf.* Gass and others, 1963; Sutherland, 1965; Baker 1978, 1990; Weaver and others, 1979). In particular, it contains a much lower Zr content than the most evolved dacites collected *in situ* on the island (92–178 ppm and > 600 ppm, respectively). Floating Protector Shoal pumice was dispersed by marine currents around Antarctica following its eruption in 1962 (Gass and others, 1963) and specimens can still be collected from

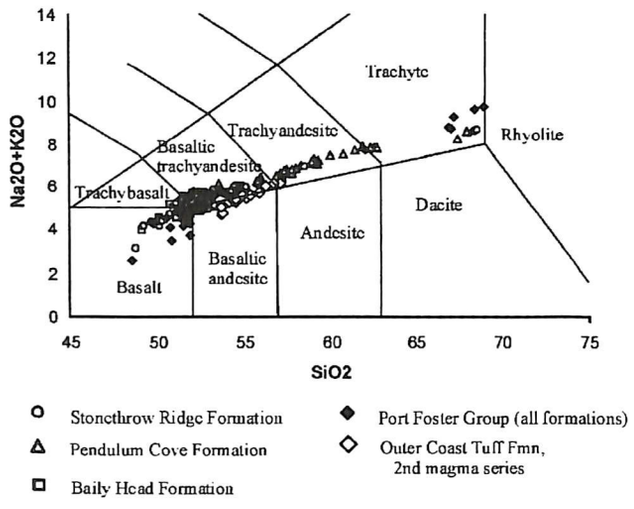

Fig. 3.26. Classification of magma types found on Deception Island, based on the TAS diagram of LeBas and others (1986). Note the presence of a small silica gap and an absence of rhyolite compositions.

many beaches in the South Shetland Islands. On a TAS (total alkalis–silica) classification diagram, the Deception Island lavas plot on a continuous trend that crosses the divide between alkaline and subalkaline suites (Fig. 3.26). Using the root names for each field (Le Bas and others, 1986), they correspond principally to basalts (mainly subalkali basalts, rare alkali basalts), basaltic trachyandesites, trachyandesites and trachytes. Most of those names have clear alkaline affinities, yet the Deception compositional series also has close affinities to tholeiites (below) and most authors have referred to the lavas as basalts, basaltic andesites, andesites and dacites with no genetic connotations, a practice that is followed here.

Lavas on Deception Island are aphyric to sparsely porphyritic (small phenocrysts (< 1 mm), typically only a few per cent by volume), but are rarely highly porphyritic, with 25–35% phenocrysts in some basalts and basaltic andesites. Although there are no detailed mineral–chemical studies, petrographical investigations, supplemented by electron microprobe analyses of

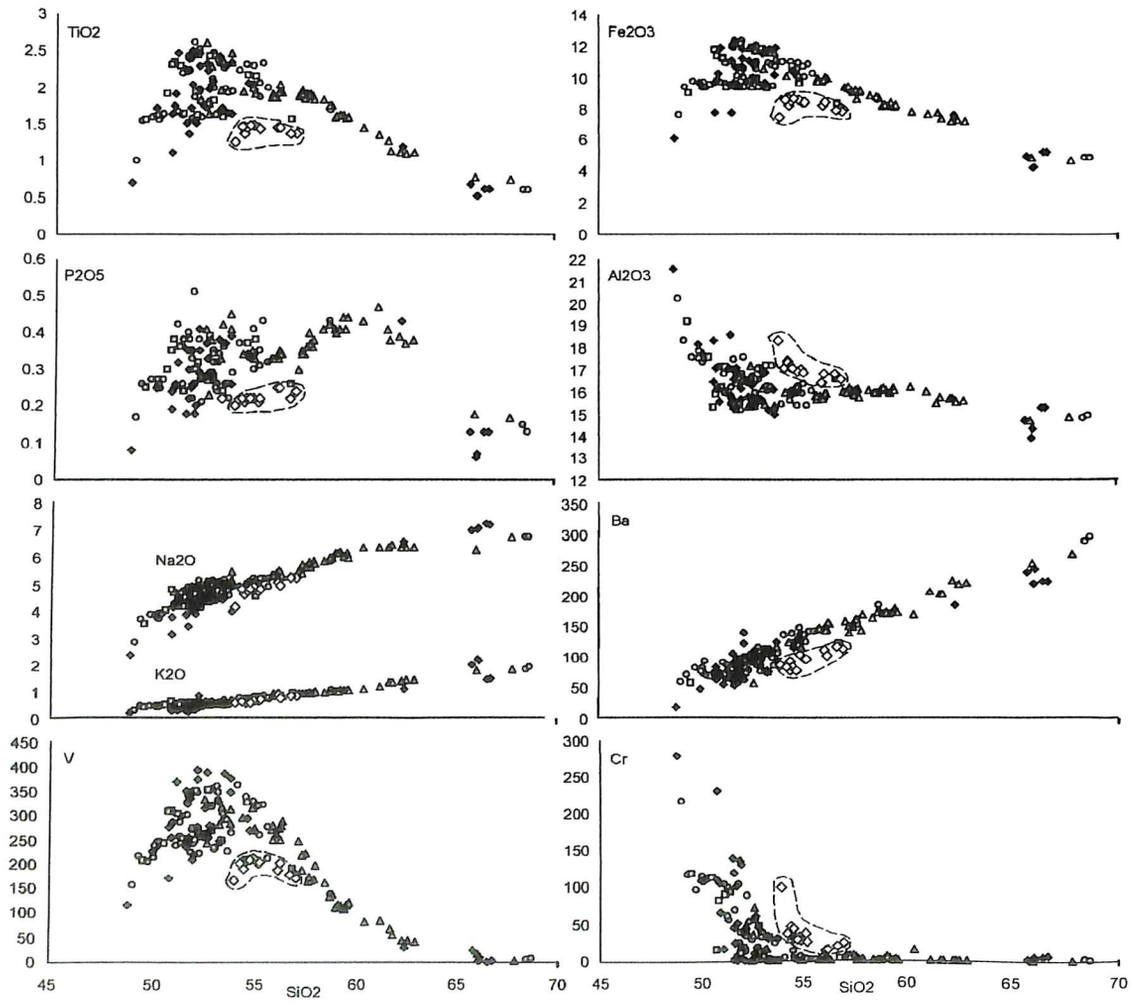

Fig. 3.27. Harker diagrams for selected major and trace elements. Note the unusual wide scatter of compositions among the basalt and basaltic andesite magmas (not caused by phenocrysts in these predominantly phenocryst-poor rocks), and the presence of a compositionally distinctive magma (open diamond symbols) associated with the eruption of the Outer Coast Tuff Formation. Symbols as in Fig. 3.26.

Table 3.2. Summary petrography of Deception Island magmas (based principally on McReath (in Baker and others, 1975), Weaver and others (1979) and unpublished observations of JL Smellie)

Composition	*Mineralogy*	*Textural features*
Basalt	Phenocrysts of calcic plagioclase, forsteritic olivine, pyroxene (augite) Groundmass calcic–intermediate plagioclase, olivine, pyroxene (augite pigeonite), opaque oxide; rare K-feldspar	Mainly intergranular or intersertal Mainly 10-20% phenocrysts, rarely up to 35%
Basaltic andesite/ andesite	Phenocrysts of intermediate plagioclase, pyroxene (augite, hypersthene), opaque oxide (magnetite, ilmenite, Ti-magnetite in andesites only); rare fayalitic olivine Groundmass intermediate plagioclase, augite, opaque oxide	Intergranular, intersertal; mainly pilotaxitic in the andesites Usually few % phenocrysts, rarely up to 35% in basaltic andesites
Dacite	Phenocrysts of sodic plagioclase, pyroxene (augite, hypersthene), fayalitic olivine, opaque oxide (ilmenite with Ti-magnetite lamellae); rare anorthoclase, apatite Groundmass of sodic plagioclase, K-feldspar, opaque oxide, pyroxene	Mainly pilotaxitic or hyalopilitic

phenocryst phases, indicate that there are clear variations in the mineralogy with magmatic host composition. They are summarized in Table 3.2. Important mineralogical characteristics include: groundmass olivine, pigeonite and possible alkali feldspar and biotite in the basalts; groundmass and rare phenocrystic hypersthene in the andesites and dacites, along with phenocrysts of fayalitic olivine, opaque oxide, anorthoclase and rare apatite; plagioclase and clinopyroxene are present as phenocryst and groundmass phases throughout the series, but evolve continuously in composition from An_{85} to An_{15} (bytownite–oligoclase) and $Ca_{43}Mg_{46}Fe_{11}$ to $Ca_{39}Mg_{36}Fe_{25}$ (augite–ferroaugite), respectively (Weaver and others, 1979). There are also compositionally related textural differences: the andesites and dacites usually show prominent felsic pilotaxitic or hyalopilitic textures, whereas intersertal and intergranular textures are characteristic of the less evolved lavas. The mineralogy is unusual. Groundmass olivine and alkali feldspar are characteristic of alkali basalts, and anorthoclase is a typical phase in trachytes. Conversely, tholeiitic series contain groundmass pigeonite, and McReath (in Baker and others, 1975) observed that the progression of ferromagnesian phases (pigeonite in the basalts, replacement of olivine by orthopyroxene in the andesites/dacites, and fayalitic olivine in the dacites) is a tholeiitic fractionation series. Similar mineralogies have been observed in basalts and basaltic andesites in magmatic series on Isla Tortuga (Gulf of California) and Santorini (Aegean Sea; Batiza, 1984; Huijsmans, 1985).

In normative characteristics, almost all the analysed rocks are saturated or oversaturated, with a low-pressure differentiation trend from olivine tholeiites towards Q-normative compositions. However, a small proportion of basalt analyses are *ne*-normative (Weaver and others, 1979), and it may be those samples that contain the groundmass olivine recorded (*cf.* Macdonald and Katsura, 1964). The high content of total alkalis is principally an effect of unusually high Na_2O contents, which are generally > 4% (Fig. 3.27). However, K_2O contents are relatively low, comparable with many island arc tholeiite and calc-alkaline series, and the series is sub-alkaline in K_2O–SiO_2 characteristics. All of the Deception lavas have high Na/K ratios and they are matched only by those in mid-ocean ridge basalts (MORB). The basalts show strong enrichments in Fe_2O_3T, TiO_2, MnO, P_2O_5, V and $Fe_2O_3T/(Fe_2O_3T+MgO)$ with fractionation, which are characteristic of tholeiitic magmas (Fig. 3.27). In general, K, Rb and Ba are at the lower ends of the ranges observed in calc-alkaline suites, overlapping with those in island arc tholeiites (IAT) and even MORB, whilst TiO_2 and Y are higher than in most IAT but are close to those of back-arc basin (BAB) and ocean-island basalts (*cf.* Knittel and Oles, 1995). Significant enrichment in Ba and Sr, compared with most ridge basalts, has been observed by other authors (e.g. Peccerrillo and others, 1991) and suggests affinities to plate margin basalts but, in general, most incompatible elements are enriched in Deception basalts relative to N-MORB. This is illustrated on an N-MORB-normalized multi-element diagram, in which the spidergrams have the humped profiles similar to oceanic island tholeiites (Fig. 3.28). Relative depletion of Nb and Ta (a feature of arc magmas), whilst present, is not marked. Chondrite-normalized REE ratios are slightly fractionated (La_N/Yb_N ratios 2.2–2.9 in the basalts) and resemble those in some BABB, IAT and ocean island tholeiites (e.g. Saunders and others, 1979; Knittel and Oles, 1995; Fig. 3.28). Thus, the Deception Island magmas do not easily "pigeon-hole" in any simple classification of magma types (Smellie, 1990). They are probably best regarded as a tholeiitic series with quasi-alkaline characteristics caused mainly by enhanced Na_2O contents.

McReath (in Baker and others, 1975) suggested, on the basis of a comparatively small sample set, that there may be two compositionally distinctive magma series on Deception Island, identified by high-alumina and high-iron trends, although samples with intermediate compositions were also present. They also highlighted a significant silica gap affecting andesites and dacites (61–66% SiO_2). With the much larger data set now available, a silica gap is still present although slightly smaller than formerly indicated (63–66% SiO_2; Fig. 3.26). In addition, the distinction into two compositional series is blurred by more abundant samples with intermediate compositions, and the significance of the original distinction is unclear. Indeed, an unusually broad scatter of compositions is a feature of the basaltic and basaltic andesite rocks on Deception Island.

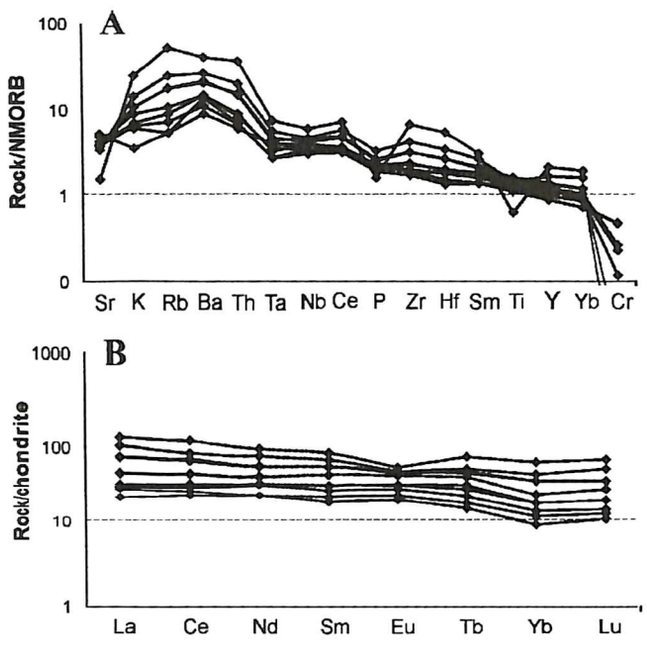

Fig. 3.28. N-MORB- and chondrite-normalized multi-element diagrams for basalts—dacites from Deception Island (all stratigraphical groups; normalising values after Sun and McDonough, 1989). The patterns resemble those of some BABB, IAT and ocean island tholeiites; a subduction influence is suggested by the presence of a small negative Nb—Ta 'anomaly'.

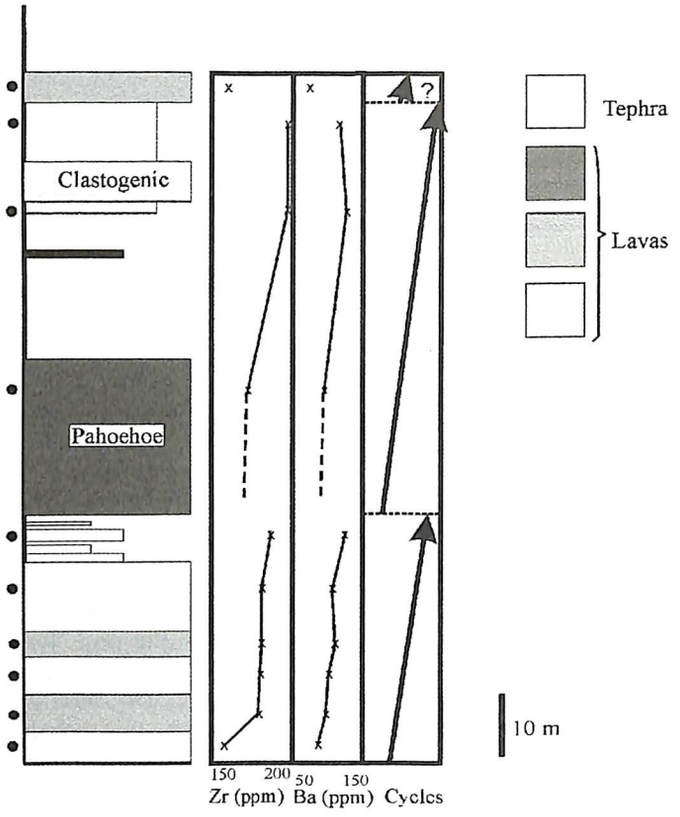

Fig. 3.29. Sketch section through the Basaltic Shield Formation at northern Stonethrow Ridge. Zr and Ba values for analysed samples are plotted in their correct stratigraphical position. Both of these (and other) indices show possible cyclical variations up-section. Note that the section depicted is composite because of incomplete exposure. It assumes that the lava outcrops are in their original relative positions and not displaced by caldera-related faults.

Basalts or basaltic andesites form 80% of the analysed samples. This reflects the compositional make-up of all the stratigraphical formations except the late post-caldera Pendulum Cove Formation, which contains a much higher proportion of andesites and dacites (*c.* 45%; mainly andesites; Figs 3.25 and 3.26). There is no serial trend to more evolved compositions with time and it is evident that basaltic and basaltic andesite magmas were available at all stages of evolution of the Deception volcano. This is well illustrated by a sequence of lavas of the Basaltic Shield Formation at northern Stonethrow Ridge, which shows cyclical compositional variations. Moving up-sequence, the Stonethrow Ridge lavas show at least two basic to evolved cycles, and a reversal to less evolved lava at the top of the section may indicate the base of a third cycle (Fig. 3.29). Even small pyroclastic eruptions, such as those which occurred between 1967 and 1970, show a surprisingly wide range of compositions (e.g. Baker and others, 1975). To achieve the wide compositional range in the relatively small volumes characteristic of Deception Island eruptions suggests:

1) the existence of multiple small compositionally stratified magma chambers feeding eruptions, and
2) a larger melt accumulation zone at depth replenishing the small chambers at much shallower crustal levels.

By contrast, some clusters of tuff cones extending laterally a few kilometres erupted compositionally very restricted magma (e.g. the Crater Lake cone cluster; Fig. 3.18). Dacite was erupted only rarely on the island. It forms lavas at Ronald Hill, Collins Point and the un-named headland 2 km west of Collins Point, and was extruded from a N–S-trending dyke within the crater at Cross Hill. White dacite pumice and obsidian also occur within the Outer Coast Tuff Formation (in caldera wall outcrops west of Cross Hill and on top of Cathedral Crags), and form the lithologically distinctive late post-caldera White Ash Member south-west of Cross Hill. Evidence for magma mingling is present in many of the dacite pumices.

Harker diagrams for major elements show continuous variations of increasing K_2O and Na_2O, and decreasing MgO and CaO. TiO_2, Fe_2O_3T and MnO initially increase, to about 53–54% SiO_2, and decrease steadily thereafter (Fig. 3.27). P_2O_5 shows a similar pattern to Fe-Ti-Mn oxides, but peak values occur at higher SiO_2 contents (59–60%). Among the trace elements, Rb, Ba, Th, REE, Y, Zr, Nb, Hf, Ta and probably Cs (Cs data are few) show a continuous increase, whilst Sr, Cr, Ni, Sc and Co decrease. V shows a similar pattern of increasing then decreasing contents mirroring those of Fe-Ti-Mn oxides. Among the REE, slight negative Eu anomalies are developed in the silicic andesites and dacites on chondrite-normalized diagrams (Fig. 3.28). The element variations are consistent with low-pressure crystal fractionation involving the observed phenocryst phases (i.e. olivine-calcic plagioclase-clinopyroxene (basalts)—plagioclase-clinopyroxene (intermediate compositions)—sodic plagioclase-

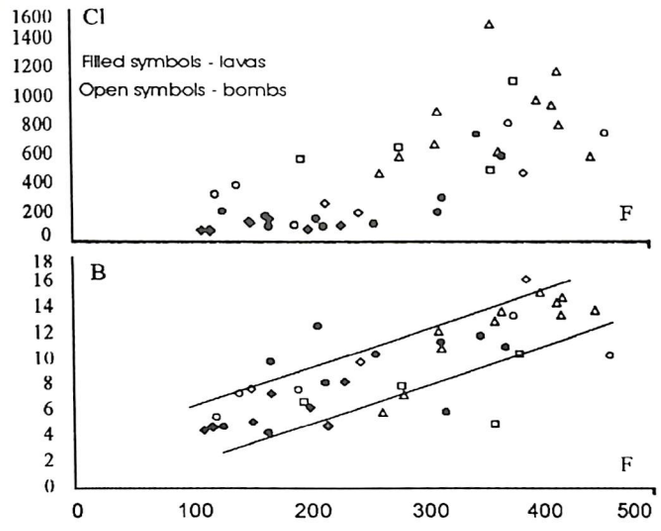

Fig. 3.30. Diagrams showing Cl and B abundances plotted against F. Each of the three elements is incompatible but the wide scatter of values suggest that substantial modification of the original magmatic abundances has occurred. The scatter is particularly broad for Cl (see text for further explanation).

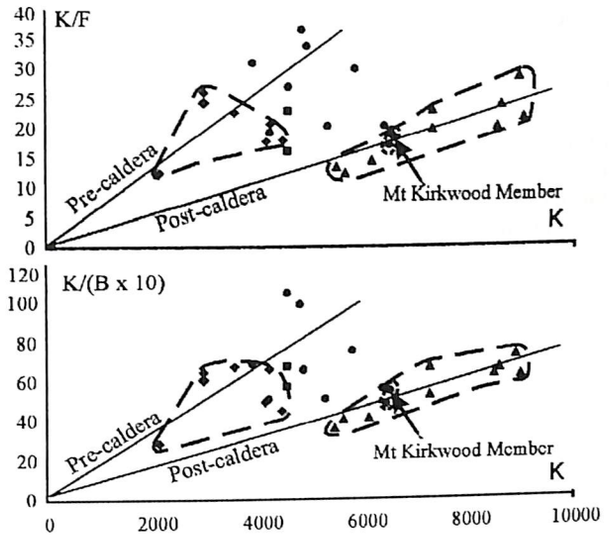

Fig. 3.31. Diagrams showing K/F and K/(Bx10) plotted *versus* K. Two diverging trend of increasing K/F and K/B ratios with increasing fractionation (increasing K) are clearly present in both diagrams. The trends appear to reflect the volcanic stratigraphy, with the change from one trend to the other occurring in post-caldera times, possibly related to a major magma mingling event that may have triggered the paroxysmal eruption that created the Outer Coast Tuff Formation and led to caldera collapse. See text for further explanation; symbols as in Fig. 3.26.

clinopyroxene- Fe olivine-magnetite [-anorthoclase-orthopyroxene-apatite] (andesites–dacites)).

There is new evidence that the eruption of the Outer Coast Tuff Formation involved the interaction of two magma series. This is indicated by XRF analyses of juvenile bombs and unpublished microprobe analyses of siderometane lapilli (analyses of the author), which show a clear separation into two series based on TiO_2, Fe_2O_3, MnO, Al_2O_3 and P_2O_5 relationships, and Cr, Ni, V and Ba variations (Fig. 3.27). The outer Coast Tuff Formation is the only stratigraphical unit on the island to show this feature, which indicates mingling of two magmas. There is also speculative evidence from the volatile element geochemistry for a major event involving mixing of two magmas at the end of the pre-caldera period (below).

Numerous publications include Sr isotope data (Halpern, 1970; Faure and others, 1971; Baker and others, 1975; Keller and others, 1992; Peccerillo and others, 1991), but there are few published data for Nd and Pb isotopes (Keller and others, 1992). Sr ratios range from 0.70318 to 0.70361, and Nd from 0.51291 to 0.51308 (ranges from Smellie and I.L. Millar, unpublished data; Appendix 4). Despite the comparatively wide range for a single volcano, there are no obvious variations with time. Sr and Pb isotope ratios of Deception Island are similar to other volcanoes in Bransfield Strait, but Sr isotope ratios are significantly higher (Keller and others, 1992, 2002). The range of Sr and Nd ratios is relatively wide but falls within the mantle array. There is no evidence for significant interaction with crust (Keller and others, 1992; Peccerillo and others, 1991). However, this need not imply that crustal interaction did not occur. Isotope ratios in South Shetland Islands volcanic rocks are generally similar to intra-oceanic arcs (lacking crustal assimilation; *cf.* Smellie and others, 1984; Birkenmajer and others, 1991), and older crust beneath Deception Island is likely to be relatively young and thin (Ashcroft, 1972; Guterch and others, 1991). Thus, in an absence of isotopically distinctive crustal rocks, any interaction with Deception Island magmas may be difficult to detect.

Volatiles: F and B compositions in Deception Island magmas were reported by Smellie and others (1992). Cl was also analysed by those authors concurrently with F and B but the results of the Cl analyses are unpublished (Smellie and A. Hofstetter, unpublished data). The results of the entire data set are discussed here. F–K_2O relationships for the basaltic samples were shown to overlap with those of basalts from continental and oceanic tholeiites (including within-plate tholeiites and tholeiites from back-arc basin spreading centres), and some island arcs. B abundances (typically 4–16 ppm) are high relative to MORB and OIB (*c.* 1 and 2–3 ppm, respectively) but overlap with those of island arc basic–intermediate lavas (2.2–46 ppm; Morris and others, 1990) and indicate a significant subduction influence on Deception Island magmas (Smellie and others, 1992). Because of fractionation effects, Cl contents vary widely in Deception Island basalts (80–>300 ppm) and it is hard to make meaningful comparisons with basalts from known tectonic settings. *Average* Cl abundances in Deception basalts (*c.* 150–180 ppm) are possibly more similar to those in Mount St Helens arc basalts and back-arc basin basalts in eastern Scotia Sea (115–120 and 120 ppm, respectively), than to mid-Atlantic Ridge, Mariana Trough (back-arc) and Mariana (oceanic) arc basalts (60, 300 and 1070 ppm; Garcia and others, 1979; Muenow and others, 1980; Shevenell and Goff, 1993). Cl abundances in within-plate tholeiites are very variable (*c.* 50–1280 ppm in Hawaiian tholeiites; Garcia and others, 1989) and encompass the range observed on Deception Island.

On Deception Island, the F–B volatile contents were related by Smellie and others (1972) to the volcano-tectonic evolution of the island. Measured F and B abundances are lower in the pre-caldera lavas compared with the late post-caldera tuff cones (Pendulum Cove Formation; see below). Early post-caldera lavas (Baily Head Formation and Stonethrow Ridge Formation) were shown to contain broadly intermediate F–B abundances. F and B contents both acted incompatibly in Deception magmas, but the generally greater variations shown by abundances in sideromelane lapilli obtained from tephras (compared with lavas) suggest that F and/or B may have been preferentially adsorbed onto some lapilli during or after eruption, although the data scatter is not great (Fig. 3.30). Cl variations show a division into two relatively ill-defined trends in which lava samples have significantly lower Cl contents than occur in bombs and sideromelane lapilli. That defined by the crystalline lava samples may reflect more complete Cl degassing and therefore lower Cl solubility at atmospheric pressures compared to the glassy bombs and lapilli. Conversely, the higher Cl contents in bombs and sideromelane lapilli may reflect interaction with Cl-rich seawater during explosive hydrovolcanic eruptions, or chemical adsorption onto particle surfaces, either in an eruption plume or by post-eruptive wind-blown sea spray (*cf.* Oskarsson, 1980). Because of the wide range of unsystematic Cl variations, it is unlikely that the compositional data set for Cl can be interpreted unambiguously in terms of magmatic evolution.

Two diverging trends are shown on diagrams of ratios involving K, P, F and B (Fig. 3.31). Because K, P, F and B are all highly incompatible elements in basaltic magmas, their relative abundances should be unaffected by closed-system crystal fractionation or variable partial melting of a homogeneous mantle source composed of the observed phenocryst phases in Deception lavas. Thus, the observed variations in the ratios are unlikely to occur in a magma evolving in a closed system, and they were interpreted as evidence that the system was open to some or all of those elements during part or all of its history, and that the pre- and post-caldera magmas evolved in different ways. Either an external source has affected abundances of those elements, or the crustal chamber has undergone periodic replenishment, perhaps by influxes of small batches of less evolved magma (open system fractionation of O'Hara, 1977). A possible external source suggested by Smellie and others (1992) was variable magmatic interaction with crustal material, possibly slivers of granitic crust beneath the volcano. F-bearing apatite, amphibole and possibly phlogopite are likely mineral phases in the upper crust or possibly mantle responsible for the K–P–F variations observed. The different pre- and post-caldera trajectories of K/F and K/B ratios may also reflect:

1) variations in the efficiency of the crustal scavenging process, which could have been enhanced in post-caldera times by increased fracturing in the upper crust following caldera collapse, and/or
2) a major influx and mixing with a batch of magma with significantly different ratios of those elements.

Thus, Smellie and others (1992) postulated that, throughout the history of the volcano, mafic magma in an upper crustal magma chamber underwent continuous open system fractionation involving the frequent influx and eruption of small batches of fresh magma, and/or the magma chamber interacted with the enclosing crust. By those methods, contents of K, P, F and B, and ratios involving those elements, were changed in the evolving liquids. It was also speculated that a larger influx of compositionally different mafic magma, possibly triggered by the regional extensional tectonics, occurred at the end of the pre-caldera period. Such an event could explain the presence of two diverging compositional trends. A major magmatic influx would cause thermal perturbations, convection and mixing within the pre-existing, stratified magma chamber, eventually resulting in a large-volume eruption by explosive degassing and caldera collapse. Alternatively, scavenging efficiency in the upper crust may have been enhanced by increased fracturing following caldera collapse.

4 Geomorphology

by J. López-Martínez and E. Serrano

Introduction

The morphology of Deception Island is clearly influenced by the fact that the island is a volcano, and it exhibits a large variety of landforms and deposits derived from the volcanic activity. A second important aspect from the geomorphological point of view is the presence of glaciers covering approximately 57% of the island surface. The ice has interacted with the volcanic activity, remodelling original volcanic landforms, accumulating moraines, and producing ice retreats and re-advances linked to eruptions and geothermal activity as well as to climate. Apart from the two main geomorphological processes – volcanic activity and glacial action – other processes have also contributed to the formation and evolution of the Deception Island relief. They are mainly processes linked to streams and lakes formed from melting ice and snow, periglacial activity producing gelifraction, slope processes, and the presence of permafrost. In addition, coastal and submarine geomorphological processes provide additional important evidence of recent changes in the relief of the island.

The location of Deception Island in Bransfield Strait presupposes the presence of a cold oceanic climate, characteristic of maritime Antarctica. In the South Shetland Islands there is a mean annual temperature of about –3°C, precipitation ranging from 470 to 700 mm, frequent summer rain (above 100 mm) and a moderate annual thermal amplitude (approximately 8–10°C) (Schwerdtfeger, 1970; Serrano and López-Martínez, 2000). Meteorological records from the Argentine station on Deception Island between 1948 and 1967 show a mean annual temperature of –2.9°C and, in the warmer months 1.1°C, absolute minimum –30°C and maximum usually between 4 and 6°C with an absolute maximum value of 10°C (Igarzabal, 1974). The measured mean annual precipitation is 510 mm.

The island is an active volcano with a history of recent eruptions, the last of them being in 1967, 1969 and 1970. Together with current geothermal activity, there have been significant geomorphological changes in the island, some very recent. The geomorphological map of Deception Island (BAS GEOMAP 6-B, back pocket) shows the distribution of the different landforms classified by their origin.

Structural geomorphology

Landforms related to the volcanic activity and to the geological structure are an essential component of the Deception Island landscape. A dominant element is the

Fig. 4.1. View of craters and lakes in the area of Telefon Bay constructed during the 1970 eruption. The glaciated crest in the background is Stonethrow Ridge.

Fig. 4.2. Multiple craters south-west of Goddard Hill, formed during the eruption in 1970.

flooded caldera, Port Foster, connected to the open sea through Neptunes Bellows. The slopes of the outer side of the caldera rim preserve landforms associated with the pre-caldera edifice. However, the original morphology is not completely preserved because of marine erosion on its outer part, the collapse of its inner flanks and changes brought about by post-caldera volcanic activity. A series of more or less concentric scarps in the inner part of Port Foster are related to caldera collapse.

Apart from the two large-scale landforms (the main volcanic edifice and the caldera), there are many minor volcanic landforms, such as tuff cones, tuff rings and cinder cones. Most of the cones and craters are located in the inner part of the caldera, where there are at least 60 relatively well-preserved craters and whose original landforms can be reconstructed and mapped. The areas with the densest concentrations of craters are around Telefon Bay (Figs 4.1 and 4.2) and along the northern slopes of the crest of Mount Kirkwood (Fig. 4.3). In the Telefon Bay area there are craters that originated during the 1967 and 1970 eruptions, several of which are very well preserved. Some of the craters are occupied by lakes.

Fig. 4.3. View of the northern slope of Mount Kirkwood. The debris-strewn lower glacier slopes below Mount Kirkwood are the locus of a linear chain of small craters formed in 1842. Neptunes Bellows is the narrow channel visible in the background.

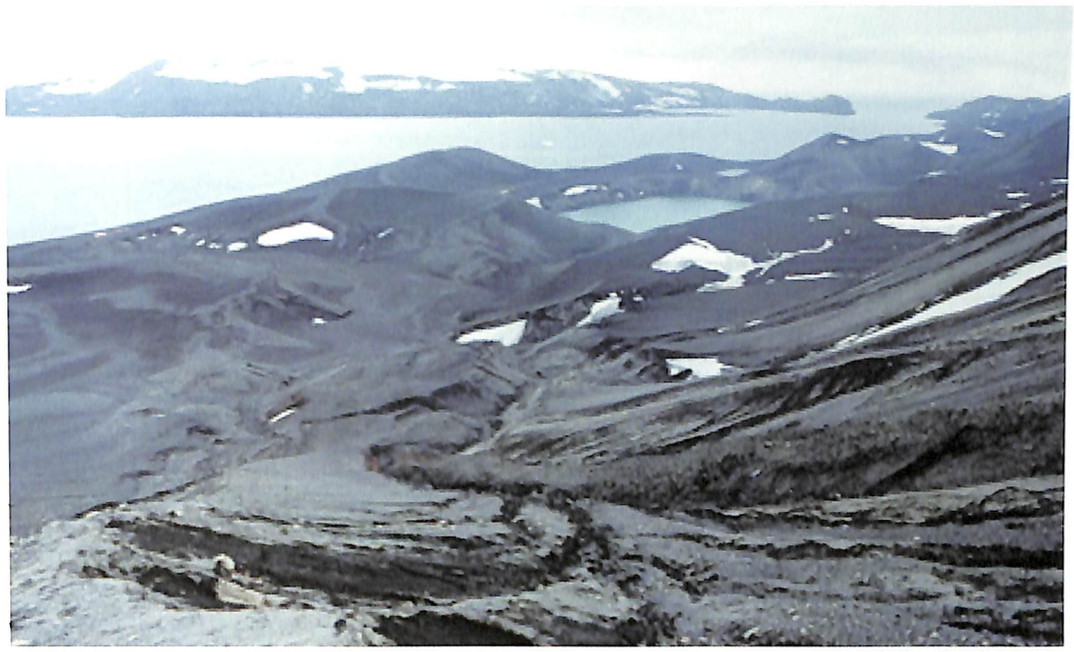

Fig. 4.4. View of Crater Lake (middle distance). A thin lava flow mantles part of the steep caldera slope in the foreground, and a more extensive lava flow occupies the prominent high terrace to the right overlooking Crater Lake. Mount Pond and Neptunes Bellows are visible in the background.

On the outer side of the caldera rim, there are several volcanic edifices that show linear distributions along evident fracture lines; this is particularly well shown by lines of craters aligned on ENE-trending fractures that extend between Telefon and Stonethrow ridges across to Macaroni Point, on the north-eastern side of the island.

A series of lava flows are located on the outer and the inner sides of the main divide. The most extensive and voluminous flows are located in the south-western part of Kendall Terrace, with other smaller ones, such as those on the northern side of Mount Kirkwood (BAS GEOMAPs 6-A and 6-B, back pocket; Fig. 4.4).

Some discernible scarps of different sizes, present in several places within the glaciers, are considered to correspond to subglacial structural landforms. The most notable are those, more or less parallel to the main divide of the island, that are located on both sides of Mount Pond and Mount Kirkwood.

Fig. 4.5. Abundant steam rising from a heated beach ridge at Pendulum Cove.

Fig. 4.6. Arcuate crevasses appearing on the surface of a glacier extensively covered by pyroclasts on the southern side of Telefon Ridge.

During the preparation of the geomorphological map, the existence of a series of sub-circular depressions in the surface of some glaciers was noticed on air photographs and their presence is recorded here for the first time. The most conspicuous of these are located east of a line from Mount Pond to Goddard Hill (between the main divide and Costa Recta), and on the western side of Mount Pond (BAS GEOMAP 6-B, back pocket). The depressions have diameters of about 100–300 m, their margins are locally imprecise and crevasses in their vicinity trend subparallel to their margins. We interpret such supraglacial depressions as the result of recent or even current thermal activity under the ice.

The existence of thermal anomalies can be observed at first hand at different places of the island (Fig. 4.5) where there are fumaroles, heated ground or the presence of deposits of fumarolic activity. BAS GEOMAPS 6-A & 6-B extend the previous knowledge of evidence for the existence of thermal anomalies (López-Martínez and others, 1996). Most evidence for the existence of thermal

Fig. 4.7. Tephra layers in glacier ice near the coast south-west of Mount Kirkwood.

Fig. 4.8. Prominent gully cut in volcanic debris-covered glacier ice and associated fluvio-glacial sediment fan on the beach north of Pendulum Cove.

Fig. 4.9. Flat-floored valley on Kendall Terrace.

Fig. 4.10. Stratified tephra layers overlying relict ice core at the southern end of Stonethrow Ridge. The hammer is 33 cm in length.

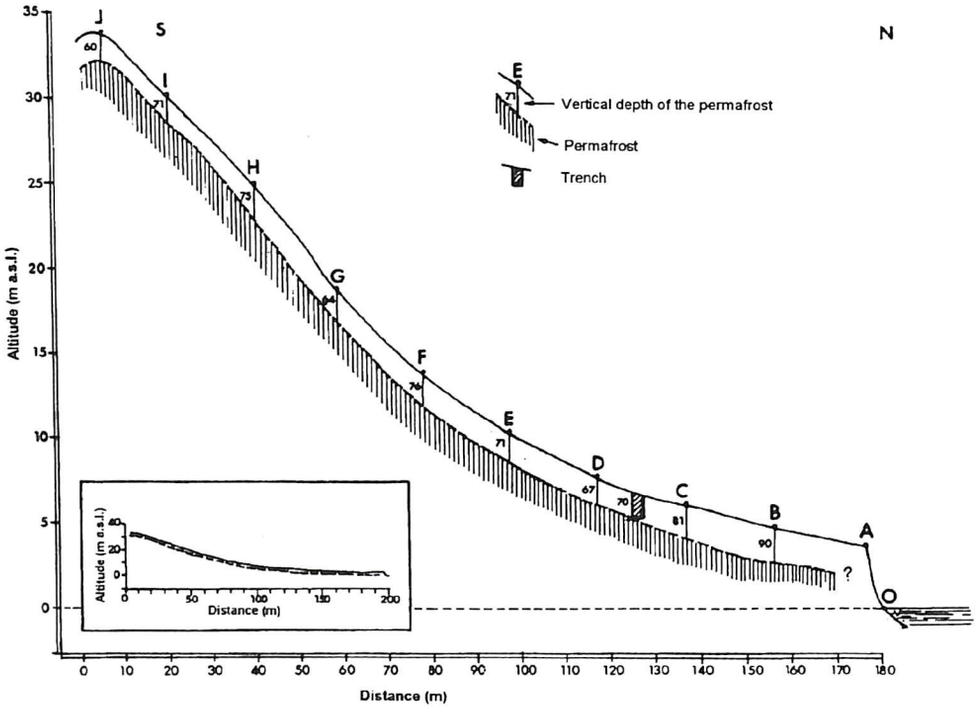

Fig. 4.11. Profile showing the position and thickness of the active layer on a slope near Gabriel de Castilla station (Spain). Indicated thicknesses are in metres.

activity occurs around the coast of Port Foster. However, there are also fumaroles north of Mount Pond, north of Whalers Bay, north-west of Base Decepción (Argentina) and on the western slopes of Stonethrow Ridge, west of Fumarole Bay. The highest recorded temperatures were measured in Fumarole Bay (approximately 99°C (López-Martínez and others, 1996; Villegas and others, 1997) and 108°C (measured in February 1987; J.L. Smellie, personal communication)).

Glacial geomorphology

Glacier ice occupies about 57% of the surface of Deception Island, even in areas where, because of extensive cover by pyroclastic debris, the presence of a glacier can only be detected by means of flux signs on the surface (Fig. 4.6), or by the contrast in morphology with respect to adjacent areas without ice. Areas where the debris cover is relatively important include the glaciers between Pendulum Cove and Telefon Bay, and the glacier extending to Port Foster west of Mount Pond. Thus debris accumulation on the glacier surfaces is variable and two types of glacial surfaces, namely debris-free or with debris/pyroclastic cover, are differentiated on the geomorphological map. Tephra and lapilli layers are evident in some ice profiles (Fig. 4.7; *cf.* Orheim, 1972*a,b*).

The general stability of the ice fronts and ice cover on the island has been influenced not only by climatic fluctuations but also by the effects of volcanic eruptions. Evidence of glacial retreat due to recent volcanic eruptions, e.g. east of Telefon Bay and the northern slopes of Mount Kirkwood, is demonstrated where the glaciers have not recovered to their pre-eruption extent. This may be a function of their not having yet reached equilibrium or because the ice supply area has been modified. In addition, fluvio-glacial sediment fans are relatively common in the island (Fig. 4.8)), and there are also lahar deposits, e.g. in Whalers Bay, where a jokulhlaup severely damaged the British station in 1969.

Many moraines on the island show recession ridges and several are ice-cored. The locations of these deposits are shown on the geomorphological map. Because of the modifying effects of the volcanic activity and problems associated with the preservation of ancient moraines it has not yet been possible to reconstruct the history of ice fluctuations.

Periglacial and fluvial geomorphology

Deception Island experiences a cryonival morphoclimate, with a relatively high availability of water in summer and frequent freeze-thaw cycles. Such features favour periglacial processes and the presence of an active layer, which is usually saturated in summer.

In the South Shetland Islands there is a high diversity of periglacial landforms: 26 types of periglacial landforms linked to gelifluction, gravitational and active layer processes have been recognized (Serrano & López-Martínez, 1998, 2000). On Deception Island, periglacial landforms and deposits consist mainly of debris slopes and fans, even slopes, solifluction lobes and flat-floored valleys (Fig. 4.9). Patterned ground and other periglacial

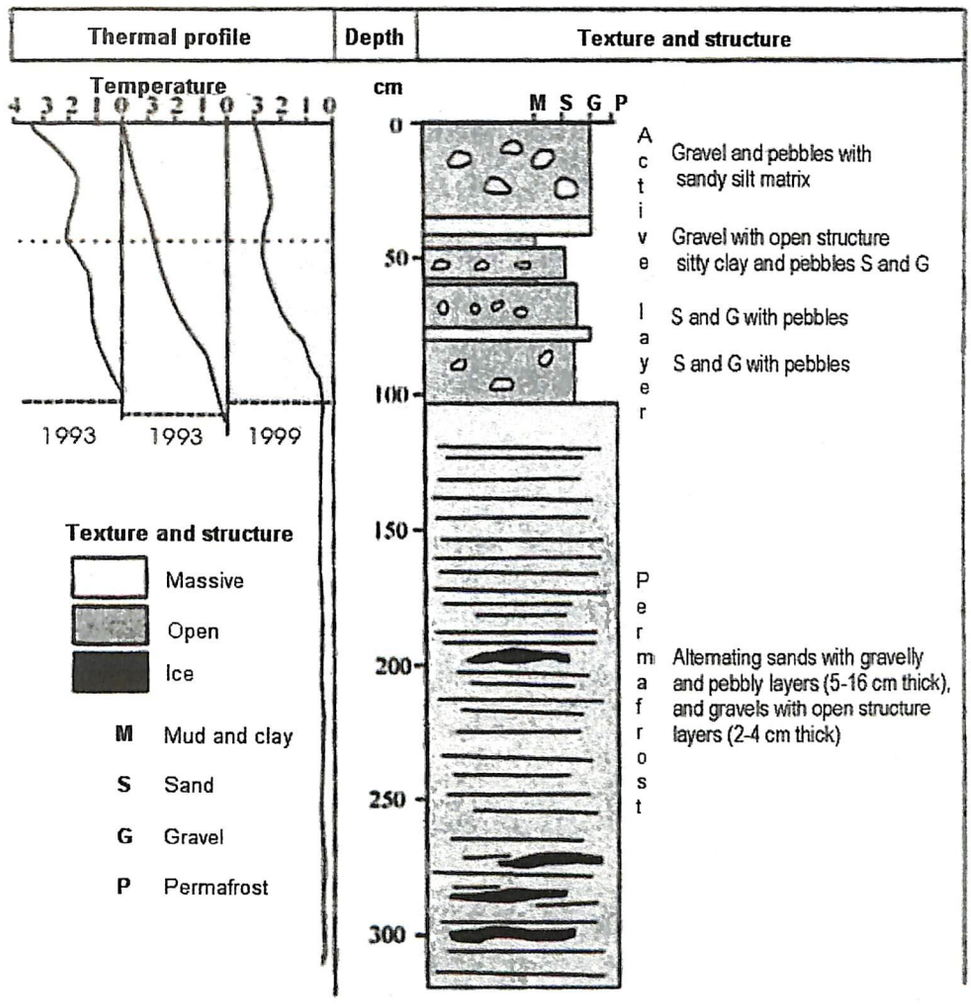

Fig. 4.12. Trench profile through permafrost and active layers at a site near Gabriel de Castilla station (Spain).

landforms, very common on other islands of the archipelago, are not usually present due to the even grain size of the clasts, permeability of the surface and the mobility of the clasts on the slopes.

On Deception Island, ice is extensively covered by pyroclastic debris; the ice may occur locally as ice masses but elsewhere it is within the permafrost (Fig. 4.10). In places, where glaciers are completely covered by pyroclasts, structures within the pyroclastic cover serve to demonstrate flow and hence the presence of ice at depth (Fig. 4.6). Permafrost has been identified at 10 cm or greater depths (Corte and Somoza, 1954; López-Martínez and others, 1996; Serrano and López-Martínez, 1998; Serrano and others, 2002). Studies of the active layer, carried out on an even slope inclined at 5–10° in the vicinity of Base Gabriel de Castilla (Spain), have provided information about the structure of the active layer. The vertical thickness of the active layer was measured at between 60 and 90 cm thick along a profile, by probing with steel rods (Fig. 4.11, López-Martínez and others, 1996). Additional observations in the same area, using vertical electrical sounding and a 3 m-deep trench, included groundwater temperatures of 0.6°C in springs linked to the permafrost, definition of the structure of the active layer and part of the permafrost, and measured temperature gradients in the active layer (Fig. 4.12, Serrano and others, 2002).

Surface drainage takes place via a network of streams constrained by the volcanic morphology of the island. The drainage pattern is generally radially outward outside the caldera, and towards Port Foster within the caldera. The drainage system is also affected by the ease of erosion and transport of the pyroclastic ground cover. In some areas, streams have cut deep ravines in slopes covered by loose pyroclasts (e.g. north-west of Pendulum Cove; Figs 4.8 and 4.13). However, in other areas, especially where stream gradients are less steep (e.g. Kendall Terrace), small flat-floored valleys have formed (Fig. 4.9). The drainage network is locally diverted around the volcanic edifices but, elsewhere, streams have cut through cones and craters (e.g. south-west of Gabriel de Castilla station (Spain); Fig. 4.4).

Maximum ice melting occurs in January, when there is a strong correlation between stream discharge rate and air temperature. The increased discharges also enable greater numbers of larger particles to be transported as bedload (Inbar, 1992) and a high total sediment flux into Port Foster.

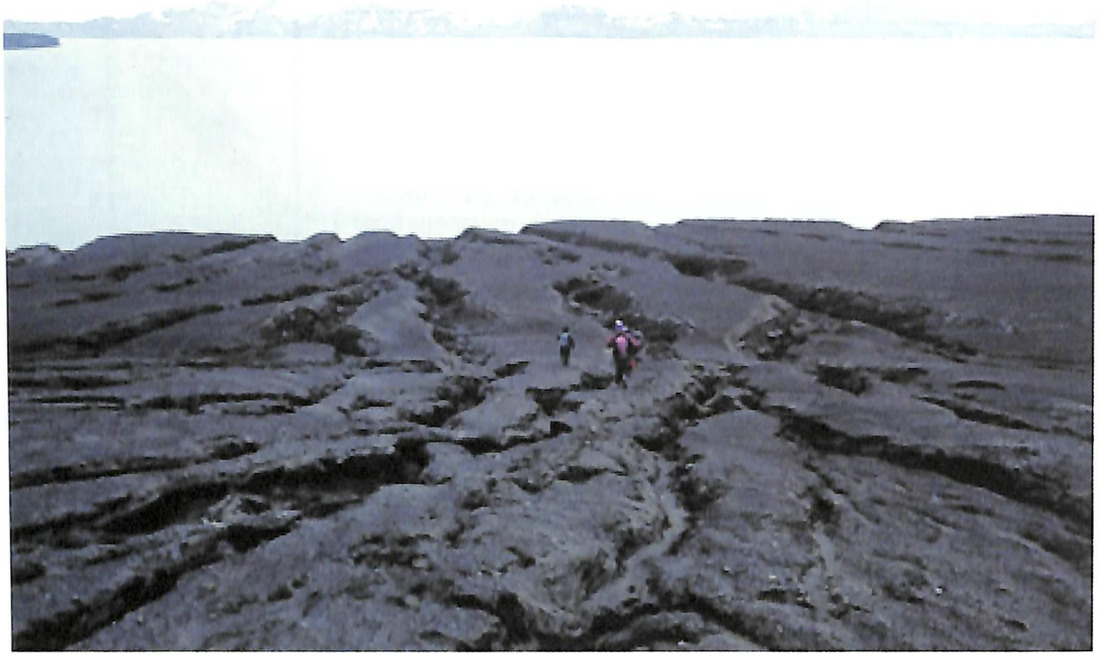

Fig. 4.13. Prominent stream channels cut in unconsolidated tephra between Pendulum Cove and Telefon Bay.

However, Cooper and others (1998) have deduced shallowing rates as high as 0.3–0.5 m a^{-1} for Port Foster. These are much higher than might be expected for normal sedimentation within a caldera of its size and they concluded that volcano-tectonic resurgence may have played a major role in the shallowing activity.

Coastal and submarine landforms

There is a notable morphological contrast between the steep outer coast of the island and the generally low beaches around Port Foster. The outer perimeter consists mainly of vertical rock cliffs about 20–40 m high; these are remarkably uniform in height along the northern and western coasts (e.g. in front of Kendall Terrace; Fig. 4.14) and in the southern area (e.g. Cathedral Crags). The cliffs show signs of landward retreat caused by sea erosion, with numerous islets, stacks and rocks awash present (see geomorphological map, back pocket).

Fractures have an influence on the coastal shape, as can be observed at Macaroni Point and the two headlands located immediately to the west, where there is a saw-tooth

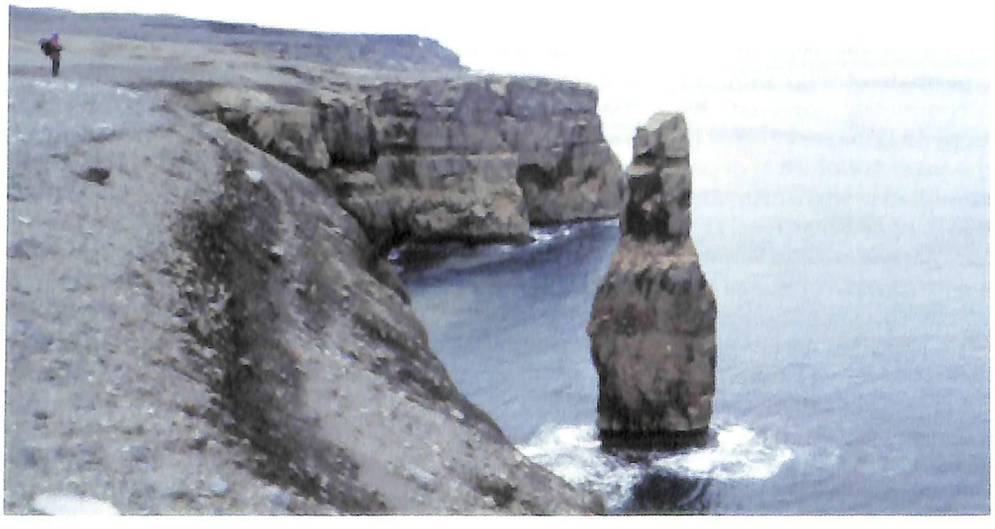

Fig. 4.14. Cliff and stack on the outer coast of Kendall Terrace.

Fig. 4.15. View of the Costa Recta, looking south toward Baily Head, showing the spectacularly linear shape and the beach at the foot of extensively debris covered glacier ice on the right side. A small sediment fan fed by glacier meltwater is present exiting onto the beach in the low foreground.

arrangement of headlands following the lines of fractures.

A remarkable feature of the outer coast of Deception Island is the presence of a linear coast on the eastern side of the island, named Costa Recta (Fig. 4.15). It is about 7 km long and marked by an ice cliff up to 30–40 m high resting directly on a beach. The existence of this feature has been ascribed a structural (fault-related) origin by most authors. However, there is no evidence for the existence of such a fracture in the outcrops located at the two ends of Costa Recta: at Macaroni Point and Baily Head, respectively. In our opinion, the influence of ice supply and marine erosion of the glacier front must also be considered. The glacier covering the eastern slopes of Mount Pond (539 m), the highest point of the island, is the largest glacier on the island and its boundary with the sea is located between two rocky bluffs at Macaroni Point and Baily Head. It is more likely that the linear form of Costa Recta results from a combination of protection of the glacier by the two erosion-resistant headlands and wave erosion at the glacier front.

Raised beaches have not been found on Deception Island, although these are a common feature of other islands in the South Shetland Islands archipelago. Their absence is probably the result of active geomorphological modification of the island related to volcanic activity, and the ease with which the volcanic clasts are remobilized. Because of the enhanced erosion and transport of unconsolidated volcanic detritus, and the increased availability of water in summer, there is a considerable movement of debris through the drainage network, resulting in a high sediment supply into Port Foster.

The morphology of the marine shelf surrounding the volcano is poorly known. However, the submarine morphology indicates a much larger volcano than is apparent from the map, with a basal diameter of at least 30 km (Smellie 1990). On the north and west sides, the edifice has been eroded to form an extensive shallow submarine platform 3–5 km wide and depths < 100 m (probably storm wave base). The topography, sediments and geological structure of the sea floor within Port Foster are much better known and are described in Chapter 5 (see also Rey and others, 1992; BAS GEOMAP 6-B, back pocket).

5 Submarine morphology and seismic stratigraphy of Port Foster

by J. Rey, A. Maestro, L. Somoza and J.L. Smellie

Since the early 1980s there have been numerous geophysical investigations of Port Foster, Deception Island (e.g. Kowalewski and others, 1990; Rey and others, 1990, 1992, 1994, 1995, 1996; Grad and others, 1992; Somoza and others, 1994). In this chapter, we focus principally on the results of several mainly Spanish geophysical investigations since 1986. Port Foster was examined by continuous seismic reflection profiling (using Sparker, Geopulse and 3.5 kHz sub-bottom Profiler) and rock dredge hauls during Antarctic cruises Exantarte 87-88, 88-89, 89-90 and 90-91 (Fig. 5.1). Track-line positions were fixed by GPS, with sub-metre resolution. The bathymetry and submarine morphology of Port Foster were determined during several B/O *Hesperides* cruises, mainly by multibeam echo sounder and parametric narrow-beam sub-bottom profile echo sounder TOPAS (Topographic Parametric Sound).

Tectonic setting

Deception Island is the only active volcano known in the Antarctic Peninsula region, with eruptions in 1967, 1969 and 1970. The island is situated at the confluence of two major tectonic structures: the south-western end of Bransfield trough (a marine deep in Bransfield Strait with nascent spreading centre caused by NW–SE extension) and a postulated southerly extrapolation of the Hero Fracture Zone (a former transform fault; Fig. 5.2). Bransfield trough is also crosscut by NW–SE-trending fractures that divide the structure into segments (Grad and others, 1992). The relatively high seismicity and historical eruptive activity on Deception Island probably reflect a continuous release of seismic energy through a regionally extensive NE–SW-trending fracture system associated with the Bransfield Strait rift system (Martí and others, 1990).

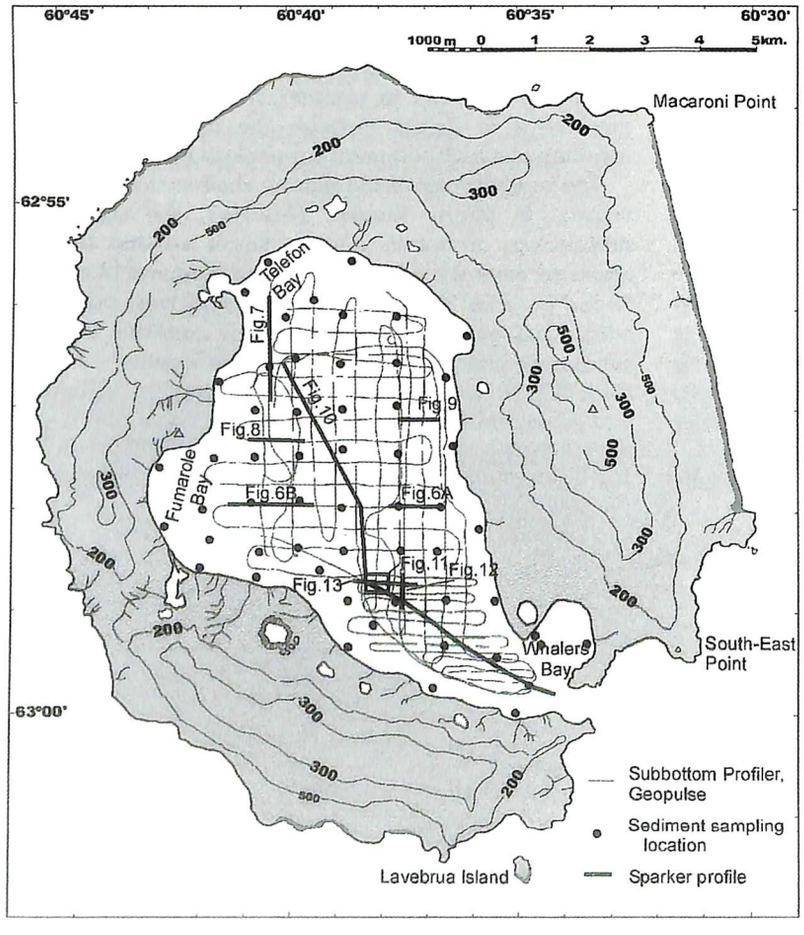

Fig. 5.1. Map showing the positions of seismic track lines (sub-bottom Profiler 3.5 kHz, Geopulse 300 J and Sparker 4 500 J) and sediment sampling grid in Port Foster.

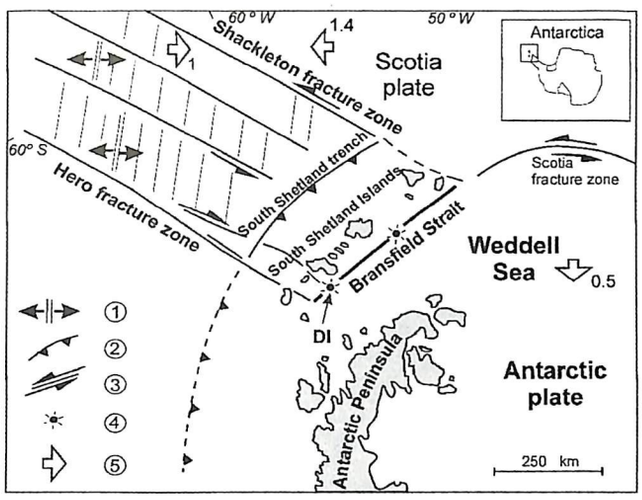

Fig. 5.2. Sketch map showing a simplified regional tectonic framework for Deception Island (after Rey and others, 1995). 1, ocean spreading centre; 2, subduction zone (dashed where inactive); 3, oceanic fracture zone; 4, volcano; 5, plate motion vector (cm/yr; Minster and Jordan, 1978); DI, Deception Island.

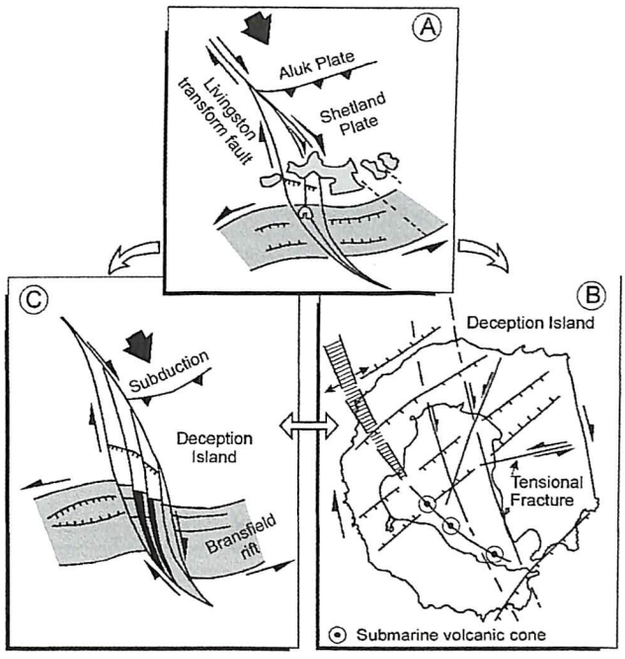

Fig. 5.3. Cartoons illustrating a geodynamic model used to explain recent seismic activity in western Bransfield Strait and fracturing on Deception Island. The 'Livingston transform fault' is a splayed offshoot of the Hero Fracture Zone (Fig. 5.2; after Rey and others, 1996).

Traditionally, the flooded caldera of Deception Island (Port Foster) is thought to be a consequence of a volcano-tectonic catastrophic collapse of the volcanic edifice along arcuate and radial faults (Holtedahl, 1929; Olsacher, 1956; Hawkes, 1961; Casertano, 1963; Baker and others, 1975; Birkenmajer, 1992; Smellie, 2001*b*). However, seismic and other geophysical studies have demonstrated NE–SW linear trends seemingly at odds with a simple volcano-tectonic model of caldera subsidence, in which arcuate patterns should be expected (Ortíz and others, 1992). Since the discovery that the influence of regional fracture systems can also be recognized on the island (Smellie, 1988), an alternative model for caldera formation has arisen involving passive collapse of the volcano superstructure along intersecting orthogonal fault systems induced solely by regional tectonics (Martí and others, 1996). Both models depend on differing interpretations of the geological history of the island: Martí and others (1996) denied the existence of a major caldera-forming eruptive event, whereas Smellie (2001*b*) ascribed such an origin to the Outer Coast Tuff Formation, a thick, island-wide stratigraphical unit formed entirely of pyroclastic current deposits (see Chapter 3).

The fracture systems and distribution of historical eruptions on Deception Island, and recent evidence for fault-related hydrothermal activity in the sedimentary sequences in Port Foster, can probably be related to regional tectonic effects associated with the situation of the volcano at the intersection between the Bransfield Strait rift and the transcurrent Hero Fault Zone (Fig. 5.3). The central part of Bransfield Strait corresponds to a zone of transtension, melt migration and crustal separation with clearly identified extensional faults (Ashcroft, 1972; Baker and McReath, 1971; Grad and others, 1992; Barker and Austin, 1998). Conversely, a zone of transpression with compressional structures exists outboard of the island, on the continental shelf of Livingston Island. Both sets of structures can be reconciled within a model of right-lateral strike-slip movement caused by south-easterly translation of the Aluk plate in Drake Passage relative to a stationary Antarctic plate (e.g. Pelayo and Wiens, 1989; González-Casado and others, 2000). Deception Island is situated within an extensional zone related to the transcurrent movement (right-lateral simple shear). The direction of maximum extension is approximately NNW–SSE, orthogonal to the direction of transcurrent movement. Within this conceptual framework, the distribution of the recent eruptive centres on the island, and hydrothermal centres within Port Foster, can be related to a system of NNW–SSE splay faults that are also hypothesised to cross Livingston Island. Although their positions on Livingston Island are unknown, fractures consistent with the hypothesis have been identified on seismic sections on the shelf area to the south of that island (Fig. 5.4), and secondary tensional structures may also have been responsible for guiding the emplacement of submarine cones and intrusive domes within south-eastern Port Foster (see below).

Fracture systems

Several submarine fracture systems have been identified seismically within Port Foster, although none shows on the present featureless basin floor (Fig. 5.5; Rey and others, 1990). Both these and lineaments postulated from satellite imagery on the island itself (e.g. Martí and others, 1996) form an important orthogonal system with NNW–SSE (160–170N) and NE–SW (045N–060N) trends similar to regional tectonic structures (Ortíz and others, 1990; Rey and others, 1995; Fig. 5.5). These structures are probably responsible for the linear shapes of parts of the outer coast of the island (most obvious between Baily Head and Macaroni Point; see Fig. 3.23) and, probably, for several of

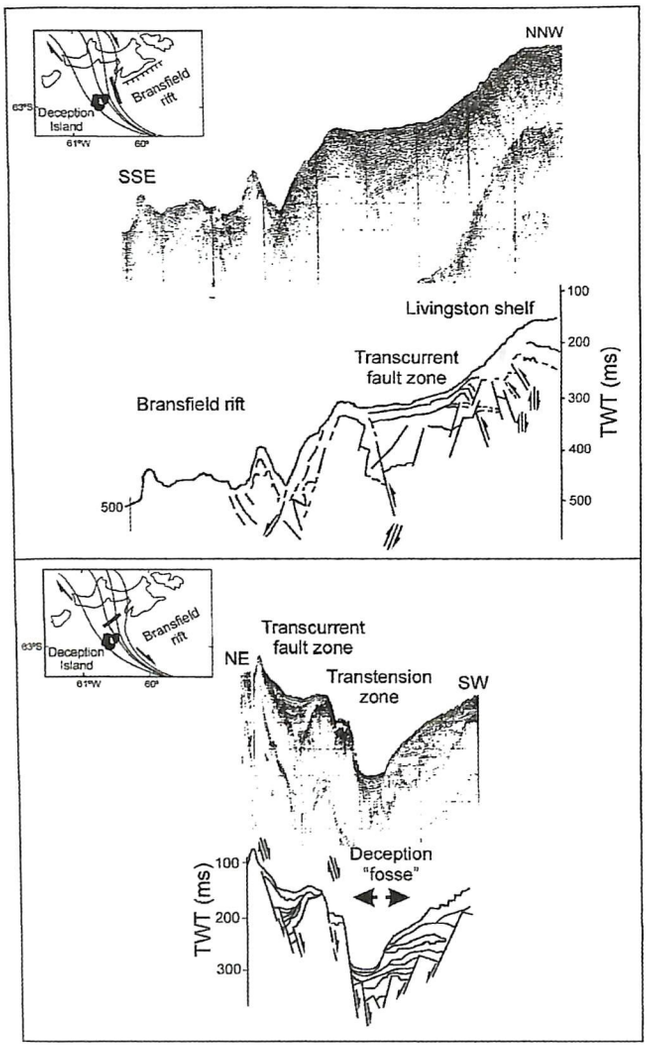

Fig. 5.4. Seismic profiles (Sparker 4 500 J) obtained on the shallow shelf platform north and east of Deception Island, and their schematic interpretation within a conceptual dextral strike-slip zone between Deception and Livingston islands (*cf.* Fig. 5.3; after Rey and others, 1996).

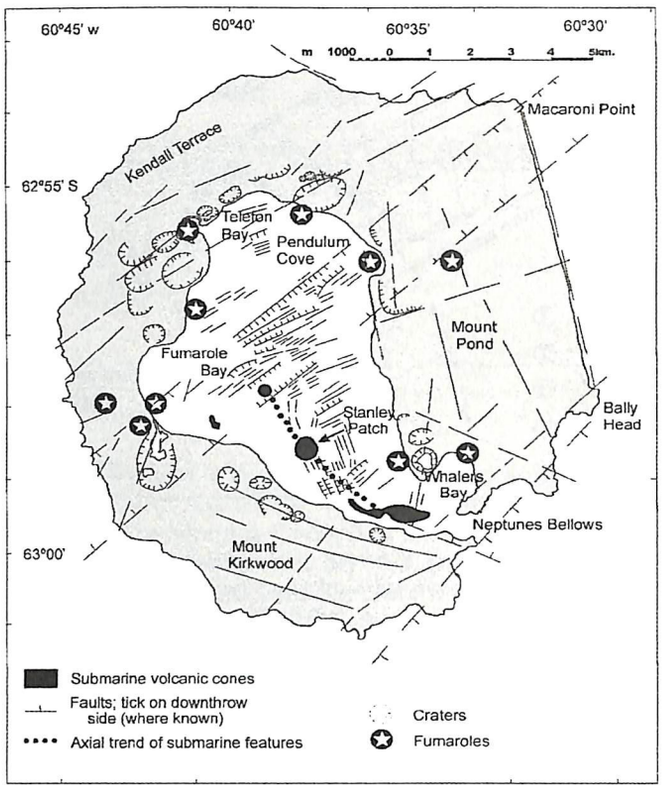

Fig. 5.5. Sketch map showing systems of fractures, volcanic cones and fumarolic areas on Deception Island and in Port Foster (modified after Rey and others, 1997). Most of the subaerial fractures indicated are inferred from morphological evidence and presence of lines of craters.

the linear crater chains on the island. Several strong negative magnetic anomalies identified also have NNW-trending orientations and have been related to fractures with those orientations (Ortíz and others, 1992). Finally, a subordinate system of fractures strikes 115–120N in the southern part of the island, around Mount Kirkwood, and was probably responsible for fixing the location of the linear crater chains that erupted there in 1839–1842 (Rey and others, 1995).

Mapping of submarine fault systems from a dense network of seismic profiles (Rey and others, 1990) has verified the existence of a major zone of faults trending 060N across the interior of the bay. Those faults are associated with several graben-like structures. Whilst not extending to the sea floor, they are associated with the deepest parts of Port Foster. Persistent, long-lived fumarolic activity at Pendulum Cove, Fumarole Bay and possibly shoreward of the 1967 land centre appear to be related to this north-easterly-trending system of fractures (Ortíz and others, 1987). The 160–170N-trending fracture system is poorly defined on the marine seismic profiles, and has only been identified in the south-easterly sub-basin in Port Foster. Two of the submarine pyroclastic cones in Port Foster (including Stanley Patch) and an elongate, high-level dome-like intrusion between Stanley Patch and Neptunes Bellows have a 150N alignment and may also be structurally controlled.

Submarine morphology of Port Foster

Port Foster has formed in a flooded central caldera depression. It is an elongate lagoon 6 x 10 km in diameter connected to the open sea through a narrow passageway named Neptunes Bellows. It is also a magnificent natural harbour that was used extensively during the early whaling period (see Chapter 1), particularly at Whalers Bay.

Port Foster contains at least two sub-basins (Rey and others, 1992; Cooper and others, 1998): a large and deep northerly sub-basin, and a much shallower southerly sub-basin that extends into Whalers Bay. The northern (largest) sub-basin is almost flat-bottomed, approximately circular and crater-like, with steep rough flanks. It is surrounded by a continuous shelf that is about 500 m wide and extends to 60 m depth, at which point it plunges to about 120 m with gradients of 11 to 22.5%, then gently deepens to 166 m centrally. The eastern and western slopes of the northern sub-basin are steeper and higher than elsewhere. The most extensive shallow flanking shelf of the northern sub-basin is beneath Fumarole Bay, which slopes gently to a break of slope at about 120 m. The flat bottom of the basin is broken

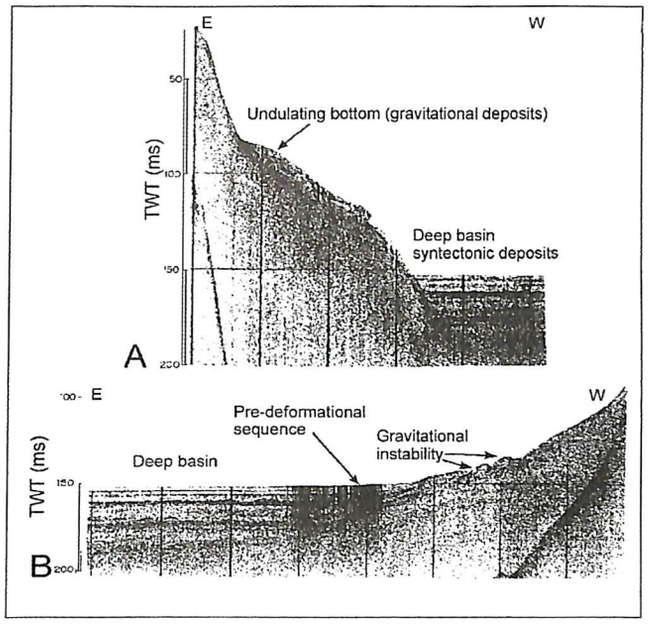

Fig. 5.6. Examples of two sub-bottom Profiler 3.5 kHz seismic profiles obtained within Port Foster, showing undulating slope (A)- and slope bottom (B)- topographies caused by active gravitational slides and slumps. The locations of the seismic sections are indicated in Fig. 5.1 (after Rey and others, 1992).

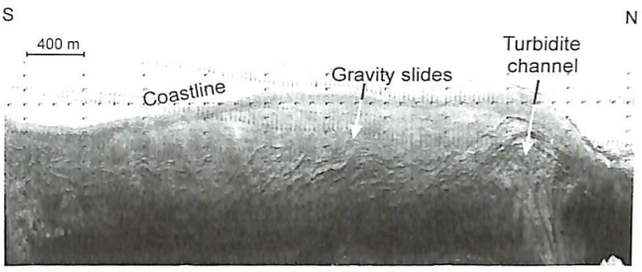

Fig. 5.7. Side-scan sonar record (100 kHz) showing undulating sea floor caused by active slides and other gravitational instabilities. A, gravity slides and slumps scars formed by creep processes; B, turbidite channel. The location of the section is shown in Fig. 5.1.

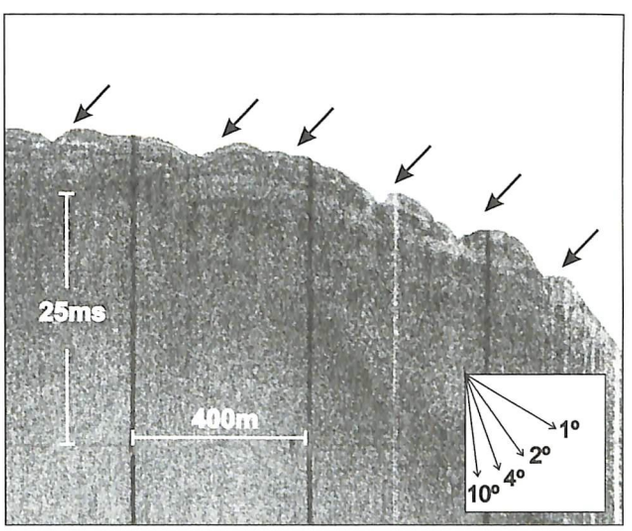

Fig. 5.8. Sub-bottom Profiler 3.5 kHz seismic profile obtained within Port Foster, showing slump scars (arrowed) formed by slow creep movement, probably aided by hydrothermal softening of the underlying volcaniclastic layers. The location of the section is shown in Fig. 5.1.

only by a single small pyroclastic cone or dome at its southern margin; a second small cone structure is also present on the south side of the broad Fumarole Bay shelf (Fig. 5.5). By contrast, the floor of the southern sub-basin has an uneven bottom morphology, with a depth generally < 110 m. It extends from Stanley Patch (a submarine pyroclastic cone) to Whalers Bay.

Submarine morphological features in Port Foster can be grouped genetically, as follows (modified mainly after Rey and others, 1992; see BAS GEOMAP Sheet 6-B, back pocket).

Features associated with tectonic instability: The asymmetrical geometry of Port Foster is probably due to neotectonic processes. Seismic studies have identified an ENE-verging monoclinal structure with a major NNW–SSE-trending axis located on the south-west side, which has lowered the caldera floor on its north-east side (Rey and others, 1990; Cooper and others, 1998; see Fig. 3.24). Thus, Port Foster can be considered as a half graben with an active western margin where the slope is rougher and slump scars and undulating bottom topography are common and formed because of slope instability. The north-western slopes are steeper and higher and show fewer features due to slope instability (Figs 5.6 and 5.7). Characteristic submarine morphologies include the following:

a) Undulations on the sea floor are confined to the marginal slope areas (Figs 5.6 and 5.7). The features appear to line up parallel to the main fracture directions and their abundance suggests that they have probably formed repeatedly because of tectonic instability.

b) Slump scars probably formed by gravitational sliding are mainly located on the south-western slopes of the basin, 2.5 and 3 km south-east and north-west of Stanley Patch (Rey and others, 2000; Fig. 5.8). The slump scar lengths vary between 4 and 300 m, although they can extend up to 500 m parallel to the coast (Figs 5.6 and 5.7). They have a low relief (2–10 m) and were probably formed during multiple slumping phases. It is possible to define three sub-types of slump-related structures formed by mass movement: (1) gravity slides (slumps) that reached the base of slope (Fig. 5.6), (2) slump scars formed by slow creep movements (Figs 5.7 and 5.8), and (3) rotational slides that show a slump-scar back-wall similar to subaerial analogues (Fig. 5.9).

c) Depositional lobes are sedimentary deposits generated by turbiditic progradational processes (Fig. 5.6). They occur on the basin floor and are rooted at the topographical break where the basin slopes give way to the flat basin floor.

Features associated with volcanism: Each of the submarine volcanic cones is characterized by relatively steep slopes

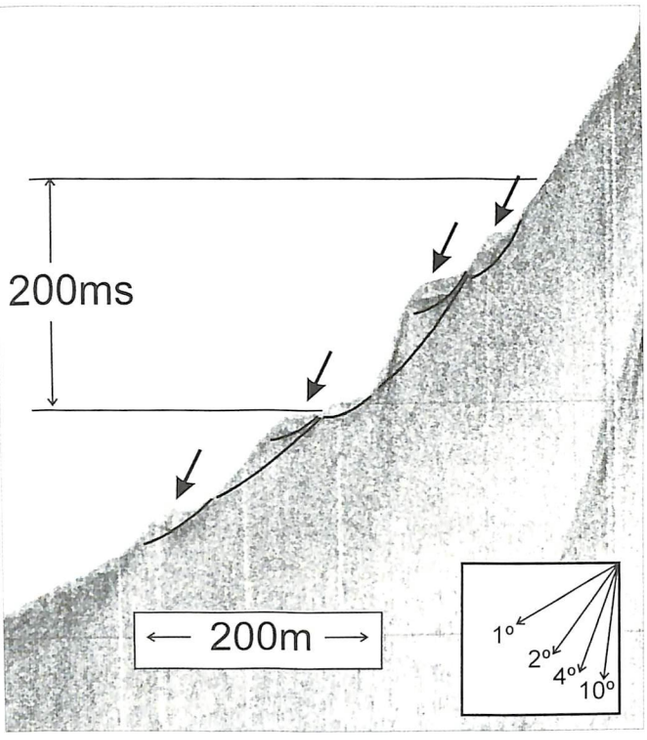

Fig. 5.9. Sub-bottom Profiler 3.5 kHz profile obtained within Port Foster, showing rotational slides with slump-scar back-walls similar to analogous subaerial structures. The location of the section is shown in Fig. 5.1.

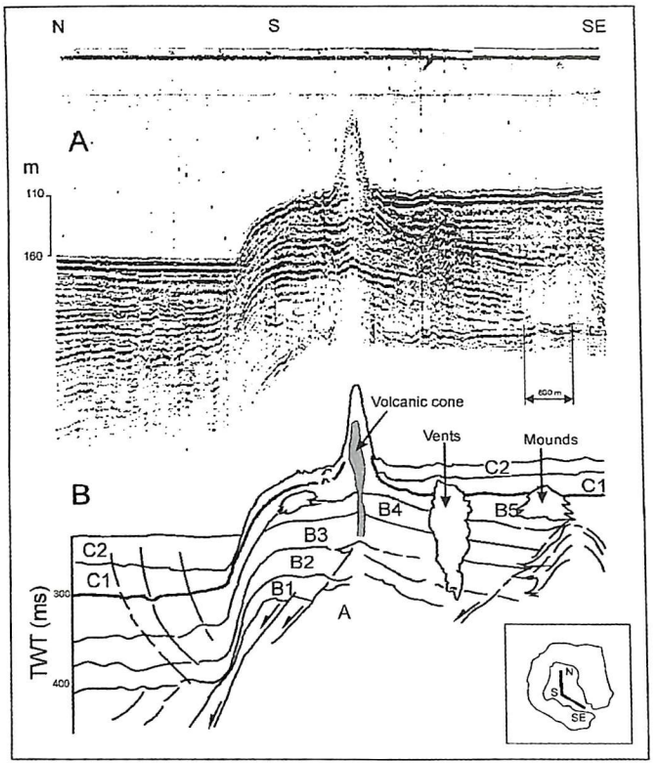

Fig. 5.10. Composite seismic reflection profile (Sparker) (A) and its interpretation (B) obtained across Port Foster, showing the seismo-acoustic depositional units described in the text (A, B and C) and associated volcanic and hydrothermal structures (after Rey and others, 1995). Inset shows the location of the profile (see Fig. 5.1).

and a dome-like or cone morphology. In vertical section, the structures extend continuously to at least 50 m depth below sea floor, and they cut across and deform the deeper sedimentary sequences (Fig. 5.10). They are situated mainly in the southern part of Port Foster and together they have an arcuate NNW–SSE alignment. The largest cone (Stanley Patch) rises more than 50 m from the sea floor and it has a small summit depression about 100 m across (likely crater; Figs 5.11 and 5.12).

Features associated with changes in eustasy:

a) Progradation wedges are particularly prominent on the eastern and south-western sides of the basin margin, usually at depths of about 120 m. They are sedimentary units and seismic imaging shows the broad outcrops to have an internal prograding sigmoid geometry strongly resembling till deltas (Fig. 5.13; *cf.* Alley and others, 1989). The till deltas on Deception Island are related to episodes of glacier growth and stagnation during low sea level stages (e.g. King and Fader, 1986).

b) Linear runnels, grooves and channels have U-shaped sections and are incised into the basin slopes, particularly the lower slopes on the eastern side of the basin (Fig. 5.12). They are typically orientated roughly perpendicular to the coastline and they resemble glacial marks made by moving ice (Belderson and others, 1972). They are associated with the progradation wedges, and are frequently located in the topset areas of till deltas.

Features associated with deep-water hydrodynamic processes: These are current-generated structures, including sand waves (ripples) and small sandbars, that occur along channel margins close to Neptunes Bellows.

Sediment distribution in Port Foster

Using dredge samples and sidescan sonar imagery of the basin floor, the distribution of sediment types within Port Foster has been mapped by Rey and others (1990, 1992; see BAS GEOMAP Sheet 6-B, back pocket). Sediment mean grain size variations are related to the proximity of the coastline and water depth. Proximal sediments (water depths < 50–70 m) consist of volcaniclastic (mainly pyroclastic?) gravels and morainic deposits, whereas deeper-water regions are dominated by sands and muds. The sediment grains were probably formed by a variety of processes: pyroclastic, glacial, periglacial, nival, aeolian and marine (Rey and others, 1990, 1992). The pattern of water circulation in Port Foster is not well-known, but there are signs that bottom currents locally influenced the distribution of sand and mud and sediment bedforms in shallow-water areas. For example, at Neptune Bellows current velocities associated with tides are enhanced because of confinement by the narrow channel, and ripple marks are developed along the channel margins (Rey and others, 1990).

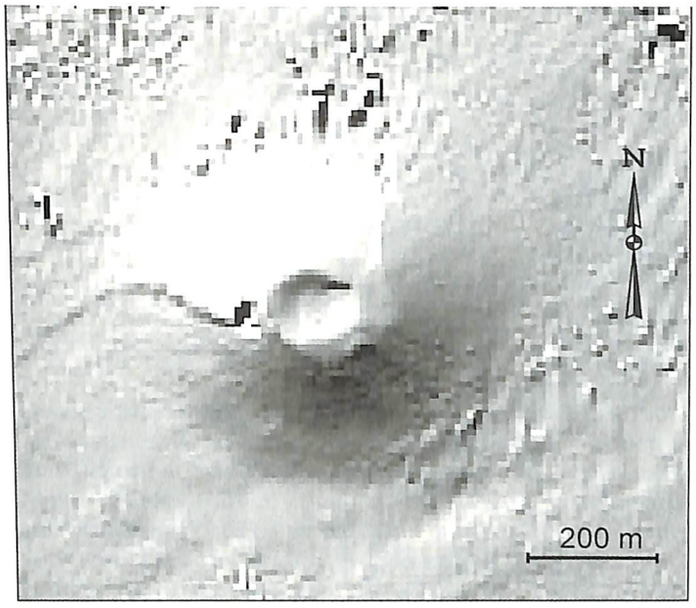

Fig. 5.11. Multibeam sea-floor relief image of Stanley Patch, first identified as a volcanic edifice in 1987 (British Antarctic Survey, 1987); see Fig. 5.1 for location.

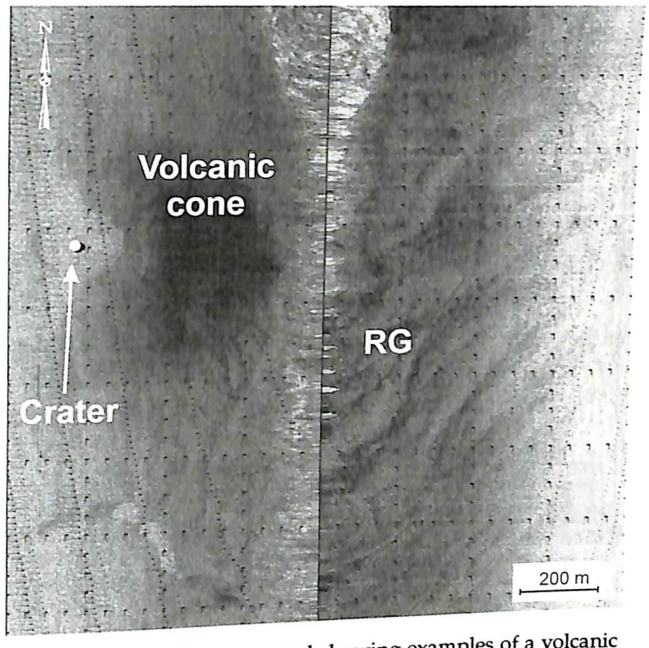

Fig. 5.12. Side-scan sonar record showing examples of a volcanic cone with summit crater (Stanley Patch), linear runnels and grooves (RG) (after Rey and others, 1992); see Fig. 5.1 for location.

Sediment thicknesses reach at least 80 m on the western side of Port Foster. If they are << 10 000 years in age (Smellie, 2001*b*; and see Chapter 7), a high sediment accumulation rate is implied (*c.* 1 cm a^{-1}). The high rates can be explained by the enclosed nature of the sedimentary basin, a provenance dominated by easily eroded unconsolidated pyroclastic material, enhanced sediment transport during annual spring thaw periods and episodes of glacier melting associated with eruptions, and glacial activity.

Seismo-acoustic stratigraphy of Port Foster

Seismic reflection profiles obtained in Port Foster show several well-defined seismo-acoustic sequences, high-level magmatic intrusions, stratigraphically confined hydrothermal mounds and fault offsets. The positions of the magmatic intrusions are apparently related to extensional fractures that affect the sedimentary deposits. Three seismo-acoustic sedimentary units are identified, each separated by tectonically enhanced unconformities. Each unconformity is interpreted in terms of deformation events that disturbed the geometry of the sedimentary materials (Fig. 5.10).

The basal unit (A) is acoustically transparent and is correlated with the precaldera lithofacies mapped on the island, including the extensive and thick Outer Coast Tuff Formation (syn-caldera; Smellie, 2001*b*). The intermediate unit (B) consists of several sub-units (B1-B5), each separated by unconformities and apparently formed synchronously with several significant volcanic and tectonic events (see Chapter 3). The sub-units contain three types of distinctive structures: mounds, cones and irregular, sub-vertical, acoustically diffuse structures (Fig. 5.10). The mound-like structures are situated at the bases of unconformities between sub-units B3 and B5; they are intercalated with the adjacent successions of evenly stratified sediments. The cones crop out on the present

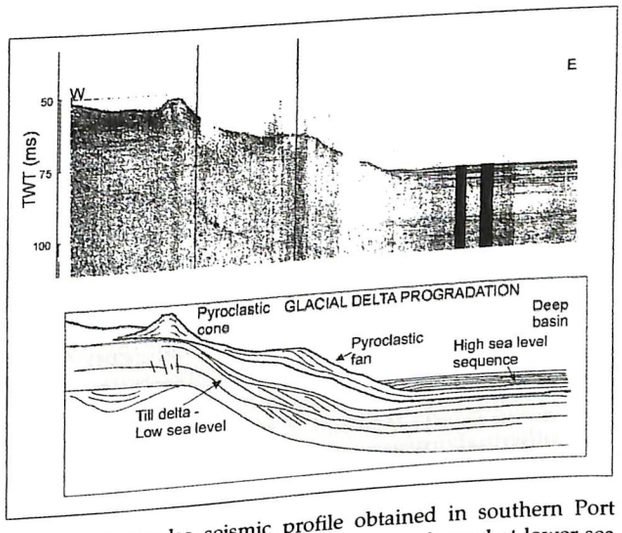

Fig. 5.13. Geopulse seismic profile obtained in southern Port Foster, showing possible till delta sequence formed at lower sea level than present, and later deeper-water deposits associated with higher sea level (after Rey and others, 1992); see Fig. 5.1 for location.

sea-floor and form prominent symmetrical edifices that rise up to 50 m, the largest being Stanley Patch. The third type of structure has irregular steep margins and is acoustically diffuse, in which internal sediment stratification can be faintly discerned and is locally deformed. These structures are interpreted to have been superimposed on the sediment succession by upward fluid transport. They locally extend up into the base of the uppermost acoustically defined unit (C). Unit C occupies a broad trough-like structure formed by deformation of the underlying units A and B by the large-scale monoclinal structure described above. It is divided into two sub-units

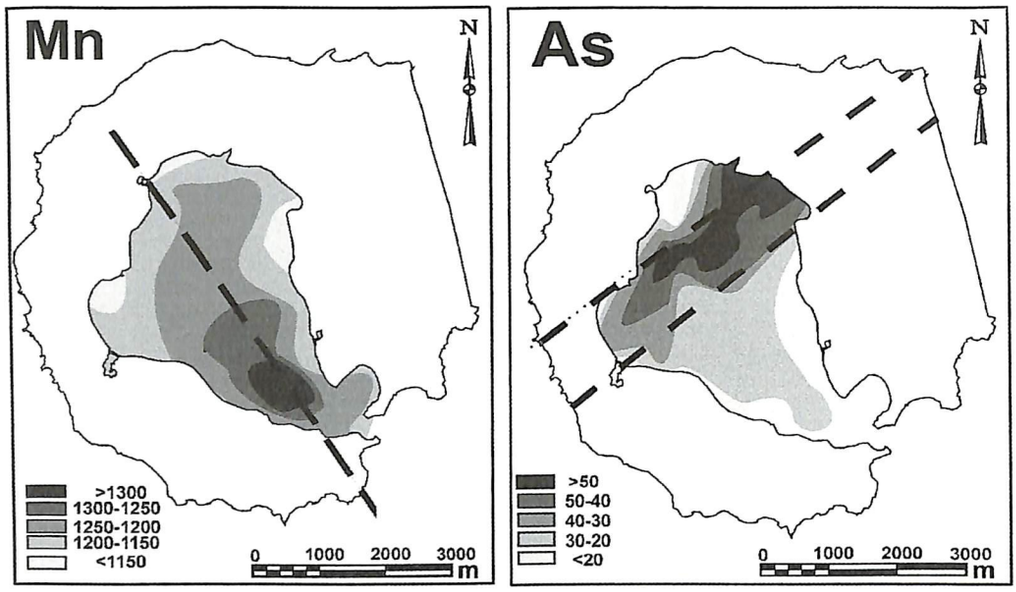

Fig. 5.14. Contoured maps showing variations of Fe and As abundances (in ppm) in dredge samples from Port Foster; the dredge sites are shown in Fig. 5.1. Note that the highest contents in Mn also coincide with the positions and NW–SE alignment of submarine volcanic cones and domes shown in Fig. 5.10; the highest contents in As reflect a NE–SW alignment comparable with the fracture system thought to be responsible for many of the long-lived fumaroles and hot springs on the island (after Rey and others, 1997).

(C1, C2) separated by an unconformity and is composed of evenly stratified horizontal sediments, and a chaotic acoustic facies that is interpreted as slumped sedimentary deposits. Unit C is affected by numerous normal and reverse faults.

Although Rey and others (1997) correlated the three seismo-acoustic sedimentary units with the lithostratigraphy proposed by Birkenmajer (1992), many problems are associated with the details of that stratigraphy (see Smellie, 2001*b*). Thus, it is safer to simply ascribe a general post-caldera age to the Port Foster sequences rather than pursue specific lithostratigraphical correlations.

Hydrothermal processes and geochemical variations

Hydrothermal activity, such as fumaroles and hot springs, is apparently associated mainly with a system of NE–SW fractures in several areas (e.g. Fumarole Bay, Pendulum Cove, former Telefon Bay and possibly Whalers Bay; Ortíz and others, 1987, 1992; Ramos and others, 1989). Those authors proposed that hydrothermal fluids are produced by venting of shallow aquifers heated convectively (to *c.* 200°C) by gases released from an underlying magma chamber.

On the basis of geochemical studies of dredge samples obtained in Port Foster, a recent mineralization system has been described, which shows significant geographical variations in element distribution patterns (Rey and others, 1995, 1997). Although the contents of these elements in the sediment samples analysed are apparently high (e.g. Fe_2O_3: 10.75%, Mn: 1361 ppm), the abundances are within the range shown by unaltered Deception Island magmas (Appendix 4). However, there are distinct NNW–SSE and NE–SW asymmetrical element-specific distribution patterns of enrichment 'anomalies', which may reflect a structural control on the positions of the fluid emissions:

1) Fe, Mn, Na and K abundances progressively decrease from Neptunes Bellows north-west into Port Foster (essentially coincident with the positions of several submarine cones and domes; Fig. 5.5), and
2) abundances of As, Al, Ca, Mg and K are greatest in a well defined SW–NE-trending zone above the northern sub-basin (Fig. 5.14).

Rey and others (1997) suggested that the formation of the two zones of contrasting element enrichments may be time controlled, but there is currently no way of dating reliably the mineralization of Port Foster sediments.

6 Volcanic hazard

by J.L. Smellie

Deception Island is an active volcano. Explosive eruptions were witnessed in 1842, 1967 and 1969, and the products of many more are documented (Chapter 3 and Appendix 3). Most visitors notice that the low-lying coastal area surrounding Port Foster contains many pyroclastic cones with conspicuous craters, representing former eruptive centres. Because they are little eroded, the cones are very young and probably erupted in historical times (i.e. < *c.* 1 000 years old). Eruptions are likely to occur again in the same area, and those eruptions represent one of the volcanic hazards represented by Deception Island that are discussed in this chapter.

A distinction exists between volcanic hazard and volcanic risk:

a) *Hazard* is a specified volcanic phenomenon that has a probability of occurring within a given period of time.
b) *Risk* is the possibility of a loss occurring caused by that hazard, e.g. loss of life or property.

Volcanic risk can also be defined by

Risk = hazard x value x vulnerability

where hazard is the probability of occurrence, value is a selected attribute such as human lives or monetary value of an area or property, and vulnerability is defined as the proportion (%) of that value likely to be lost in the event of volcanic activity. The purpose of this chapter is to describe the nature and geographical distribution of volcanic hazards on Deception Island (see inset map on BAS GEOMAP 6-A (back pocket)).

Apart from an early paper by Roobol (1982), the hazards posed by Deception Island are largely unassessed, despite its continued use during each austral summer, as a site for scientific research and as a popular tourist destination. Hazard maps and assessments are fundamental for the preparation of emergency plans designed to mitigate the impact of a volcanic eruption and save lives.

Past eruptive behaviour of the volcano

The past history of a volcano is often the best guide to how it will erupt in the future, particularly if observed eruptions and the human history associated with the volcano are limited. The eruptive history of Deception Island can be described in four major phases.

Phase 1: The earliest phase, comprising subaqueous eruptions, constructed at least 80% of the volcanic edifice and was responsible for its overall form as a volcanic shield with gentle surface gradients. Because it is entirely submerged, it has not been examined. By comparison with uplifted and exposed oceanic volcanoes elsewhere, it is inferred to be formed of pillow lava and hyaloclastite breccia, which would have formed non-explosively mainly during subaqueous effusion (Smellie, 2001*b*).

Phase 2: The shoaling and early subaerial emergence of the volcano is represented by rocks of the Fumarole Bay and Basaltic Shield formations, respectively. Those were formed by lava fountaining from several, possibly co-eruptive centres in shallow water, and a small subaerial edifice constructed during low-energy explosive eruptions and lava effusion.

Phase 3: The sudden connection of magma between two magma chambers beneath Deception Island probably triggered the caldera-forming eruption on Deception Island. That eruption is the only large-scale event known to have affected the volcano, and the eruption characteristics (dynamics, dominant lithofacies, etc) are significantly different from other eruptions on the island. Seawater probably flooded the vent, resulting in a relatively low, dense eruption column, whose collapse formed multiple pyroclastic density currents (mainly pyroclastic flows). The products of that eruption (Outer Coast Tuff Formation) draped the entire island with a minimum thickness of 70–80 m, and the present margins of the island may have been enlarged by 6 or 7 km in all directions. Collapse of the Port Foster caldera occurred at the end of the eruption. Seismo-acoustic studies have also identified large slumped sections of the submerged outer flanks of the island (and east side of Mount Pond?), which may have formed during or immediately following caldera collapse.

Phase 4: In early post-caldera time, eruptions occurred from centres widely scattered across the island, along fissures imposed on the island by regional tectonics. All later post-caldera eruptions, including all those in historical times, were confined to centres in a 1.5 km-wide annular zone within the caldera. All of the post-caldera eruptions were of small volume (e.g. < 0.05 km^3 for each of the eruptions in 1967 to 1970). Eruptions were of two types. At low elevations around the shores of Port Foster, they were highly explosive and hydrovolcanic, because of the impact of seawater and groundwater on the erupting magma. In addition to tephra fall, fast-moving pyroclastic currents (mainly surges, rarely pyroclastic flows) are

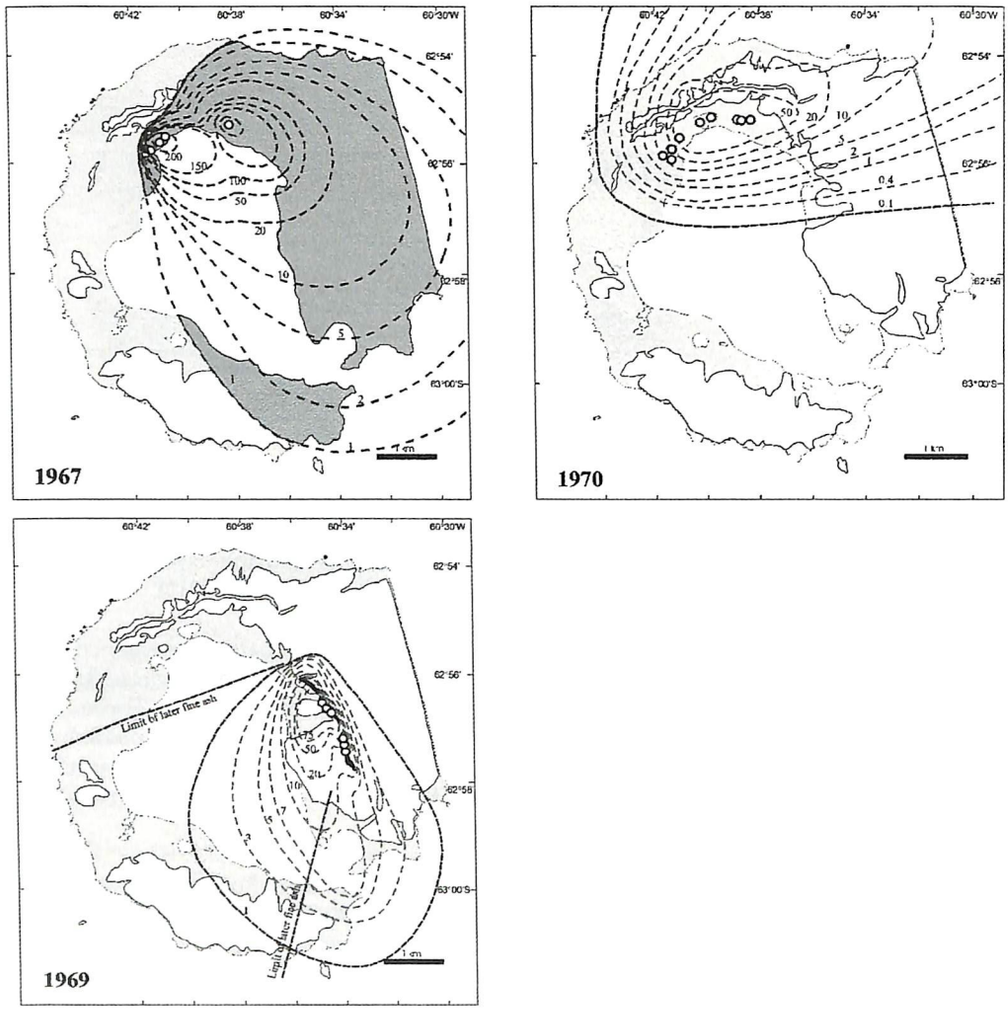

Fig. 6.1. Sketch maps showing the distribution and average thicknesses (in cm) of ash falls during eruptions on Deception Island in 1967, 1969 and 1970 (after Baker and others, 1975). Small open circles in each diagram indicate the location of the erupting centres.

characteristic of these eruptions. At higher elevations, principally around the crest of the caldera rim, eruptions were much less explosive and commonly involved lava effusion. However, eruptions from centres situated beneath glaciers at any elevation released substantial volumes of meltwater, often highly charged with debris (lahars or volcanic mudflows).

Future eruptive behaviour of the volcano

Examination of the historical record (Appendix 3) shows that the eruptive pattern appears to be one of several eruptions closely spaced in time followed by several decades of dormancy (Roobol, 1982). However, even the most detailed record, that of tephra layers in the Mount Pond glacier, may record only half the eruptions that occurred on the island during the period represented (Orheim, 1972*b*). Conversely, eruptions during the 20th Century (Appendix 3), suggest that the frequency inferred from ice tephra has probably slowed slightly from that in the late 18th and 19th Centuries (i.e. from one eruptive period every 17 years to one every 33 years). If this style of historical eruptions is continued, any new eruptions will probably be of small volume and from centres within the caldera. Both lava effusion and explosive eruptions are likely. Fallout of tephra will probably only affect those parts of the island down-wind of the centres, as occurred during the 1967–1970 eruptions (Fig. 6.1). However, the presence of Deception Island tephras dispersed > 800 km (in the Scotia Sea; Moreton and Smellie, 1998)) suggests that some post-caldera eruptions may have been much more violent than experienced in recent centuries.

The discovery of significant present-day inflation of the sea floor in part of Port Foster suggests the possibility that the caldera may be resurging, raising the possibility of another caldera collapse and associated large-scale eruption (Cooper and others, 1998). Seismo-acoustic studies of Port Foster also suggest that there has been step-like deformation of the caldera floor in the past related to resurgence, although there is no known link to coincident eruptions (Chapter 3). The eruptive style and probability of occurrence of eruptions related to a further caldera collapse are hard to assess. The first (and only known) caldera-forming eruption was apparently triggered by the interaction of two magmas, and the probability of a similar event recurring is probably very low. In addition, explosivity during an eruption within Port Foster will probably be reduced by hydraulic pressure and water

flooding the vent, until the vent is built to very shallow levels. Finally, so long as small eruptions take place around the caldera margins, it seems likely that pressures in the magma chamber will be relieved and prevent a climactic caldera collapse eruption.

Types of volcanic hazards identified

Note: *the volcanic activity described below is that which is most likely to pose a significant hazard to persons and vessels on and around Deception Island. It is not a catalogue of all volcanic phenomena that may occur. A summary hazard map is included as an inset in BAS GEOMAP 6-A accompanying this booklet.*

Ash fall: During an explosive eruption, the magma is torn apart by the expansion of dissolved gases. Particles of the magma are thrown into the air as ash, pumice and lapilli, where they freeze and fall to the ground. Larger particles follow ballistic trajectories close to the vent (normally within a few hundred metres), but finer particles (mainly ash, smaller lapilli and pumice) are entrained in the eruption column above the vent. The column (or plume) typically reaches elevations of several km very rapidly, and may exceed 10 km. It is driven mainly by expanding heated air and it drifts downwind. Because prevailing winds on Deception Island are mainly from the west (> 50% of winds; Hydrographic Department, 1974), the eastern side of the island is at greatest risk from the effects of ash fall. However, in the three best-documented eruptions, between 1967 and 1970, very little of the island escaped at least some ash fall (Fig. 6.1; Baker and others, 1975). In documented eruptions of Deception Island, the columns probably rose < 10 km, unlike much higher columns at other volcanoes. The ash and other particles fall out of the cooling drifting cloud, with larger particles and thickest deposits closest to the vent. Such fall deposits can extend many tens to hundreds of kilometres. For example, ash from the 1970 eruption fell on King George Island, > 150 km away (Baker and others, 1975), and numerous layers of Deception Island ash are preserved in marine sediments in the Scotia Sea, > 800 km distant (Moreton and Smellie, 1998). Close to the erupting vent, a thick accumulation of ash can be very hot and heavy, causing severe damage to wooden buildings. For example, the abandoned Chilean station at Pendulum Cove was buried and burned down as a result of falling ash from the 1969 fissure eruption, the closest vents being situated 400–500 m away. Otherwise, ash fall and ballistic projectiles endanger people by impact, burial, causing ingestion of fine particles in air and water, and carrying noxious gases, acids and salts.

Pyroclastic currents: These are amongst the most hazardous of volcanic events. They vary widely but share many characteristics. All are gravity-driven, rapidly moving, ground-hugging or inflated mixtures of hot rock fragments and gases. Two main types are often distinguished, *flows* and *surges*. Pyroclastic flows have a relatively high concentration of solids, whereas pyroclastic surges have lower solid concentrations. Laterally-directed blasts (as occurred in the 1980 Mount St Helens eruption) are a third possible category of pyroclastic current, formed where depressurisation of a magma chamber is precipitated catastrophically by a mountain landslide, but it is probably an unlikely occurrence on Deception Island. A continuum probably exists between these three types of pyroclastic currents. Pyroclastic currents are often very hot (300–>800°C) and move at high speeds (10 to several hundred metres per second). Pyroclastic flows consist of a dense basal flow that hugs the ground, together with a preceding or overriding turbulent ash-cloud surge. Convection of ash particles from the moving current can also distribute falling ash. Investigations on the island indicate that pyroclastic flows occurred but have been uncommon during most of the history of the volcano; they were abundant only during the caldera-forming eruption (Outer Coast Tuff Formation). Conversely, pyroclastic surges are the most characteristic feature of many Deception Island eruptions. Surges typically travel faster than pyroclastic flows. Unlike pyroclastic flows, which will be restricted by topography and flow in valleys, the more-expanded hot gas and ash mixtures in surges can flow across topography. On Deception Island, mapped surge deposits only extend about 1.5 km from known vents. They can travel much farther, but on Deception Island are unlikely to form a serious threat > 2 km from vents, *in most cases*. Although some surges may be hot, similar to pyroclastic flows, most of those on Deception Island were probably relatively cold and contained water and/or steam at temperatures mainly below the boiling point of water. Any eruptions within or at low elevations around the margins of Port Foster are likely to be characterised by abundant pyroclastic surges. It should be noted that pyroclastic currents can travel across water. Death is likely for people caught up in a pyroclastic current.

Lava flows, lava domes and lava fountains: Erupting magma that has lost most of its gases forms lava flows, domes and/or lava fountains. Eruptions of this type on Deception Island probably occurred at low effusion rates, and the lava tended to produce many small flows that piled up near their vents and did not extend long distances. Conversely, larger-volume eruptions of lava created lava flows that mantled the south and west coasts and parts of Kendall Terrace. Lava fountaining is common throughout the eruptive history of the island. The first eruption observed, in 1842 by the sealer Smiley (Wilkes, 1845), was probably of that type. Conversely, lava domes are unknown on Deception Island, but they may occur in future. Domes usually form from relatively viscous magma, and their sudden collapse can generate hot rock-falls or even small pyroclastic flows and/or surges. The major hazard from lava flows is damage or destruction by burying, crushing or burning everything in their paths. They are confined in valleys and can be easily outrun. Lavas can also cause floods by melting snow and ice, but the interaction is usually not explosive. Where lavas enter lakes or the sea, they commonly form low platforms known as lava-fed deltas (e.g. Punta de la Descubierta, headland south of Entrance Point, South East Point). Lava-fed deltas are very common in oceanic volcanoes and are being constructed currently in an eruption on Hawaii. Apart from a tendency for large slabs (hundreds of metres in extent) of the upper surface of a platform to collapse into the sea, and for small explosions between hot lava and seawater, they are generally not very dangerous.

Structural collapse and rock falls: Volcanoes are susceptible to large-scale structural collapse due to steep volcanic slopes containing weak materials, and presence of faults. Slope failures, including rock falls, slides, avalanches and sector collapse, can be triggered suddenly and move very rapidly. They can cause secondary hazards such as tsunamis and even unleash eruptions (*cf.* Mount St Helens, 1980). On a smaller scale, rock falls in strategically important places can cause major problems. For example, the collapse of Cathedral Crags could easily block Neptunes Bellows and prevent ship egress to/from Port Foster.

Hydrothermal eruptions: Because Deception Island is an island, with lakes and a large area covered by glaciers, water is important. It is heated by magma at depth, and returns to the surface in steamfields, fumaroles and hot pools (see below). The process is illustrated in the pattern of seismic activity, which shows peak activity in days following heavy snowfall or rain (Almendros and others, 1997; Villegas and others, 1997). However, in hydrothermal systems, the hot water can flash to steam, perhaps triggered by earthquakes fracturing the volcano, and cause small but powerful explosions. Damage from hydrothermal eruptions is unlikely to extend more than a few hundred metres from the vent. Such explosions may occur without warning, but they are probably rare on Deception Island.

Volcanic gases: Volcanic eruptions are driven by expanding gases, mainly water and carbon dioxide, but including poisonous minor gases such as sulphur dioxide, hydrogen sulphide, chlorine and fluorine. These gases are also emitted from fractures in the ground between eruptions. They can also be very hot. For example, gases with measured temperatures exceeding 250°C were recorded in fumaroles 10 months after the 1967 eruptions (Orheim, 1970). They are usually only present in toxic amounts very close to vents, particularly the heavy gases (e.g. carbon dioxide and hydrogen sulphide) in poorly ventilated craters. Deception Island is a windy place and its craters are comparatively shallow and well ventilated. Noxious volcanic gases are therefore likely to be a minor hazard.

Steamfields, fumaroles, heated ground: Deception Island contains several areas of heated ground, etc, which are a conspicuous and normal surface expression of heat escape on the island. All but one are confined to the caldera, and they are long lived (Baker and others, 1975; Roobol, 1980). They are mainly situated around the shores of Port Foster, but examples occur on the summit of a hill 500 m north-west of the Argentine station, at the north end of the Mount Pond ridge, and on the outer slopes west of Stonethrow Ridge. Temperatures of most are < 40–60°C, but a beach pool at Pendulum Cove commonly reaches 70°C and fumaroles at Fumarole Bay are generally 100–107°C. Temperatures fluctuate daily, typically in response to tides. Sudden subsidence of the sea floor beneath Whalers Bay in 1920–21 also caused the sea to boil and blistered the paint on ships' hulls (Hydrographic Department, 1974; Appendix 1). In addition to the possible presence of noxious gases and hydrothermal explosions, people may be scalded by unprotected exposure to steam or very hot water (e.g. Pendulum Cove).

Lahars and floods: A lahar is a moving mixture of volcanic debris and water. It may be hot (few hundred °C) or cold. Lahars on Deception Island are likely to be cold. The physical properties of lahars are controlled by grain size and water content, but they typically have relatively high yield strength, bulk density and apparent viscosity. With variable sediment bulking, flow transformations between lahars and watery floods occur. Flow velocities vary greatly according to channel dimensions, volume and grain size distribution; published examples vary from 1.3 to 40 m/sec, with mean values of about 20–30 m/sec (Blong, 1984). Lahars moving at high velocities can surmount topographical barriers. They are generated in several ways, including expulsion of sediment from crater lakes, and avalanching of water-saturated debris during slope failure or bursting of dams. Pyroclastic currents can transform into (hot) lahars by incorporation of meltwater from snow and ice. Because of their high bulk density and velocity, lahars destroy and/or bury structures in their path, as happened to the British scientific station at Whalers Bay in the 1969 eruption on Deception Island (Baker and others, 1975). Lahars have sharply defined topographical limits (i.e. valley confined) and people can usually climb quickly to safety away from areas threatened by lahars. They are a characteristic feature of meltwater floods associated with subglacial eruptions and are likely to have affected Deception Island frequently in the past (Smellie, 2002). For example, the prominent deep and broad flat-bottomed valley situated about 0.5 km west of Crater Lake is carved through thick ash deposits. The valley contains a misfit stream (i.e. a stream too small to have eroded the surrounding valley), which is sourced in the steep backing caldera cliff. It is likely that the valley was eroded mainly during a flood of meltwater released by an eruption beneath the Mount Kirkwood glacier.

Earthquakes: Volcanic earthquakes on Deception Island are generated by explosions, movement of lava, heated water and gases at depth and associated crack formation, and large-scale mass movements (e.g. Correig and others, 1997). Tectonic forces may also affect Deception Island and are caused by plate movements associated with deep consumption of Pacific Ocean floor at the South Shetland trench and plate separation in Bransfield Strait. It can often be difficult to distinguish between the different earthquake mechanisms. Volcanic earthquakes are typically small and shallow, seldom exceeding magnitude 5 on the Richter scale. During January 1992, unusually high seismicity on Deception Island included several magnitude-3 events. These are the largest recorded so far and can be detected by persons in favourable locations on the island without the use of instruments. Conversely, tectonic earthquakes or large mass movements can exceed magnitude 7. Damage caused by earthquakes is typically restricted to proximal areas, as a result of ground shaking and cracking. The earthquakes can also trigger mass movements that may lead to avalanches, rock falls and lahars. Many eruptions are preceded by increased seismicity (i.e. number, magnitude and duration of

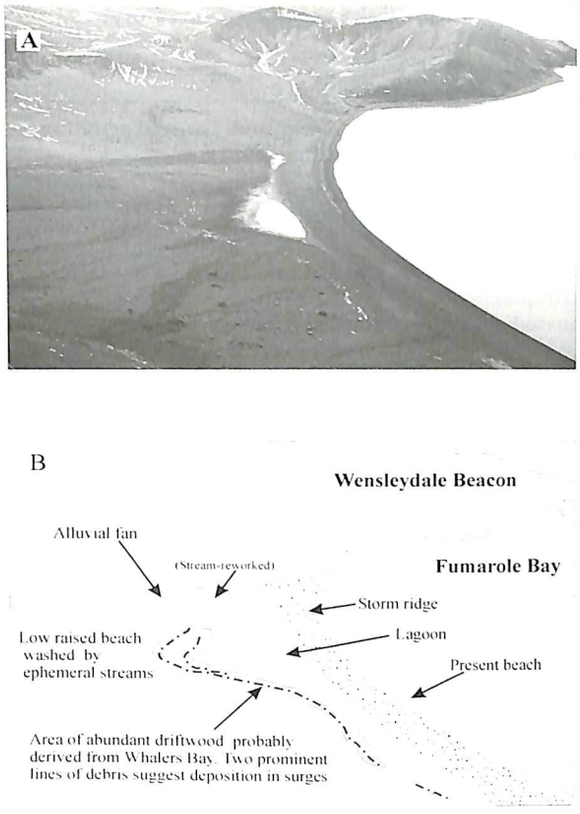

Fig. 6.2. View looking north to Wensleydale Beacon (A) and sketch (B) showing distribution of abundant driftwood on raised beach area facing Fumarole Bay. The driftwood was probably driven ashore by tsunami surges during the 1969 eruption. Photograph taken by the author in February, 1994.

earthquakes) and it is a useful, if crude, indication of impending eruption (e.g. 1969 eruption on Deception Island; Baker and others, 1975; Smellie, 2002).

Tsunamis and standing waves: Tsunamis are unusually high sea waves or wave trains that are generated by the sudden displacement of water caused by fault displacements of the sea floor, large mass movements of the land, or some submarine eruptions. They travel at high speeds through deep water and increase in height when approaching shores. Tsunami triggered by eruptions and slope failures have occurred at Deception Island in the past (Fig. 6.2), with consequences for ships both outside the island and in Port Foster. Because Port Foster is virtually landlocked, volcanic explosions and sea floor movements within the basin can set up oscillatory standing waves. Waves oscillating at least 1.5 m were recorded during the 1967 eruption and made small boat operations hazardous (Baker and others, 1975); this is especially true in the narrow shallow channel at Neptunes Bellows.

Suggested alert scheme for eruptions on Deception Island

No alert scheme has been published for Deception Island although, in view of the comparatively high levels of human activity on the island (by Antarctic standards, at least), one is clearly needed. For an alert scheme to be put in place, a seismic network should be placed immediately around the volcano and monitored throughout the year by trained scientists. On Deception Island, this is currently not the case. However, Spanish seismologists monitor seismographs on the island for about two months annually (generally between late December and late February). As that period also corresponds to the major period of tourist activity on the island, it is probably acceptable as a minimum level of volcano monitoring, and it is certainly much better than no monitoring at all. The simple scheme presented in Table 6.1 is adapted from that used by the Alaska Volcano Observatory (U S Geological Survey; http://www.avo.alaska.edu/avo4/updates/color_code.html). It is well suited to Deception Island and is recommended. Captains of vessels proposing to enter Deception Island, or pilots of aircraft flying near to the island should pay attention to any bulletins on the current state of activity of the volcano that are issued from either the senior seismologist at the Spanish station on the island, or by an appropriate spokesperson representing a recognised scientific authority operating in the Antarctic (e.g. British Antarctic Survey, Spanish Antarctic Programme or National Science Foundation (USA)).

Escape strategy in case of a volcanic eruption on Deception Island

In view of the wide range of volcanic hazards identified above, and with the increasing numbers of tourists now visiting Deception Island, it is important to identify escape routes on the island in case of a sudden volcanic eruption. The following escape strategy could form the basis for a more comprehensive strategy for the island. This section is based on the premise that eruptions will be similar to those documented in 1967–1970, i.e. with a limited geographical impact on the island (code orange alert state; Table 6.1). Nevertheless, a sudden collapse of the caldera could result in a much more serious eruption, with potentially devastating effects on anyone on the island at the time and a low probability of escape. However, the likelihood of caldera collapse is very low and such an event would probably be preceded by significant precursory activity, particularly widespread ground inflation and associated earthquakes, during several days or weeks prior to the eruption.

1. Inner coast areas are likely to be hazardous because of ash fall, possible pyroclastic surges (within *c.* 2 km of an eruption centre), tsunami and irregular rapid tidal oscillations. Tidal effects are likely to be pronounced by water ramping onto beaches, and they may prevent the use of inner coast beaches for boat uplift. People may therefore have to be uplifted from the outer coast.
2. If ships are present within Port Foster when an eruption occurs, they should depart the island immediately, ideally after uplifting all people ashore. Masters of vessels should observe extreme caution whilst departing Neptunes Bellows because of tidal rips and surges, which are enhanced at the narrow shallow entrance channel. They should also avoid routes that skirt close under Cathedral Crags, because of the possibility of rock falls from the unstable cliffs.

Table 6.1. Alert scheme for eruptions on Deception Island (modified after system used by USGS Alaska Volcano Observatory)

Colour code	*Alert state*	*Description*	*Action*
GREEN	**No eruption is anticipated**	Volcano is quiet, in dormant state. Normal seismicity and fumarolic activity occurring. This is the normal alert state for Deception Island	None required. Normal activities unrestricted
YELLOW	**An eruption is possible in the next few weeks and may occur with little or no additional warning**	Volcano is restless; an eruption may occur. Increased levels of small earthquakes detected locally and/or increased volcanic gas emissions. An example of a code yellow alert state occurred in January 1992, when the area around the Argentine station experienced ground inflation of 20 cm, increased ground and seawater temperatures and a much increased incidence and magnitude of shallow earthquakes caused by magma movement (unpublished report by Ortiz, Garcia and Risso, 1992)	Normal activities may occur on the island but no vessels to leave persons ashore unattended. Vessels to remain near shore parties at all times
ORANGE	**Explosive eruption occurring or is possible within a few days and may occur with little or no warning. Ash plume(s) not expected to reach 10 000 m above sea level**	Volcano in eruption or eruption may occur at any time. Increased numbers and/or magnitudes of local earthquakes. Extrusion of lava flows (non-explosive eruption) may be occurring. The Deception Island eruptions of 1839, 1842 and 1967 to 1970 correspond to a code orange alert state. Those eruptions were comparatively small, ash plumes probably only reached a few km in elevation and evacuations took place successfully; no lives were lost	All persons to depart the island immediately. No vessels to enter Port Foster. All aircraft to give the island a wide safety margin. Vessels and/or aircraft may usefully remain within a few miles of the island (well away from any volcanic plumes) to observe and record the eruption, taking all necessary precautions. These restrictions to remain in force until advised that the island has returned to a code **green** alert
RED	**Major explosive eruption is in progress or expected within 24 hours. Large ash plume(s) expected to exceed 10 000 m above sea level**	Significant eruption is occurring or major explosive activity expected at any time. Strong earthquake activity detected even at distant monitoring stations. The only eruption of Deception Island that definitely corresponded to a code red alert is the caldera collapse eruption (date unknown). However, numerous eruptions have distributed volcanic ash more than 800 km away, in the Scotia Sea, and were probably sufficiently violent to have had plume(s) exceeding 10 000 m and to be accorded a code red status	All persons to depart from the island immediately, although code red eruptions likely to destroy all life on much or all of the island very quickly. No vessels or aircraft to come closer than 50 km from the island (or further if conditions dictate). These restrictions to remain in force until advised that the island has returned to a code **green** alert

3. All rescuing vessels and helicopters should avoid passing through or under the eruption clouds because of the damaging effects of gritty ash particles on machinery.
4. Escape routes to the outer coast of the island are shown in Fig. 6.3. All escape routes from the inner bay to the outer coast are strenuous, both climbing up on to the caldera rim and (in most cases) descending again on the outside. The caldera wall is steep (impassable cliff in places) and draped in highly mobile scree. It is impossible to use ground vehicles (e.g. ATVs) to transport people out of the caldera. Although exit routes are passable for ATVs at two places, much skill and local knowledge of the routes are required and the routes are impassable to ATVs carrying a passenger.
5. All routes to the outer coast will take hours to complete, ranging from about two hours for the easiest route (Whalers Bay to Baily Head) to three or four hours (or more) if the unnamed bay on the north coast or at Macaroni Point are the only options. These are minima and based on times likely to be taken by young relatively fit persons. The routes are physically arduous as most surfaces are yielding (mainly composed of coarse ash and lapilli). Exhaustion is likely and should be anticipated, even in fit persons.

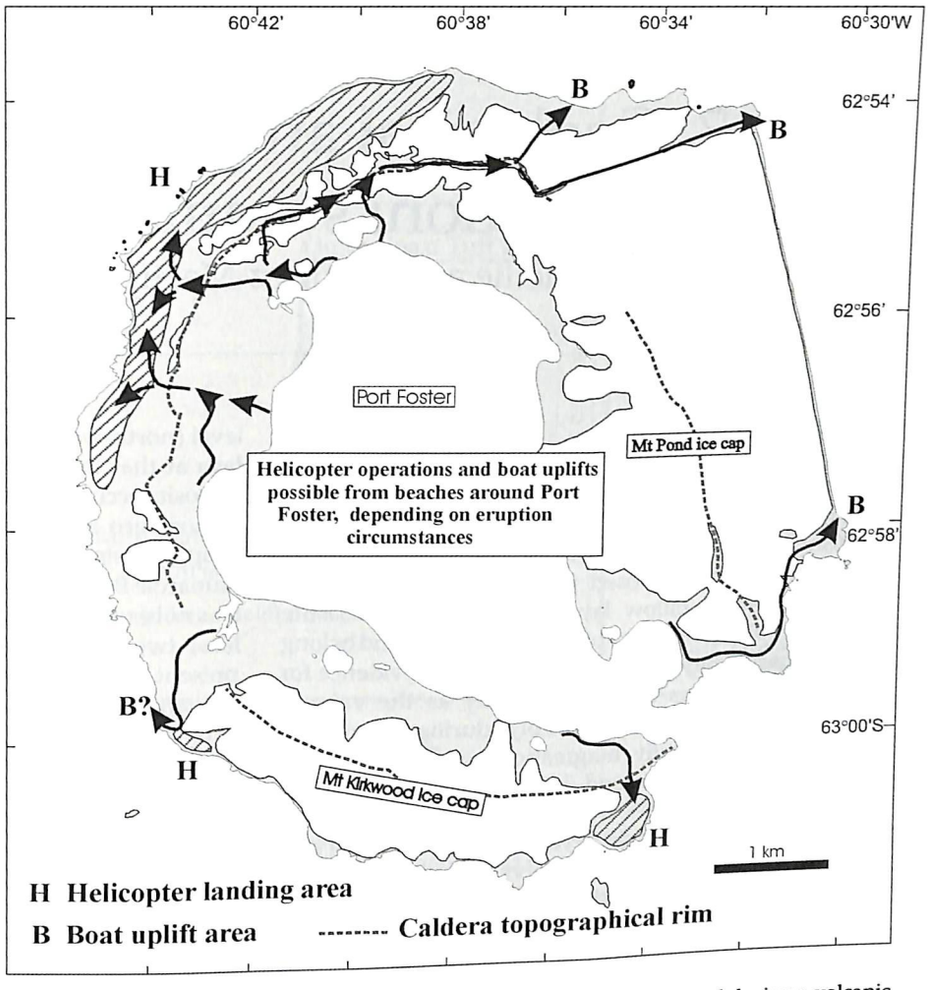

Fig. 6.3. Sketch map showing suggested escape routes on Deception Island during a volcanic crisis corresponding to no more than a code orange alert state. Although helicopter uplifts can probably be effected, with variable difficulty, almost anywhere, the best areas are indicated on the diagram by hatching. Note that all routes are physically exhausting for most persons.

Descending to beaches on the outer coast is also generally difficult because of steep slopes. Apart from routes shown from Goddard Hill to Macaroni Point and the unnamed bay on the north coast (Fig. 6.3), there are no recommended safe routes over snow and ice. Because of important difficulties peculiar to glaciers (e.g. crevasses, whiteout, slippery surfaces), other glacier travel should be avoided unless with trained guides using suitable equipment (e.g. ice axes, ropes, harnesses). Such equipment is unlikely to be readily available in an emergency.

6. Helicopter uplifts are usually the best option as most of the outer coast beaches are narrow, bouldery and shelve steeply into deeper water, causing beach surf even on calm days. Some beaches (e.g. north of Punta de la Descubierta) also have a submerged offshore bar hazardous to small boats. If wind conditions are suitable, it may be possible to uplift people by helicopter from the inner coast. The most appropriate action can be judged at the time. The best sites for uplift by helicopter are shown in Fig. 6.3.

7 Geological and geomorphological evolution: summary

by J.L. Smellie and J. López-Martínez

Geological evolution

The early history of Deception Island is essentially unknown. About 80% of the island is below sea level and therefore inaccessible but it has a low-profile and, by analogy with better-exposed volcanoes, it is likely to be formed largely of pillow lava and coeval hyaloclastite breccia. The oldest deposits preserved on the island belong to the Fumarole Bay Formation. They show evidence for possibly subaqueous explosive activity as the volcano approached sea level and, possibly, during emergence. Eruptions were initially magmatic, broadly resembling pyroclastic deposits formed in subaerial Hawaiian or Strombolian eruptions. However, there is abundant evidence for a subaqueous environment in the basal unit (lava lobe member), and several unusual clast characteristics of the overlying scoria member can be interpreted as evidence for subaqueous fire-fountaining activity. The gradual upward transition into the stratified lapilli tuff member, interpreted as a tuff cone capping sequence, is compatible with shoaling and likely emergence of the vents. The coarse grain size of the dominant scoria member deposits, and presence of very large bombs, indicate that the deposits are proximal to the original eruptive centres and that multiple centres were involved. At one locality (Cathedral Crags), at least two vents were co-eruptive, but the isolated nature of the other outcrops makes it impossible to ascertain contemporaneity of Fumarole Bay Formation eruptions across the island. It is likely that, during the shoaling and emergence phase, Deception Island consisted of several small coalesced centres broadly similar in concept (but not in outcrops) to the polygenetic pre-caldera edifice envisaged by Hawkes (1961), rather than the single tall stratocone postulated by other workers (e.g. Baker and others 1975; Birkenmajer, 1992; Martí and Baraldo, 1990).

If the interpretation of the Fumarole Bay Formation is correct, it indicates that sea level was relatively high during the shoaling and emergent stage of the volcano, and had an elevation > 100–150 m above present datum (Fig. 7.1). Alternatively, eruptions may have taken place within a water-filled subglacial vault, but there is no clear evidence for the presence or extent of any glacial cover during that period. By contrast, the succeeding Basaltic Shield Formation consisted of essentially dry effusive and weakly pyroclastic activity that was entirely subaerial. It constructed a small basaltic shield volcano with an original basal diameter inferred to be about 8 km. Although outcrops of the Basaltic Shield Formation crop out at sea level (north-west outer coast), it is uncertain whether the lava at that locality was subaerial. The lowest subaerial deposits occur at c. 70 m above sea level in the caldera wall in northern Stonethrow Ridge, indicating that sea level dropped significantly after the activity forming the Fumarole Bay Formation. The small shield volcano (which was not exclusively basaltic) experienced eruptions from at least two centres, with a more distant centre (within present-day Port Foster) responsible for the lower sequence, and a proximal centre (probably a small flank vent relative to the earlier centre) forming the upper sequence. Had the centres in the Fumarole Bay Formation continued in their activity, it is likely that they would have evolved into overlapping subaerial effusive shields similar to that forming the Basaltic Shield Formation.

Tephra of the succeeding Outer Coast Tuff Formation (OTF) is draped unconformably over both the Fumarole Bay and Basaltic Shield formations and there is some evidence in Stonethrow Ridge that it thins over topographic highs. The OTF is the most geographically widespread formation, and outcrops suggest that it formerly draped the entire island to a minimum depth of 70 m. The formation contains no lavas and it is entirely formed of tephra deposited from a variety of pyroclastic currents, mainly dense pyroclastic flows. There was significant involvement of water with the eruption and the eruption columns were probably low, dense and collapsed frequently, resulting in multiple pyroclastic currents and their deposits. Evidence for at least two compositionally different magma series involved in the eruption suggests that influx of fresh magma to a stratified magma chamber may have been responsible for destabilising that chamber and possibly acted as a trigger for the OTF eruption. The eruption was followed by collapse of the Deception Island caldera. Although the mass of the eruption is unknown because of extensive erosion of the deposits, a minimum volume of about 30 km^3 is inferred from the size of the caldera. Such a volume would have been capable of extending the coastline of the island by 6 or 7 km in all directions, at least (calculated assuming (unrealistically) that a thickness of 70 m is maintained). Because evidence for water interaction during the eruption is present throughout the OTF, it implies that a large volume of water was involved, which presumably could only be seawater. This suggestion is supported by a study of the alteration mineralogy (Martí and Baraldo, 1990). Such an interpretation suggests that the OTF vent(s) were below sea level at the time, and it is even conceivable that the eruption columns were largely subaqueous. The tops of

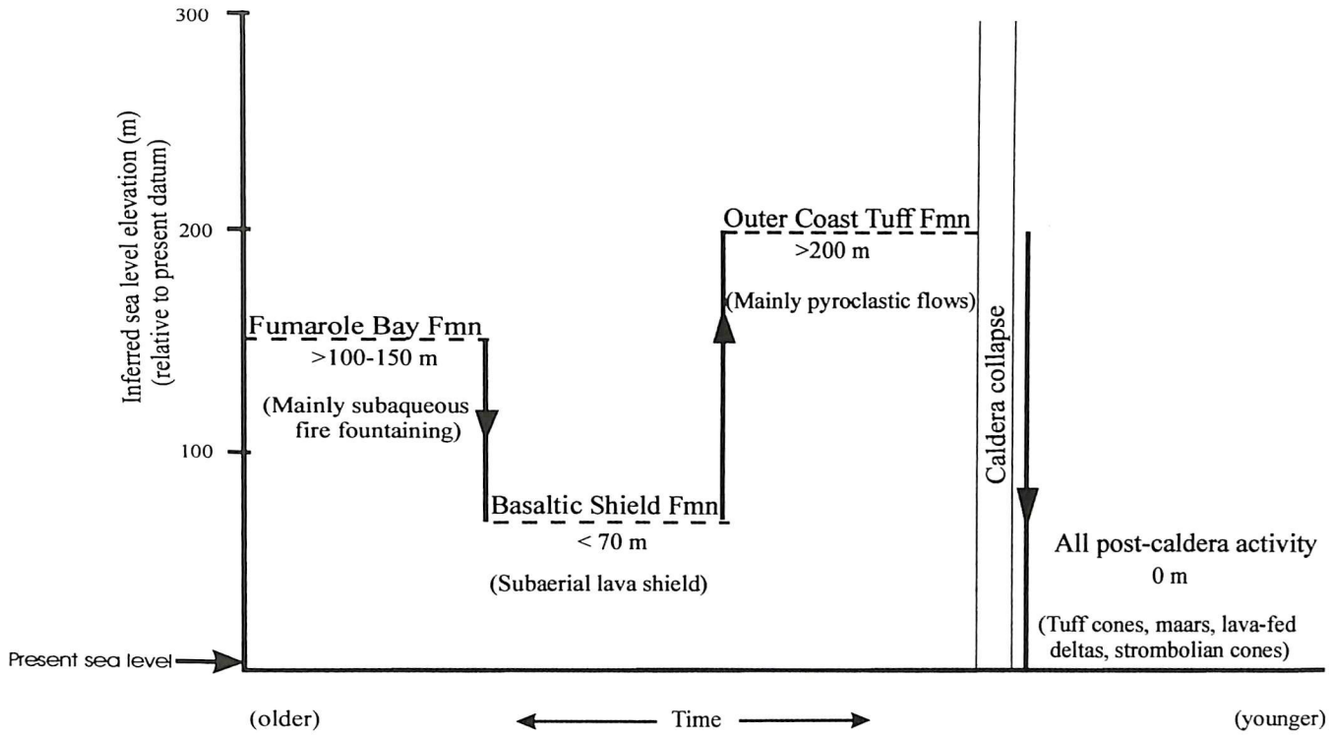

Fig. 7.1. Schematic diagram showing changes in sea level at different times during the lifetime of Deception Island. Elevations are relative to present datum and are minima, calculated from inferred elevations of vents associated with each of the stratigraphical units (see text). The changes are likely to have been caused by a combination of eustasy, volcano tectonism and regional tectonics, the relative influence of which is unquantified at present.

the highest outcrops in the caldera wall occur today at about 200 m elevation. As the deposits were formed from pyroclastic gravity flows, that gives a minimum elevation for the erupting vent, which in turn suggests that relative sea level had risen at least 130 m since eruption of the preceding Basaltic Shield Formation.

The nature of the caldera collapse (e.g. whether piecemeal, trapdoor or chaotic) has not been examined in detail. However, there is substantial evidence that regional tectonics have exerted a significant influence on the island, in the distribution of linear fractures, faults and eruptive fissures (Smellie 1989; Rey and others, 1992, 1995; Martí and others, 1996). Together with the distribution of present-day seismic activity, which shows no caldera-related annular distribution of epicentres (Vila and others, 1992), these observations have led to the hypothesis that the caldera may be simply a topographical feature caused by collapse of the volcano summit due to instability within an extensional tectonic regime - i.e. a passive response unrelated to a caldera-forming eruption (e.g. Martí and others, 1996). However, a link to volcano tectonics and a large caldera-forming eruption also seems plausible based on studies by Smellie (2000), and it is likely that an interplay between regional and volcano-induced stresses has acted on the island. Seismic studies within the caldera suggest that the caldera is resurgent and the underlying surface of pre-caldera rocks has undergone repeated vertical movements (*cf.* Fig. 3.24; Cooper and others, 1998). Moreover, the presence of at least three morphological sub-basins within Port Foster (Cooper and others, 1998) suggests the possibility of unsystematic multiple collapse episodes or nested sub-calderas.

Early pyroclastic activity within the caldera formed tuff cones, indicating that eruptions were hydromagmatic and that the caldera was flooded with seawater soon after collapse. For the caldera to become flooded indicates that the encircling caldera wall must have been breached to permit the sea to flood in. There is seismic evidence for collapse deposits (slides, slumps) on the submerged south-eastern outer flanks of the island (Acosta and others, 1992), and early post-caldera sector collapse probably created the large horseshoe-shaped scar east of Mount Pond, now covered by the Mount Pond glacier. In addition, there are prominent topographical lows in the encircling caldera ridge, which may correspond to breached sections (e.g. at Vapour Col and between Goddard Hill and Mount Pond). These are now partly occupied by post-caldera tuff cones. The presence of tuff cone relicts (Baily Head Formation) at those localities indicates a very early post-caldera age for the formation of the breached sections.

The post-caldera volcanic activity consists of numerous small-volume eruptions from centres scattered across the island, both within and outside of the caldera. Roobol (1982) estimated that the 1967, 1969 and 1970 eruptions each ejected only < 0.05 km^3 of pyroclastic products. The eruptive behaviour is related to the local hydrology, with magmatic eruptions from small fissure-related scoria cones along the topographical rim of the caldera and on the outer slopes of the island, and tuff cones and maars situated at lower elevations (Baker and others, 1975). There has been

a marked focusing of the post-caldera activity to within the caldera in historical times, at least (Pendulum Cove Formation and Stonethrow Ridge Formation (Mount Kirkwood Member)). Magmatic activity has also created several prominent lava platforms, mainly around the south-east and south-west outer coast. These are probably the subaerial carapaces of lava deltas, corresponding to 'topset beds' in sedimentary deltas, whose lavas were sourced in vents situated on the backing caldera ridge. The lava platforms probably overlie thick deposits of cogenetic hyaloclastite breccia disposed in steep-dipping foreset beds. Effusive activity was particularly important on the outer slopes of Mount Kirkwood, extending all the way between Punta de la Descubierta and Entrance Point, a distance of more than 8 km.

Unusual slump deposits in a Stonethrow Ridge Formation outcrop on the north outer coast (2 km west of Macaroni Point) show evidence of wet emplacement, which may indicate that sea level was a few tens of metres higher than present during their formation. By contrast, all other post-caldera activity can be related to a sea level essentially indistinguishable from present datum. Eustatic sea level has varied continuously throughout the Phanerozoic (Haq and others, 1987) and to expect that the several post-caldera outcrops were erupted at significantly different times, when sea levels fortuitously happened to be at coincident elevations, seems to stretch credibility. Rather, it seems likely that these post-caldera outcrops are very young (<< 10 000 years?). It is also notable that the range in sea level elevations interpreted for both pre- and post-caldera outcrops (> 200 m; Fig. 7.1) is probably outside of the range of variations that can easily be ascribed to fluctuating eustatic sea levels (probably < 100 m; Haq and others, 1987). Therefore, the changes in relative sea level inferred for Deception Island probably also include volcano-tectonic and/or regional tectonic effects, which are unquantified at present.

Basalt magma has been available repeatedly throughout the history of the volcano, but more evolved compositions are commoner in the younger deposits (Pendulum Cove Formation and Mount Kirkwood Member of the Stonethrow Ridge Formation). There is a wide compositional range in many individual eruptions, suggesting that the eruptions were sourced in compositionally well-stratified magma chambers. The repeated eruption of basaltic magmas, together with small-volume eruptions showing a wide range of compositions, suggest that a large melt accumulation zone, broadly basaltic in composition through repeated replenishment, may exist at depth and is feeding several relatively small shallow magma chambers. The latter are the source of most or all of the post-caldera eruptions.

Geomorphological evolution

As an active volcano with a complex geological history and a Quaternary age (< 0.7 Ma; Valencio and others, 1979; Keller and others, 1992), Deception Island has changed its morphology progressively with time. It is often not easy to reconstruct the succession of original primary landforms and their locations due to the lack of unambiguous field evidence. According to Smellie (1988, 1989), the submarine (inaccessible) part of the present edifice represents about 80% of the volume of the volcano. There is no direct morphological evidence of the shape of the older volcano during its submarine period, but deductions can be made for the later-submarine to early subaerial phase by interpreting the stratigraphical succession preserved on the island today. Most authors have interpreted the early edifice as a single large stratocone (e.g. Holtedahl, 1929; Martí and Baraldo, 1990; Birkenmajer, 1992). However, the most recent study (Smellie, 2001*b*) suggested that the pre-caldera outcrops consist of the products of several relatively small, overlapping and probably co-eruptive centres superimposed on the larger submarine construct, not dissimilar in concept to the early polygenetic edifice envisaged by Hawkes (1961).

The period of predominantly submarine activity was followed by a large-volume catastrophic eruption characterised by the generation of multiple pyroclastic flows. Deposits of the eruption draped the edifice and may have extended it laterally by several km compared with the coastline of the island today. The prominent shallow (< 100 m) submarine platform, that is particularly well-developed north and west of the island, was probably cut across products of that eruption. That climactic event was followed by caldera collapse (Holtedahl, 1929), along fractures that may already have been induced on the island by regional tectonics related to its location in an actively extending young marginal basin (Smellie, 1988, 1989; Martí and Baraldo, 1990; Rey and others, 1992, 1995; Martí and others, 1996). The shallow submarine basin of Port Foster probably formed very soon after caldera collapse, by marine inundation via gaps in the caldera ring created by local sector collapse. Subsequently, all known post-caldera eruptions have been small in volume and ranged from lava effusion (sometimes feeding conspicuous lava-fed deltas where the lavas reached the coast) to multiple small cones of Strombolian, Surtseyan and maar-types (Chapter 3).

Evidence exists of numerous eruptions during the 19th and 20th centuries. They are preserved mainly as tephra layers within the island's ice caps (Orheim, 1972*a*,*b*). The first eruption observed, in 1842, affected the "whole south side" of the volcano (Wilkes, 1845). It produced a line of small cinder cones on the northern slopes of Mount Kirkwood (identified by Hawkes, 1961, and dated (lichenometric method) by Birkenmajer, 1991). By contrast, the sources of several close-spaced eruptions between 1906 and 1912 (Appendix 3), represented as tephras in ice, are unknown despite their very young age coinciding with the period of summer occupation by the whaling industry. In general, the sources of vents on the island responsible for the numerous tephra layers in ice are unknown.

The best known geomorphological changes on any part of Deception Island are those due to the eruptions of 1967, 1969 and 1970. Those eruptions were entirely explosive and formed several tuff cones, maars and lahars, with consequent major topographical changes at Telefon Bay, western slopes of Mount Pond, Pendulum Cove and Whalers Bay (well documented by Baker and others, 1975). Important changes occurred in the Telefon Bay area due to the eruption that began in December 1967. The activity was concentrated in three craters, resulting in the construction of a small island, and a larger crater about 2 km to the east. The same area experienced further geomorphological modification during a new eruption in 1970, forming a

second series of craters at the foot of the caldera wall facing Telefon Bay, between Cross Hill and Goddard Hill. New land measuring 1700 m by 400 m large strip was created between the small island formed in 1967 and the former Telefon Bay coastline, but some of that new land was partially removed to form several small flooded maars. Another seven conspicuous craters were formed close to Goddard Hill in 1970, variably 50 to 300 m in rim diameter and up to 150 m deep. Mudflows associated with the 1970 volcanic activity in the Goddard Hill area modified the shape of the large crater created previously in the 1967 eruption. The numerous notable changes in morphology caused by the 1967 and 1970 eruptions are obvious when older maps of the island (e.g. Hawkes, 1961) are compared with those made subsequent to 1970 (e.g. Servicio Geográfico del Ejército and Universidad Autónoma de Madrid, 1994; see back pocket).

In contrast to those which occurred in 1967 and 1970, eruptions in February 1969 were from multiple small cinder cones in a series of *en echelon* fissures that crossed the Mount Pond ice cap (Baker and others, 1975; Smellie, 2002). Widespread meltwater floods affected most of the area between Whalers Bay and Pendulum Cove, and a combination of lahars and pyroclastic fall deposits generated by the eruption caused the destruction of British and Chilean stations at those localities. As well as the tephra and lahar deposits that accumulated on land, the enhanced water runoff caused by glacier melting significantly increased the supply of sediment to Port Foster.

Although Deception Island is seismically active (e.g. Vila and others, 1992*a*,*b*) and is currently only dormant (as shown by the presence of several steam-emitting fumaroles; Ortiz and others, 1987; López-Martínez and others, 1996), there have been no major geomorphological changes on the island since the last eruption in 1970. However, a comparison of historical bathymetric records for Port Foster up to 1993 suggested that uplift rates on the basin floor are locally unusually high (0.3–0.5 m a^{-1}). Such rates exceed the sedimentation rates expected in calderas of a similar size and suggest that volcano-tectonic resurgence or tectono-magmatic activity is currently taking place (Cooper and others, 1998).

Fractures exert a strong influence on the large-scale morphology of several parts of the island, and on the locations of craters. This is particularly well seen in the shape of rock cliffs west of Macaroni Point, as linear sections of the caldera rim, and as aligned chains of craters on Kendall Terrace and flanks of Mount Kirkwood. There is also continuing morphological evolution of the island due to present-day ice erosion, gravitational slope processes, runoff of meteoric water and the erosive action of wind and sea. The mobility of the unconsolidated, often vesicular and light pyroclasts is very high and several recently-formed craters and parts of Port Foster are rapidly being infilled. Together with summer ice ablation, these processes ensure that a relatively high proportion of sediment is transported into Port Foster and the surrounding Bransfield Strait.

ACKNOWLEDGEMENTS

The inclusion of the topographic map of Deception Island with BAS GEOMAP 6 (see back pocket) is by courtesy of the Centro Geográfico del Ejército (the former Servicio Geográfico del Ejército, SGE). The co-operation of the SGE was also invaluable during the publication of the present geological and geomorphological maps: SGE undertook the digitization and printing of the geological and geomorphological maps under a co-operative venture between SGE and the Universidad Autónoma de Madrid. Aerial photographs from the Falklands Islands and Dependencies Aerial Survey Expedition (1956–1957) and several photographic sets obtained in the 1970s and 1980s by HMS *Endurance* for the British Antarctic Survey were used during the preparation of the geological and geomorphological maps. We are grateful to the captains, and crews of RRS *Bransfield*, RRS *John Biscoe*, HMS *Endurance*, R/V *Hespérides* and *Las Palmas*, all personnel at Gabriel de Castilla and Decepción stations on Deception Island, and our field assistants and other colleagues on the island (Dr L. Greenfield, A Morton, D. Mason) for their support during the several expeditions required to conduct this work. Our grateful thanks are also extended to Dr T. Millar, Alaska Volcano Observatory (AVO), for information explaining the AVO volcano alert scheme. Finally, publication of this GEOMAP would not have been possible without the foresight, encouragement and insightful editing of Dr M.RA. Thomson, former Head of Geology Division, British Antarctic Survey, for which we are particularly grateful.

REFERENCES

ACOSTA, J., HERRANZ, P., SANZ, J.L. *and* UCHIPI, E. 1992. Antarctic continental margin: geologic image of the Bransfield Trough, an incipient oceanic basin. (*In* POAG, W.C. *and* DE GRACIANSKY, P.C., *eds. Geologic evolution of Atlantic continental rises*. New York, Van Nostrand Reinhold, 49–61.

ALGUACIL, G., ALMENDROS, J, DEL PEZZO, E., GARCÍA, A., IBAÑEZ, J.M., LA ROCCA, M., MORALES, J. *and* ORTIZ, R. 1999. Observations of volcanic earthquakes and tremor at Deception Island, Antarctica. *Annali di geofisica*, **42**, 417–436.

ALLEY, R.B., BLANKENSHIP, S.T., ROONEY, S.T. *and* BENTLEY, C.R. 1989. Sedimentation beneath ice shelves. The view from ice stream B. *Marine Geology*, **85**, 101–10.

ALMENDROS, J., IBANEZ, J.M., ALGUACIL, G., DEL PEZZO, E. *and* ORTIZ, R. 1997. Array tracking of the volcanic tremor source at Deception Island, Antarctica. *Geophysical Research Letters*, **24**, 3069–3072.

ARISTARAIN, A.J. *and* DELMAS, R.J. 1998. Ice record of a large eruption of Deception Island volcano (Antarctica) in the XVII th century. *Journal of Volcanology and Geothermal Research*, **80**, 17–25.

ASHCROFT, W.A. 1972. Crustal structure of the South Shetland Islands and Bransfield Strait. *British Antarctic Survey Scientific Reports*, No. 66, 43 pp.

BAKER, P.E. 1978. The South Sandwich Islands: III. Petrology of the volcanic rocks. *British Antarctic Survey Scientific Reports*, No. 93, 34 pp.

BAKER, P.E. 1990. The South Sandwich Islands. Summary. (*In* LEMASURIER, W.E. *and* THOMSON, J.W., *eds. Volcanoes of the Antarctic plate and southern oceans. Antarctic Research Series, 48*. Washington, D.C., American Geophysical Union, 360–395.)

BAKER, P.E. 1990. D.2. Deception Island. (*In* LEMASURIER, W.E. *and* THOMSON, J.W., *eds. Volcanoes of the Antarctic plate and southern oceans. Antarctic Research Series, 48*. Washington, D.C., American Geophysical Union, 316–321.)

BAKER, P.E., DAVIES, T.G. *and* ROOBOL, M.J. 1969. Volcanic activity at Deception Island in 1967 and 1969. *Nature, London*, **224**, 553–60.

BAKER, P. E. *and* MCREATH, I. 1971. Geological investigations on Deception Island. *Antarctic Journal of the United States*, **6**, 85–86.

BAKER, P.E., MCREATH, I., HARVEY, M.R., ROOBOL, M.J. *and* DAVIES, T.G. 1975. The geology of the South Shetland Islands: V. Volcanic evolution of Deception Island. *British Antarctic Survey Scientific Reports*, No. 78, 81 pp.

BARALDO, A. *and* RAPALINI, A.E. 2000. Emplacement temperatures of Recent pyroclastic deposits at Deception Island, Antarctica, determined by paleomagnetism. *Journal of South American Earth Sciences* (in press).

BARKER, P.F. 1982. The Cenozoic subduction history of the Pacific margin of the Antarctic Peninsula: ridge crest-trench interactions. *Journal of the Geological Society, London*, **139**, 787–802.

BARKER, D.H.N. *and* AUSTIN, J.A. 1994. Crustal diapirism in Bransfield Strait, West Antarctica: evidence for distributed extension in marginal-basin formation. *Geology*, **22**, 657–660.

BARKER, D.H.N. *and* AUSTIN, J.A. 1998. Rift propagation, detachment faulting, and associated magmatism in Bransfield Strait, Antarctic Peninsula. *Journal of Geophysical Research*, **103**, 24017–24043.

BARTH, T.F.W. *and* HOLMSEN, P. 1939. Rocks from the Antarctandes and the Southern Antilles. Being a description of rock samples collected by Olaf Holtedahl 1927–1928, and a discussion of their mode of origin. *Scientific Results of the Norwegian Antarctic Expedition*, **18**, 64 pp.

BATIZA, R. 1984. Geology, petrology, and geochemistry of Isla Tortuga, a recently formed tholeiitic island in the Gulf of California. *Geological Society of America Bulletin*, **89**, 1309–1324.

BATIZA, R., FORNARI, D.J.M., VANKO, D.A. *and* LONSDALE, P. 1984. Craters, calderas, and hyaloclastites on young Pacific seamounts. *Journal of Geophysical Research*, **89**, 8371–8390.

BELDERSON, R.H., KENYON, H.H., STRIDE, A.H. *and* STUBBS, A.R. 1972. *Sonographs of the Sea Floor*. Amsterdam, Elsevier.

BIRKENMAJER, K. 1991. Lichenometric dating of a mid-19th century lava eruption at Deception Island (West Antarctica). *Bulletin of the Polish Academy of Science, Earth Sciences*, **39**, 1–9.

BIRKENMAJER, K. 1992. Volcanic succession at Deception Island, West Antarctica. A revised lithostratigraphic standard. *Studia Geologica Polonica*, **101**, 27–82.

BIRKENMAJER, K. 1995*a*. Some young volcanic features at Whalers Bay, Deception Island volcano, South Shetland Islands (West Antarctica). *Studia Geologica Polonica*, **107**, 131–143.

BIRKENMAJER, K. 1995*b*. Volcano-structural evolution of the Deception Island volcano, West Antarctica. *Terra Antartica*, **2**, 33–40.

BIRKENMAJER, K. *and* DUDZIAK, J. 1991. Nannoplankton evidence for Tertiary basement of Deception Island volcano, West Antarctica. *Bulletin of the Polish Academy of Sciences, Earth-Sciences*, **39**, 93–100.

BIRKENMAJER, K., FRANCALANCI, L. *and* PECCERILLO, A. 1991. Petrological and geochemical constraints on the genesis of Mesozoic–Cenozoic magmatism of King George Island, South Shetland Islands, Antarctica. *Antarctic Science*, **3**, 293–308.

BJÖRK, S., SANDGREN, P. *and* ZALE, R. 1991. Late Holocene tephrochronology of the northern Antarctic Peninsula region. *Quaternary Research*, **36**, 322–328.

BLONG, R.J. 1984. *Volcanic hazards: a sourcebook on the effects of eruptions*. Orlando, Academic Press, 424 pp.

BRECHER, H.H. 1975. Photogrammetric maps of a volcanic eruption area, Deception Island, Antarctica. *Institute of Polar Studies, Report No. 52*, 10 pp.

BRITISH ANTARCTIC SURVEY 1987. *Report for 1986/1987*. Swindon, Natural Environment Research Council, p. 88.

CAMPBELL, R.J. 2000. *The discovery of the South Shetland Islands 1819–1820. The journal of Midshipman C.W. Poynter*. London, The Hakluyt Society, 232 pp.

CAS, R.A.F. *and* WRIGHT, J.V. 1987. *Volcanic sucessions. Modern and ancient. A geological approach to processes, products and successions*. London, Allen and Unwin, 528 pp.

CASERTANO, L. 1963. Volcanic Activity at Deception Island. (*In* ADIE, R.J., *ed. Antarctic geology*. Amsterdam, North-Holland Publishing Company, 33–47.)

COOPER, A.P.R., SMELLIE, J.L. *and* MAYLIN, J. 1998. Evidence for shallowing and uplift from bathymetric records of Deception Island. *Antarctic Science*, **10**, 455–461.

CORREIG, A.M., URQUIZU, M., VILA, J. *and* MARTÍ, J. 1997. Analysis of the temporal occurrence of seismicity at Deception Island (Antarctica). *Pure and Applied Geophysics*, **149**, 553–574.

CORTE, A.E. & SOMOZA, A.L. 1954. Algunas observaciones geológicas y criopedológicas en la Antártida. *Publicación Instituto Antártico Argentino*, No 4, 131 pp.

CRIADO, C., ARCHE, A. *and* VILAS, F. 1992. Mapa geomorfológico preliminar de la Isla Decepción, Islas Shetland del Sur. (*In* LÓPEZ-MARTÍNEZ, J., *ed. Geología de la Antártida Occidental*. III Congreso Geológico de España y VIII Congreso Latinoamericano de Geología, Salamanca, Spain, 293–304.)

DIRECTORATE OF COLONIAL SURVEYS. 1955. *Falkland Islands Dependencies, South Shetland Islands, Deception Island*. DCS (Misc.) 217, 1:50 000 scale, 1st edn. London, Directorate of Colonial Surveys.

DIRECTORATE OF OVERSEAS SURVEYS. 1960. *Falkland Islands Dependencies, South Shetland Islands, Deception Island*. DOS 310 Series, 1:25 000 scale, 1st edn. London, Directorate of Overseas Surveys.

DOWNIE, R.H. *and* SMELLIE, J.L. 2001. *A management strategy for Deception Island*. Cambridge, British Antarctic Survey, 80 pp. [Unpublished]

DRUITT, T.H. 1998. Pyroclastic density currents. *Geological Society, London, Special Publications*, No. 145, 145–1821.

FANNING, E. 1833. *Voyages round the world; with selected sketches of voyages to the South Seas, North and South Pacific Oceans, China, etc. performed under the command and agency of the author*. New York.

FAURE, G., SHULZ, C.H. and CARWILE, R.H. 1971. Isotope composition of strontium in volcanic rocks from Deception Island. *Antarctic Journal of the United States*, **6**, 197–198.

FERGUSON, D. 1921. Geological observations in the South Shetland Islands, the Palmer Archipelago, and Graham Land, Antarctica. *Transactions of the Royal Society of Edinburgh*, **53**, 29–55.

FISHER, R.V. *and* SCHMINCKE, H-U. 1984. *Pyroclastic rocks*. Berlin, Springer-Verlag, 472 pp.

FLOYD, P.A. 1986. Petrology and geochemistry of oceanic intraplate sheet-flow basalts, Nauru Basin, Deep Sea Drilling Project Leg 89. *Initial Reports of the Deep Sea Drilling Project*, **89**, 471–497.

FOLCH, A. *and* MARTÍ, J. 1998. The generation of overpressure in felsic magma chambers by replenishment. *Earth and Planetary Science Letters*, **163**, 301–314.

GAVIN-ROBINSON, C. 1958. FIDASE. The story of the Falkland Islands Dependencies Aerial Survey Expedition. *Flight*, 14 June issue, 839–842.

GALINDO-ZALDÍVAR, J., JABALOY, A., MALDONADO, A. *and* SANZ DE GALDEANO, C. 1996. Continental fragmentation along the South Scotia Ridge transcurrent plate boundary (NE Antarctic Peninsula). *Tectonophysics*, **259**, 275–301.

GARCIA, M.O., LIU, N.W.K. *and* MUENOW, D.W. 1979. Volatiles in submarine volcanic rocks from the Mariana island arc and trough. *Geochimica et Cosmochimica Acta*, **43**, 305–312.

GARCIA, M.O., MUENOW, D.W., AGGREY, K.E. *and* O'NEIL, J.R. 1989. Major element, volatile, and stable isotope geochemistry of Hawaiian submarine tholeiitic glasses. *Journal of Geophysical Research*, **94**, 10525–10538.

GASS, I.G., HARRIS, P.G. *and* HOLDGATE, M.W. 1963. Pumice eruption in the area of the South Sandwich Islands. *Geological Magazine*, **100**, 321–330.

GONZÁLEZ-CASADO, J.M., LÓPEZ-MARTÍNEZ, J., GINER, J., DURÁN, J.J. & GUMIEL, P. 1999. Análisis de la microfracturación en la Isla Decepción, Antártida Occidental. *Geogaceta*, **26**, 31–34.

GONZÁLEZ-CASADO, J.M., GINER-ROBLES, J.L. *and* LÓPEZ-MARTÍNEZ, J. 2000. Bransfield Basin, Antarctic Peninsula: not a normal backarc basin. *Geology*, **28**, 1043–1046.

GONZÁLEZ-FERRÁN, O. *and* KATSUI, Y. 1970. Estudio integral del volcanism cenozoico superior de las Islas Shetland del Sur, Antártica. *Serie Científica Instituto Antártico Chileno.*, **1**, 123–174.

GONZÁLEZ-FERRÁN, O., MUNIZAGA, F. *and* MORENO, H. 1971. Sintesis de la evolución volcánica de Isla Decepción y la erupción de 1970. *Instituto Antártico Chileno, Serie Científicas*, **2**, 1–14.

GOURDON, E. 1914. Sur la constitution minéralogique des Shetland du Sud (île Déception). *C. R. Acad. Sci. Paris*, **158**, 583–586.

GRÁCIA, E., CANALS, M., FARRÁN, M., PRIETO, M.J., SORRIBAS, J. *and* GEBRA Team. 1996. Morphostructure and evolution of the central and eastern Bransfield basins (NW Antarctic Peninsula). *Marine Geophysical Researches*, **18**, 429–448.

GRÁCIA, E., CANALS, M., FARRÁN, M., SORRIBAS, J. *and* PALLÀS, R. 1997. Central and eastern Bransfield basins (Antarctica) from high-resolution swath-bathymetry data. *Antarctic Science*, **9**, 168–180.

GRAD, M., GUTERCH, A. *and* SRODA, P. 1992. Upper crustal structure of Deception Island area, Bransfield Strait, West Antarctica. *Antarctic Science*, **4**, 469–476.

GUTERCH, A., GRAD, M., JANIK, T. *and* PERCHUC, E. 1991. Tectonophysical models of the crust between the Antarctic Peninsula and the South Shetland Trench. (*In* THOMSON, M.R.A., CRAME, J.A. *and* THOMSON, J.W., *eds. Geological evolution of Antarctica*. Cambridge, Cambridge University Press, 499–504.)

HAQ, B.U., HARDENBOHL, J. *and* VAIL, P.R. 1987. Chronology of fluctuating sea levels since the Triassic. *Science*, **235**, 1156–1167.

HALPERN, M. 1970. Rubidium-strontium dates and Sr^{87}/Sr^{86} initial ratios of rocks from Antarctica and South America: a progress report. *Antarctic Journal of the United States*, **5**, 159–161.

HATTERSLEY-SMITH, G. 1991. The history of place-names in the British Antarctic Territory. *British Anarctic Survey Scientific Reports*, No. 113 (Parts I and II), 670 pp.

HAWKES, D.D. 1961. The geology of the South Shetland Islands: II. The geology and petrology of Deception Island. *Falkland Islands Dependencies Survey Scientific Reports*, No. 27, 43 pp.

HOTELDAHL, O. 1929. On the geology and physiography of some Antarctic and subantarctic islands. *Scientific Results of the Norwegian Antarctic Expeditions 1927–1928 and 1928–1929*, No. 3, 172 pp.

HUIJSMANS, J.P.P. 1985. Calc-alkaline lavas from the volcanic complex of Santorini, Aegean Sea, Greece. A petrological, geochemical and stratigraphic study. *Geologica Ultraiectina*, No. 41, 316 pp.

HYDROGRAPHIC DEPARTMENT. 1974. *The Antarctic Pilot. Comprising the coasts of Antarctica and all islands southward of the usual route of vessels. 4th edn.* (NP 9). Taunton, Hydrographic Department.

HYDROGRAPHIC OFFICE. 1987. *Deception Island, South Shetland Islands*. Chart No. 3202, 1:50 000 scale. Taunton, Hydrographic Office.

IBAÑEZ, J.M., ALMENDROS, J., ALGUACIL, G., MORALES, J., DEL PEZZO, E. *and* ORTIZ, R. 1997*a*. Eventos sísmicos de largo periodo en la Isla decepción: evidencias de una zona volcánica activa. *Boletín de la Real Sociedad Española de Historia Natural (Sec. Geol.)*, **93**, 105–112.

IBAÑEZ, J.M., MORALES, J., ALGUACIL, G., ALMENDROS, J., ORTIZ, R. *and* DEL PEZZO, E. 1997*b*. Intermediate-focus earthquakes under South Shetland Islands (Antarctica). *Geophysical Research Letters*, **24**, 531–534.

IGARZABAL, A.P. 1974. Rasgos morfológicos de Isla Decepción, Islas Shetland del Sur, Antártida Argentina. *Contribución del Instituto Antártico Argentino*, No. 172, 31 pp.

IGARZABAL, A.P. 1977. Carta geomorfológica de Isla Decepción, Shetland del Sur, Antártida Argentina. *Contribución del Instituto Antártico Argentino*, No. 197, 26 pp.

INBAR, M. 1992. Hidrología y geometría hidráulica en litología volcánica. Estudio cuantitativo morfológico en la Isla Decepción, Islas Shetland del Sur. (*In* LÓPEZ-MARTÍNEZ, J., *ed. Geología de la Antártida Occidental*. III Congreso Geológico de España y VIII Congreso Latinoamericano de Geología, Salamanca, Spain, 337–346.)

JONES, J.G. *and* NELSON, P.H.H. 1970. The flow of basalt lava from air into water—its structural expression and stratigraphic significance. *Geological Magazine*, **107**, 13–19.

KENDALL, E.N. 1831. An account of the Island of Deception, one of the New Shetland Isles. Extracted from the private journal of Lieutenant Kendal, R.N., embarked on board his Majesty's sloop *Chanticleer*, Captain Foster, on a scientific voyage; and communicated by John Barrow, Esq., F.R.S. *Journal of the Royal Geographical Society, London*, **1**, 62–66.

KELLER, R.A., FISK, M.R., WHITE, W.M. *and* BIRKENMAJER, K. 1992. Isotopic and trace element constraints on mixing and melting models of marginal basin formation, Bransfield Strait, Antarctica. *Earth and Planetary Science Letters*, **111**, 287–303 (for 1991).

KELLER, R.A., FISK, M.R., SMELLIE, J.L., STRELIN, J.A. *and* LAWVER, L.A. 2002. Geochemistry of back arc basin volcanism in Bransfield Strait, Antarctica: subducted contributions and along-axis variations. *Journal of Geophysical Research*, **107**, B8, 10.1029/2001JB000444.

KILLINGBECK, J.B. 1977. *The role of Deception Island in the development of Antarctic affairs*. Thesis, Diploma in Polar Studies, Scott Polar Research Institute, Cambridge, 63 pp. [Unpublished]

KING, L.H. *and* FADER, G.B.J. 1986, Wisconsian glaciation of the Atlantic Continental Shelf of Southeast Canada. *Geological Survey Canada Bulletin*, **363**.

KNITTELL, U. *and* OLES, D. 1995. Basaltic volcanism associated with extensional tectonics in the Taiwan—Luzon island arc: evidence for non-depleted sources and subduction zone enrichment. *Geological Society, London, Special Publication*, **81**, 77–93.

KOKELAAR, B.P. 1983. The mechanism of Surtseyan volcanism. *Journal of the Geological Society, London*, **140**, 939–944.

KOKELAAR, P. 1986. Magma—water interactions in subaqueous and emergent basaltic volcanism. *Bulletin of Volcanology*, **48**, 275–289.

KOKELAAR, P. *and* BUSBY, C. 1992. Subaqueous explosive eruption and welding of pyroclastic deposits. *Science*, **257**, 196–201.

KOWALEWSKI, W., RUDOWSKI, S. *and* ZALEWSKI, S.M. 1990. Seismoacoustic studies within flooded part of the caldera of the Deception Island, West Antarctica. *Polish Polar Research*, **11**, 259–266.

LARTER, R.D. 1991. Debate: Preliminary results of seismic reflection investigations and associated geophysical studies in the area of the Antarctic Peninsula. *Antarctic Science*, **3**, 217–222.

LAWVER, L.A., KELLER, R.A., FISK, M.R. *and* STRELIN, J.A. 1995. Bransfield Strait, Antarctic Peninsula: active extension behind a dead arc. (*In* TAYLOR, B., *ed. Back-arc basins: tectonics and magmatism*. New York, Plenum, 315–342.)

LAWVER, L.A., SLOAN, B.J., BARKER, D.H.N., GHIDELLA, M., VON HERZEN, R.P., KELLER, R.A., KLINKHAMMER, G.P. *and* CHIN, C.S. 1996. Distributed, active extension in Bransfield Basin, Antarctic Peninsula: evidence from multibeam bathymetry. *GSA Today*, **6**, 1–6 & 16–17.

LE BAS, M.J., LE MAITRE, R.W., STRECKEISEN, A. *and* ZANETTIN, B. 1986. A chemical classification of volcanic rocks based on the total alkali-silica diagram. *Journal of Petrology*, **27**, 745–750.

LEGROS, F., KELFOUN, K. *and* MARTÍ, J. 2000. The influence of conduit geometry on the dynamics of caldera-forming eruptions. *Earth and Planetary Science Letters*, **179**, 53–61.

LÓPEZ-MARTÍNEZ, J. *and* HERNÁNDEZ-CIFUENTES, F. 1997. Toponimia antártica española. Propuesta para un primer glosario de nombres geográficos españoles. *Boletin real sociedad Española de Historia Natural (Sección Geológica)*, **93**, 229–236.

LÓPEZ-MARTÍNEZ, J., RAMOS, M., CRIADO, C., SERRANO, E. *and* NICOLÁS, P. 1996. Anomalías geotérmicas y permafrost en la Isla Decepción, Antártida. *Actas V Simposio Nacional de Estudios Antárticos*. Madrid, Comisión Interministerial de Ciencia y Tecnología, 223–234.

MACDONALD, G.A. *and* KATSURA, T. 1964. Chemical composition of Hawaiian lavas. *Journal of Petrology*, **5**, 82–133.

MARTÍ, J. *and* BARALDO, A. 1990. Pre-caldera pyroclastic deposits of Deception Island (South Shetland Islands). *Antarctic Science*, **2**, 345–352.

MARTÍ, J., REY, J. *and* BARALDO, A. 1990. Origen y estructura de la isla Decepción (Islas Shetland del Sur). (*In* CASTELLVÍ, J., *ed. Actas del III Simposium de Estudios Antárticos*. Madrid, Comisión Interministerial de Ciencia y Tecnología, 187–194.)

MARTÍ, J., VILA, J. *and* REY, J. 1996. Deception Island (Bransfield Strait, Antarctica): an example of a volcanic caldera developed by extensional tectonics. *Geological Society, London, Special Publication*, No. 110, 253–265.

MATTHIES, D., MÄUSBACHER, R. *and* SCHMIDT, R. 1990. Deception Island tephra: a stratigraphical marker for limnic and marine sediments in Bransfield Strait area, Antarctica. *Zentralblatt für Geologie und Paläontologie*, **1**, 153–165.

McPHIE, J., DOYLE, M. *and* ALLEN, R. 1993. *Volcanic textures. A guide to the interpretation of textures in volcanic rocks*. Tasmania, Tasmanian Government Printing Office, 198 pp.

MORETON, S.G. 1999. *Quaternary tephrochronology of the Scotia Sea and Bellingshausen Sea, Antarctica*. Ph.D. thesis, Cheltenham and Gloucester College of Higher Education, 164 pp. [Unpublished]

MORETON, S.G. *and* SMELLIE, J.L. 1998. Identification and correlation of distal tephra layers in deep-sea sediment cores, Scotia Sea, Antarctica. *Annals of Glaciology*, **27**, 285–289.

MORRIS, J.D., LEEMAN, W.P. *and* TERA, F. 1990. The subducted component in island arc lavas: constraints from Be isotopes and B-Be systematics. *Nature, London*, **344**, 31–36.

MOSSMAN, R.C. 1905. The recent voyage of the *Uruguay*. *Scottish Geographical Magazine*, **21**, 323–328.

MOTT, P.G. 1958. Airborne survey in the Antarctic. *Geographical Journal*, **124**, 1–17.

MOTT, P.G. 1986. *Wings over ice. An account of the Falkland Islands and Dependencies Aerial Survey Expedition 1955–57*. Long Sutton, Somerset, Peter Mott, 167 pp.

MUELLER, W. *and* WHITE, J.D.L. 1992. Felsic fire-fountaining beneath Archean seas: Pyroclastic deposits of the 2730 Ma Hunter Mine Group, Quebec, Canada. *Journal of Volcanology and Geothermal Research*, **54**, 117–134.

MUENOW, D.W., LIU, N.W.K., GARCIA, M.O. *and* SAUNDERS, A.D. 1980. Volatiles in submarine volcanic rocks from the spreading axis of the east Scotia Sea back-arc basin. *Earth and Planetary Science Letters*, **47**, 272–278.

MUÑOZ, G. 1996. Museo en la Antártica. *Boletin Antártico Chileno*, **15**, 5–8.

O'HARA, M.J. 1977. Geochemical evolution during fractional crystallisation of a periodically refilled magma chamber. *Nature*, **266**, 503–507.

OLSACHER, J. 1956. Contribución a la Geología de la Antártida Occidental. I, Contribución al conocimiento de la Isla Decepción. *Publicación Instituto Antártico Argentino*, No. **2**, 1–76.

ORHEIM, O. 1970. Glaciological investigations on Deception Island. *Antarctic Journal of the United States*, **5**, 95–97.

ORHEIM, O. 1972*a*. Volcanic activity on Deception Island, South Shetland Islands. (*In* ADIE, R.J., *ed. Antarctic geology and geophysics*. Oslo, Universitetsforlaget, 117–120.)

ORHEIM, O. 1972*b*. A 200-year record of glacier mass balance at Deception Island, southwest Atlantic Ocean, and its bearing

on models of global climate change. *Institute of Polar Studies, Ohio State University, Report* 42, 118 pp.

ORTÍZ, R., VALENTÍN, A. *and* GRIMALT, J. 1987. Actividad fumaroliana en Decepción. Estudio preliminar. *II Simposio Español de Estudios Antárticos.* Madrid, Comisión Interministerial de Ciencia y Tecnología, 229–237.

ORTÍZ RAMIS, R., GARCIA, A.G. *and* RISSO, C. 1992. *Seismic and volcanic activity in the South Shetland Isalnds and the Antarctic Peninsula environment.* Madrid, Museo Nacional de Ciencias Naturales (CSIC), 46 pp. [Unpublished]

ORTÍZ, R., VILA, J. *and* SASTRE, J.C. 1990. Actividad sísmica en el entorno de la Base Antártica Española Juan Carlos I (Islas Livingston y Decepción). (*In* CASTELLVÍ, J., *ed. Actas del III Simposium Español de Estudios Antárticos.* Madrid, Comisión Interministerial de Ciencia y Tecnología, 238–243.)

ORTÍZ, R., VILA, J., GARCÍA, A., CAMACHO, A.G., DÍAZ, J.L., APARICIO, A., SOTO, R., VIRAMONTE, J.G., RISSO, C., MENEGATTI, N. *and* PETRINOVIC, I. 1992. Geophysical features of Deception Island. (*In* YOSHIDA, Y. KAMINUMA, K. *and* SHIRAISHI, K., *eds. Recent progress in Antarctic earth science.* Tokyo, Terra Scientific Publishing Company, 443–448.)

OSKARSSON, N. 1980. The interaction between volcanic gases and tephra: fluorine adhering to tephra of the 1970 Hekla eruption. *Journal of Volcanology and Geothermal Research,* **8**, 251–266.

PALLÀS, R., SMELLIE, J.L., CASAS, J.M. *and* CALVET, J. 2001. Using tephrochronology to date temperate ice: correlation between ice-tephras on Livingston Island and eruptive units on Deception Island volcano (South Shetland Islands, Antarctica). *The Holocene,* **11**, 149–160.

PANKHURST, R.J., MILLAR, I.L., GRUNOW, A.M. *and* STOREY, B.C., 1993. The pre-Cenozoic magmatic history of the Thurston Island crustal block, West Antarctica. *Journal of Geophysical Research,* **98**, 11835–11849.

PANKHURST, R.J. *and* RAPELA, C.R. 1995. Production of Jurassic rhyolite by anatexis of the lower crust of Patagonia. *Earth and Planetary Science Letters,* **134**, 23–36.

PECCERILLO, A., TRIPODO, A., VILLARI, L., GURRIERI, S. *and* ZIMBALATTI, E. 1991. Genesis and evolution of volcanism in back-arc areas. A case history, the Island of Deception (Western Antarctica). *Periodico di Mineralogia,* **60**, 29–44.

PELAYO, A. *and* WIENS, D. 1989. Seismotectonics and relative plate motions in the Scotia Sea region. *Journal of Geophyiscal Research,* **94**, 7293–7320.

RAMOS, M., ORTÍZ, R., DIEZ-GIL, J.L. *and* VIRAMONTE, J. 1989. Anomalías térmicas y balance de flujo energético sobre el suelo del volcán Decepción, Isla Decepción (Shetland del Sur). (*In* CASTELLVÍ, J., *ed. Actas del III Simposium Español de Estudios Antárticos.* Madrid, Comisión Interministerial de Ciencia y Tecnología, 203–219.)

REY, J., DE ANDRÉS, J.R. *and* FERNÁNDEZ-LÓPEZ, J. M. 1990. Tectónica reciente en los depósitos submarinos de la Bahía de Decepción. (*In* CASTELLVÍ, J., *ed. Actas del III Symposium Español de Estudios Antárticos.* Madrid, Comisión Interministerial de Ciencia y Tecnología, 258–270.)

REY, J., SOMOZA, L. *and* HERNÁNDEZ-MOLINA, F.J. 1992. Formas de los sedimentos submarinos superficiales en Puerto Foster, Isla Decepcion, Islas Shetland del Sur. (*In* LÓPEZ-MARTÍNEZ, J., *ed. Geología de la Antártida Occidental.* Salamanca, III Congreso Geología de España & VIII Congreso Latinoamericano de Geología, Salamanca, Spain, 163–172.)

REY, J., SOMOZA, L., MARTÍNEZ-FRÍAS, J., DEL BARRIO, J. *and* BENITO, R. 1994. Caracterización geoquímica de los sedimentos volcánicos submarinos de la Isla Decepción (Antártida). *Publicaciones Especiales del Instituto Español de Oceanografía, Madrid.* Ministerio de Agricultura, Pesca y Alimentación, **18**, 95–105.

REY, J., SOMOZA, L. *and* MARTÍNEZ-FRÍAS, J. 1995. Tectonic, volcanic, and hydrothermal event sequence on Deception Island (Antarctica). *Geo-Marine Letters,* **15**, 1–8.

REY, J., SOMOZA, L. *and* MARTÍNEZ-FRÍAS, J. 1996. Evidencias tectónicas, volcánicas e hidrotermales en Isla Decepción, relacionadas con el marco geodinámico de la cuenca de Bransfield (Antártida). (*In* CACHO, J. and SERRAT, D., *eds Actas del V Simposio de Estudios Antárticos.* Madrid, Comisión Interministerial de Ciencia y Tecnología, 209–222.)

REY, J., SOMOZA, L., MARTÍNEZ-FRÍAS, J., BENITO, R. *and* MARTÍN-ALFAGEME, S. 1997. Deception Island (Antarctica): a new target for exploration of Fe-Mn mineralization? *Geological Society, London, Special Publication,* No. **119**, 239–251.

REY, J., SOMOZA, L. *and* MARTÍNEZ-FRÍAS, J. 2000. Sismicidad e inestabilidad de los sedimentos submarinos en Isla Decepción, Antártida. *Geotemas,* **1**, 345–348.

RISSO, C., BARALDO, A. *and* VIRAMONTE, J.G. 1992. Nuevos aportes al conocimiento de la geomorfología de la Isla Decepción, Islas Shetland del Sur. (*In* LÓPEZ-MARTÍNEZ, J., *ed. Geología de la Antártida Occidental.* III Congreso Geológico de España y VIII Congreso Latinoamericano de Geología, Salamanca, Spain, 293–304.)

ROOBOL, M.J. 1973. Historic volcanic activity at Deception Island. *British Antarctic Survey Bulletin,* **32**, 23–30.

ROOBOL, M.J. 1980. A model for the eruptive mechanism of Deception Island from 1820 to 1970. *British Antarctic Survey Bulletin,* No. 49 (for 1979), 137–156.

ROOBOL, M.J. 1982. The volcanic hazard at Deception Island, South Shetland Islands. *British Antarctic Survey Bulletin,* **51**, 237–245.

ROSA, R. DE, MAZZUOLI, R., OMARINI, R.H., VENTURA, G. *and* VIRAMONTE, J.G. 1995. A volcanological model for the historical eruptions at Deception Island (Bransfield Strait, Antarctica). *Terra Antartica,* **2**, 95–101.

SAUNDERS, A.D., TARNEY, J., STERN, C.R. *and* DALZIEL, I.W.D. 1979. Geochemistry of Mesozoic marginal basin floor igneous rocks from southern Chile. *Geological Society of America Bulletin,* **90**, 237–258.

SCHMINCKE, H-U *and* BEDNARZ, U. 1990. Pillow, sheet flow and breccia flow volcanoes and volcano—tectonic hydrothermal cycles in the Extrusive Series of the northeastern Troodos ophiolite (Cyprus). (*In* MALPAS, J., MOORES, E.M., PANAYIOTOU, A. *and* XENOPHONTOS, C., *eds. Ophiolites: Oceanic crustal analogues.* Nicosia, Geological Survey Department, 185–206.)

SCHWERDTFEGER, W. 1970. The climate of Antarctica. (*In* LANDBSBERG, H.E., *ed. World Survey of Climatology.* Amsterdam, Orvig, S., 253–355.)

SCIENTIFIC COMMITTEE ON ANTARCTIC RESEARCH. 1998. *Composite Gazetteer of Antarctica (south of latitude 60°S).* Rome, Working Group on Geodesy and Geographic Information, Scientific Committee on Antarctic Research. Vol. 1, 227 pp. and Vol. 2, 328 pp.

SCIENTIFIC COMMITTEE ON ANTARCTIC RESEARCH. 2000. *Composite Gazetteer of Antarctica, Supplement to the first edition.* Rome, Working Group on Geodesy and Geographic Information, Scientific Committee on Antarctic Research, 46 pp.

SCIENTIFIC COMMITTEE ON ANTARCTIC RESEARCH. 2002. *What's new in the CGA.* Rome, Working Group on Geodesy and Geographic Information, Scientific Committee on Antarctic Research, 24 pp.

SERRANO, E. and LÓPEZ-MARTÍNEZ, J. 1998. Caracterizacion y distribucion de las formas y los procesos periglaciares en las Islas Shetland del Sur (Antartida). (*In* GOMEZ, A., SCHULTE, L. *and* GARCIA, A., *eds. Procesos biofisicos actuales en medios frios. Estudios recientes.* Universidad de Barcelona, 181–204.)

SERRANO, E. *and* LÓPEZ-MARTÍNEZ, J. 2000. Rock glaciers in the South Shetland Islands, Western Antarctica. *Geomorphology,* **35**, 145–162.

SERRANO, E., GINER, J., GUMIEL, P. *and* LÓPEZ-MARTÍNEZ, J. 2002. Permafrost en las Islas Shetland del Sur (Antártida marítima). Distribución y dinámica actual. (*In* SERRANO, E. and GARCÍA DE CELIS, A., *eds. Periglaciarismo en montaña y altas latitudes.* Universidad de Valladolid, Spain, 277–296.)

SERVICIO GEOGRÁFICO DEL EJÉRCITO *and* UNIVERSIDAD AUTÓNOMA DE MADRID. 1994. *Isla Decepción/Deception Island.* 1:25000 scale, 1st edn. Madrid, Servicio Geográfico del Ejército.

SHEVENELL, L. *and* GOFF, F. 1993. Addition of magmatic volatiles into the hot spring waters of Loowit Canyon, Mount St. Helens, Washington, USA. *Bulletin of Volcanology*, **55**, 489–503.

SKILLING, I.P. 1994. Evolution of an englacial volcano: Brown Bluff, Antarctica. *Bulletin of Volcanology*, **56**, 573–591.

SMELLIE, J.L. 1988. Recent observations on the volcanic history of Deception Island, South Shetland Islands. *British Antarctic Survey Bulletin*, No. 81, 83–85.

SMELLIE, J.L. 1989. Deception Island. (*In* DALZIEL, I.W.D., *ed. Tectonics of the Scotia arc, Antarctica.* 28th International Geological Congress, Field Trip Guidebook T180. Washington, D.C., American Geophysical Union, 146–152.)

SMELLIE, J.L. 1990. Graham Land and South Shetland Islands. Summary. (*In* LEMASURIER, W.E. and THOMSON, J.W., *eds. Volcanoes of the Antarctic plate and southern oceans. Antarctic Research Series*, **48**. Washington, D.C., American Geophysical Union, 302–312.)

SMELLIE, J.L. 1999. The upper Cenozoic tephra record in the south polar region: review. *Global and Planetary Change*, **21**, 51–70.

SMELLIE, J.L. 2000. Subglacial eruptions. (*In* SIGURDSSON, H., *ed. Encyclopedia of Volcanoes.* San Diego, Academic Press, 403–418.)

SMELLIE, J.L. 2001*a*. Lithofacies architecture and construction of volcanoes erupted in englacial lakes: Icefall Nunatak, Mount Murphy, eastern Marie Byrd Land, Antarctica. (*In* WHITE, J.D.L. and RIGGS, N., *eds. Lacustrine volcaniclastic sedimentation. International Association of Sedimentologists Special Publication*, 73–98.)

SMELLIE, J.L. 2001*b*. Lithostratigraphy and volcanic evolution of Deception Island, South Shetland Islands. *Antarctic Science*, **13**, 188–209.

SMELLIE, J.L. 2002. The 1969 subglacial eruption on Deception Island (Antarctica): events and processes during an eruption beneath a thin glacier and implications for volcanic hazards. (*In* SMELLIE, J.L. *and* CHAPMAN, M.G., *eds. Volcano—ice interaction on Earth and Mars. Geological Society, London, Special Publication*, No. **202**, 59–79.)

SMELLIE, J.L. *and* HOLE, M.J. 1997. Products and processes in Pliocene–Recent, subaqueous to emergent volcanism in the Antarctic Peninsula: examples of englacial Surtseyan volcano construction. *Bulletin of Volcanology*, **58**, 628–646.

SMELLIE, J.L., PANKHURST, R.J., THOMSON, M.R.A. *and* DAVIES, R.E.S. 1984. The geology of the South Shetland Islands: VI. Stratigraphy, geochemistry and evolution. *British Antarctic Survey Scientific Reports*, No. 87, 85 pp.

SMELLIE, J.L., HOFSTETTER, A. *and* TROLL, G. 1992. Fluorine and boron geochemistry of an ensialic marginal basin volcano: Deception Island, Bransfield Strait, Antarctica. *Journal of Volcanology and Geothermal Research*, **49**, 255–267.

SMELLIE, J.L., LÓPEZ-MARTÍNEZ, J., REY, J. *and* SERRANO, E. 1997. Geological and geomorphological maps of Deception Island, South Shetland Islands. (*In* RICCI, C.A., *ed. The Antarctic region: Geological evolution and processes.* Siena, Museo Nazionale dell' Antartide, 1195–1198.)

SMITH, T.L. *and* BATIZA, R. 1989. New field and laboratory evidence for the origin of hyaloclastite flows on seamount summits. *Bulletin of Volcanology*, **51**, 96–114.

SOMOZA, L., REY, J., MARTÍNEZ-FRÍAS, J. *and* BENITO, R. 1994. Fe-Mn distribution patterns on seafloor sediments related to the discovery of submarine volcanic cones, mounds and vent structures (Deception Island, Antarctica). *European Journal of Mineralogy*, **6**, 343–344.

STAUDIGEL, H. *and* SCHMINCKE, H-U. 1984. The Pliocene seamount series of La Palma/Canary Islands. *Journal of Geophysical Research*, **89**, 11195–11215.

SUN, S-S. *and* McDONOUGH, W.F. 1989. Chemical and isotopic systematics of oceanic basalts: implications for mantle composition ands processes. *Geological Society, London, Special Publication*, **42**, 313–345.

SUTHERLAND, F.L. 1965. Dispersal of pumice, supposedly from the 1962 South Sandwich Islands eruption, on southern Australian shores. *Nature, London*, **207**, 1332–1335.

TYRRELL, G.W. 1945. Report on rocks from West Antarctica and the Scotia arc. *Discovery Reports*, **23**, 37–102.

VALENCIO, D.A., MENDÍ, J.E. *and* VILAS, J.F. 1979. Palaeomagnetism and K-Ar age of Mesozoic and Cenozoic igneous rocks from Antarctica. *Earth and Planetary Science Letters*, **45**, 61–68.

VALENZUELA, E., CHÁVEZ, L. *and* MUNIZAGA, F. 1968. Informe preliminar sobre la erupción de la Isla Decepción ocurrida en diciembre de 1967. *Boletín Instituto Antártico Chileno*, **3**, 5–16.

VILA, J., ORTIZ, R., CORREIG, A.M. *and* GARCÍA, A. 1992*a*. Seismic activity on Deception Island. *(In* YOSHIDA, Y., *ed. Recent progress in Antarctic earth science.* Tokyo, Terra Scientific Publishing Company, 449–456.)

VILA, J., MARTÍ, J., ORTIZ, R., GARCIA, A. *and* CORREIG, A.M. 1992*b*. Volcanic tremors at Deception Island (South Shetland Islands, Antarctica). *Journal of Volcanology and Geothermal Research*, **53**, 89–102.

VILLEGAS, M.T., CASELLI, A. *and* GARCÍA, A. 1997. Nuevas aportaciones al estudio de las variaciones estacionales de los gases volcánicos de la Isla decepción(Islas shetland del Sur). *Boletín Real Sociedad Española de Historia Natural (Sección geológica)*, **93**, 145–153.

WALKER, G.P.L. 1984. Downsag calderas, ring faults, caldera sizes, and incremental caldera growth. *Journal of Geophysical Research*, **89**, 8407–8416.

WEAVER, S.D., SAUNDERS, A.D., PANKHURST, R.J. *and* TARNEY, J. 1979. A geochemical study of magmatism associated with the initial stages of back-arc spreading: The Quaternary volcanics of Bransfield Strait, from South Shetland Islands. *Contributions to Mineralogy and Petrology*, **68**, 151–169.

WHITE, J.D.L. 2000. Subaqueous eruption-fed density currents and their deposits. *Precambrian Research*, **101**, 87–109.

WILKES, C. 1845. *Narrative of the United States exploring expedition, during the years 1838, 1839, 1840, 1841, 1842.* Vol. 1. Philadelphia.

WILKINS, H. 1929. The Wilkins–Hearst Antarctic Expedition, 1928–1929. *Geographical Review*, **XIX**, 353–376.

YODER, A.H. 1929. Deception Island. *The Quarterly Journal*, **19**, 211–222.

Appendix 1 Selected chronology of expeditions and historical events at Deception Island

by R.K. Headland

[Abridged and updated extracts from HEADLAND, R.K. 2001. *Antarctic Chronology.* Unpublished revision of *Chronological List of Antarctic Expeditions and Related Historical Events.* Cambridge University Press, 1989]

1820–21 British sealing voyage (from Valparaíso)

Andrew McFarlane	*Dragon*

Reported to have landed on the mainland coast of Antarctica, south of Deception Island (possibly the first such landing - but see also John Davis, 1820–22). [Neptunes Bellows, the entrance to Deception Island was known to sealers as 'Dragon's Mouth' which may be derived from this ship.]

1820–21 United States sealing voyage (from Stonington)

Benjamin Pendleton (senior commander)	*Frederick*
James P. Sheffield	*Hersilia*
Nathaniel Brown Palmer	*Hero*
Thomas Dunbar	*Free Gift*
Ephraim Williams	*Express*
Josiah C. Chester	*Essex*

Palmer, aboard the shallop *Hero*, entered Deception Island and searched for new sealing grounds; reported land on 16 November 1820 which was later named 'Palmer's Land' [Davis Coast of the Antarctic Peninsula]; he probably examined what is now known as Palmer Archipelago.

1820–22 United States sealing voyage

John Davis	*Huron*

Davis landed on the mainland coast of Antarctica, 7 February 1821 and wrote 'I think this Southern Land to be a Continent' (possibly the first such landing - but see also Andrew McFarlane, 1820–21). Davis entered Deception Island and described 'Dragon's Mouth' [Neptunes Bellows], 30 December 1821.

1828–31 British naval expedition

Henry Foster	HMS *Chanticleer*

Foster made pendulum and magnetic observations on Deception Island, which was charted; maximum and minimum thermometers left at Port Foster (collected by William Horton Smyley 1841–42, *q.v.*), sealers' graves reported.

1838–42 United States Exploring Expedition

Charles Wilkes (senior commander)	*Vincennes*

Sailed with six vessels, seven scientists and two artists to conduct an extremely broad scientific programme. Reported Bridgeman Island volcanically active; visited Deception Island.

1841–42 United States sealing voyage (from Newport)

William Horton Smyley	*Ohio*

Recovered the minimum thermometer left on Deception Island by Henry Foster (1828-29, *q.v.*, it recorded -5°F [-20.3°C]) and reported much volcanic activity on the island.

1901–03 Swedish South Polar Expedition

Nils Otto Gustaf Nordenskjöld	
Carl Anton Larsen	*Antarctic*

Tried to enter Deception Island but blocked by ice.

1906–07 Norwegian and Chilean whaling enterprise (from Punta Arenas)

Adolf Amandus Andresen	*Gobernador Bories*
?	*Cornelia Jacoba* (transport vessel) with whale-catchers *Almirante Valenzuela* and *Almirante Uribe*

Sociedad Ballenera de Magallanes used Whalers Bay, Deception Island for the first time as a site for a floating whaling factory. Andresen was accompanied by his wife and family. The company used the bay for the next 10 years, under a Falkland Islands and Dependencies Government licence from 1907. Whalers Bay became the principal anchorage for the floating factories operating in the region.

1907–08 South Shetland Islands: Four whaling companies (from Newfoundland, Norway and Chile [started 1906–07]) deployed floating factories at Deception Island during this summer, all with Falkland Islands and Dependencies Government licences. The numbers of floating factories operating at the island increased rapidly, reaching a maximum of 13 (and a shore station) in 1914–15; the last left in 1931.

1907–08 Newfoundland whaling enterprise (from St John's)

Nokard Davidsen	*Sabraon* with whale-catchers *Puma* and *Lynx*

Newfoundland Whaling Company deployed a floating whaling factory at Deception Island. Davidsen fell overboard from *Lynx* and drowned, 22 January 1908, his grave is the first in the whalers' cemetery on Deception Island.

1908 Norwegian whaling voyage

Roland Nilsen	*Telefon*

This collier, bound for Deception Island, struck Telefon Rocks, off King George Island, 26 December, and was abandoned; Adolf Amandus Andresen salvaged and moved *Telefon* to Telefon Bay, Deception Island; after winter, repairs were made and the vessel reached Punta Arenas.

1908–10 French Antarctic Expedition

Jean-Baptiste Etienne August Charcot	
Ernest Chollet	*Pourquoi Pas ?*

Expedition bunkered at Deception Island.

1909–11 South Shetland Islands: Albert Newing appointed representative for the islands by the Falkland Islands Dependencies Government, based on board floating factory Sabraon, at Deception Island. A government representative was

present on Deception Island during every summer until 26 April 1931 when whaling ceased at the islands.

1912 Falkland Islands Dependencies: Port Foster declared 'Port of Entry' from 1 October by the Falkland Islands Dependencies Government, for whaling seasons only.

1912–13 Norwegian whaling enterprise: Aktieselskabet Hektor established shore factory at Deception Island under British lease granted for 21 years from 1 October 1911. Pigs, sheep, equines and cattle introduced. Factory worked every summer until abandoned in 1931.

1913 Norwegian whaling voyage
R. Dahn *Pisagua*
This floating factory was wrecked near Deception Island. This was reported to the Governor in Stanley by the Falkland Islands Dependencies Magistrate by wireless, 25 January 1913, the first radio transmission from the Dependencies.

1915–17 Deception Island: James Innes Wilson, Falkland Islands Dependencies administrator on the island, made geological collections.

1920–21 Deception Island: The shore in the vicinity of the whaling station suddenly subsided in this season, imperilling the safety of the floating factory *Roald Amundsen*; water in the harbour boiled and removed paint from the hulls of vessels moored there.

1924 Norwegian whaling voyage: Four men from Norwegian whale-catcher *Bransfield* drowned off Livingston Island, buried at Deception Island.

1924–25 Deception Island: A violent volcanic subsidence occurred in the harbour, 4 January 1925.

1927–28 Norwegian whaling voyage: Geological observations of Deception Island made by O Holtedahl.

1928–29 Wilkins-Hearst Antarctic Expedition (Britain and United States)
Sir George Hubert Wilkins (1st expedition)
Marinius Hansen *Hektoria*
Pioneer air reconnaissance of east coast of Graham Land from Deception Island to about 71.33°S, November to January. Aircraft left at Deception Island for 1929–30 expedition.

1928–30 British expedition
Sir George Hubert Wilkins (2nd expedition)
Richard Laurence Vere Shannon RRS *William Scoresby*
Continuation of previous summer's aims. An Austin 7 motor car used for transport on Deception Island.

1928–31 Deception Island: In January 1930 a severe earthquake occurred and the floor of Whalers Bay dropped 4.6 m. A census was conducted of the island on 26 April 1931. 1930–31 was the last whaling season at Deception Island and at its conclusion the administrative post was closed until 1944 (Operation Tabarin).

1931–32 Whaling industry: Deception Island whaling station closed, April 1931.

1933–35 Ellsworth expedition (United States)
Lincoln Ellsworth (2nd expedition)
Baard Holth *Wyatt Earp*
Private expedition, planning to fly across Antarctica from the Antarctic Peninsula, frustrated by continuous bad weather. Called at Deception Island.

1934 British naval voyage
John Augustine Levers *HMS Burghead Bay*
Charted seaward coasts of Deception Island.

1941 British naval operation
Geoffrey A. B. Hawkins HMS *Queen of Bermuda*
Destroyed oil fuel installations and coal stocks on Deception Island to deny their use to German raiders.

1942 Argentine naval voyage
Alberto J. Oddera *1° de Mayo*
Visited Deception Island, January to February and on 8 February took formal possession for Argentina of the sector between longitudes 25°W and 68°34'W [68°57'W], south of 60°S; copper cylinders with corresponding notes were left at the site (the Argentine Government officially notified the United Kingdom Government of this action on 15 February 1943). Conducted hydrographic survey with the aid of an aircraft; made geological observations.

1943 British naval operation
Edward Wollaston Kitson HMS *Carnarvon Castle*
In January obliterated the Argentine marks of sovereignty left on Deception Island by *1° de Mayo* in 1942 and hoisted the British flag, leaving a record of the ship's visit (the cylinder and contents were returned to Argentina by the British Ambassador in Buenos Aires).

1943 Argentine naval voyage
Silvano Harriague *1° de Mayo*
Deposited a cylinder at Deception Island (and elsewhere), claiming for the Argentine Government the sector between longitudes 25°W and 68.57°W (68°34'W), south of 60°S, removed British emblems and painted the Argentine flag.

1943–44 British naval expedition ('Operation Tabarin')
James William Slessor Marr (in overall command)
William Robert Flett (Deception Island)
Keith Allan John Pitt *Fitzroy*
Victor Aloysius John Baptist Marchesi HMS *William Scoresby*
Permanent scientific station established at Deception Island ('Base B', 3 February 1944); Argentine emblems removed. Scientific programmes initiated included geology, biology and survey. [This was the first of a series of British expeditions by the Royal Navy, Falkland Islands Dependencies Survey (from 1945–46) and British Antarctic Survey (from 1961–62)]

Note: *The mid 1940s ushered in the modern era of essentially continuous exploration and habitation of Deception Island; for reasons of space, only abbreviated details of historical and scientific (geological) events are included here; for additional details, refer to Headland (2001).*

1946–47 Falkland Islands Dependencies Survey (Britain): Deception Island station (destroyed by fire, September 1946) rebuilt.

1947–48 Argentine expedition: New station ('Decepción', also '1° de Mayo') established on Deception Island, 25 January 1948; hydrographic and aerial photographic surveys made.

1947–48 Norwegian expedition: Research voyage; landed on Deception Island.

1948 Argentine naval voyage: Aerial photographic survey of Deception Island.

1948–49 Argentine expedition: Refuge huts built at Telefon Bay ('Thorne') and Pendulum Cove ('Pendulo'), Deception Island.

1948–49 Falkland Islands Dependencies Survey (Britain): Admiralty hydrographic unit re-surveyed Deception Island (including Port Foster and approaches).

1950–51 Argentine expedition: Five vessels; partial topographic and air survey of Deception Island, and instalment of an ionosonde.

1950–51 Falkland Islands Dependencies Survey (Britain): Routine ionospheric observations began on Deception Island, August 1951.

1952 Argentine flight: 2 Catalina aircraft flew from Rio Grande, Tierra del Fuego, to Deception Island, 7 February, returning to Buenos Aires 10 February, and again outbound on 2 March, returning 6 March.

1952–53 Argentine expedition: Refuge hut ('Teniente Lasala') built on the landing ground near Whalers Bay; dismantled by Falkland Islands Dependencies civil authorities, February 1953.

1952–53 Chilean expedition: Refuge hut built on the landing ground near Whalers Bay; dismantled by Falkland Islands Dependencies civil authorities, February 1953.

1952–53 Falkland Islands Dependencies Survey (Britain): One man died and was buried on Deception Island, 17 November 1953.

1953 First criminal law case in the Antarctic: Heard before the Falkland Islands Dependencies Magistrate on Deception Island, South Shetland Islands, 14 April; it concerned protection of wildlife. [Civil and criminal cases had been tried in Antarctic regions previously (the first at South Georgia, 24 October 1910, by a Falkland Islands Dependencies Magistrate) but this was the earliest case in the region subsequently covered by the Antarctic Treaty.]

1952–54 Falkland Islands Dependencies Survey (Britain): Deception Island surveyed by summer parties. One man died on the island.

1954–55 Chilean expedition: Station ('Presidente Pedro Aguirre Cerda') established at Pendulum Cove, 18 February 1955.

1955–56 Chilean expedition: Refuge ('Cabo Gutiérrez Varas') built near Pendulum Cove.

1955–56 Falkland Islands and Dependencies Aerial Survey Expedition [1]: Hunting Aerosurveys Ltd, under contract from the British Colonial Office, initiated a programme of vertical air photography of the South Shetland Islands and northern Antarctic Peninsula with Canso flying boats based on Deception Island; helicopters used to assist ground control parties. First private company involved in Antarctic mapping.

1956 British whaling voyage: Christian Salvesen and Company whale-catcher *Southern Hunter* wrecked while entering at Neptunes Bellows, 21 December.

1956–57 Falkland Islands and Dependencies Aerial Survey Expedition [II]: Hunting Aerosurveys Ltd, under contract to the British Colonial Office, continued air photography and survey programme started in 1955–56, again based on Deception Island using Canso aircraft.

1956–1957 Argentine Air Force: A Martin Mariner amphibious aircraft flew non-stop from Buenos and landed on Deception Island, 19 January.

1957–58 Falkland Islands Dependencies Survey (Britain): Geological study of Deception Island.

1957–58 Chilean expedition: Skidway for amphibious aircraft built on Deception Island.

1960–61 Chilean expedition: Oceanographic investigations made in Port Foster.

1961–62 Falkland Islands Dependencies Survey/British Antarctic Survey: An aircraft hangar was constructed on Deception Island.

1964–65 Argentine expedition: Sea ice survey flights made from Deception Island, January and August 1965.

1964–65 Chilean expedition: Geological investigations of Deception Island made.

1967 Deception Island: Increasing seismic activity culminating in a volcanic eruption on the island, 4 December, caused rapid evacuation of Argentine, British and Chilean stations, December. [Further eruptions occurred in February 1969 and August 1970.]

1967–68 Argentine expedition: Deception Island station closed temporarily after volcanic eruption but reopened for winter; *Bahía Aguirre* assisted in evacuation of personnel.

1967–68 British Antarctic Survey: Deception Island station evacuated after major volcanic eruptions, 4 and 7 December 1967; personnel taken aboard the Chilean vessel *Piloto Pardo* by helicopter; two volcanic vents and a new island were later examined.

1967–68 Chilean expedition: *Piloto Pardo* assisted in evacuation of Deception Island after volcanic eruptions, 4 and 7 December 1967; the Chilean station was destroyed. Chilean Air Force aircraft inspected Deception Island during and after the eruption.

1968–69 British Antarctic Survey: Deception Island station reopened, volcanological and hydrographic surveys of the island made and the landing ground re-established, January 1969; seismic activity intensified and the station was evacuated (again by *Piloto Pardo* [Chile]) as further eruptions occurred in February, which damaged several buildings. A reconnaissance was made of the eruption in March.

1968–69 British naval voyage
Peter William Buchanan HMS *Endurance*
Investigated Deception Island after volcanic eruption.

1968–69 Chilean expedition: Helicopters again assisted evacuation of British station on Deception Island following another volcanic eruption, 21 February 1969.

1969 Deception Island erupted severely, February. Argentine, British and Chilean stations evacuated; see also 1967 and 1970.]

1969–70 Argentine expedition: Volcanological studies made of Deception Island, station remained closed owing to another volcanic eruption.

1969–70 British naval voyage:
Peter William Buchanan HMS *Endurance*
Continued volcanological investigation of Deception Island.

1970 Deception Island erupted severely, 13 August. [The Argentine, British and Chilean stations on the island had been evacuated following an eruption in February 1969; see also 1967.]

1970–71 Argentine expedition: Volcanological studies of Deception Island continued.

1970–71 British Antarctic Survey: Further volcanological studies made of Deception Island; great changes found after the 1970 eruption.

1971–72 Argentine expedition: Volcanological investigation of Deception Island continued.

1971–72 Chilean expedition: Volcanological examination made of Deception Island.

1972–73 British Antarctic Survey: Inspection of volcanicity made at Deception Island.

1973–74 British naval voyage
Christopher John Isacke HMS *Endurance*
Magnetometer measurements taken on Deception Island.

1983–84 Argentine expedition: Removed, without consent, the unoccupied British Antarctic Survey scientific building from Deception Island.

1984–85 Polish Expedition: Geological and geophysical studies on Deception Island.

1986–87 British Antarctic Survey: Volcanological investigation of Deception Island.

1987–88 British Antarctic Survey: Volcanological investigation of Deception Island.

1986–88 Polish Expedition: Geological and geophysical studies on Deception Island.

1986–89 Spanish Expedition: Geophysical studies in Port Foster.

1988–89 Spanish Expedition: Geophysical studies in Port Foster.

1988–90 Spanish expedition: Summer station (Gabriel de Castilla) built on Deception Island for seismological observations.

Note. *Since 1990, scientific expeditions from several countries have visited Deception Island, and annual summer-only occupation and scientific investigations, including geological activities, have continued at the Spanish and Argentine stations, together with marine geophysical cruises to Port Foster. A complete record of scientific visits and activities of the post-1990 years does not yet exist and the chronology in this appendix is therefore curtailed at 1990. The Argentine station has largely been closed to geological observations since the late 1990s, whereas the Spanish station continues to make seismological observations. The period also included the first over-wintering since 1967, by yacht Freydis (Germany; captain: Erich Wilts) in 1991; the Freydis was partly crushed by ice, and the complement wintered in the Argentine summer station until rescued by the Argentine navy.*

Appendix 2 Gazetteer

by J.W. Thomson

Mc 49107

The gazetteer below includes all place names referred to in the text and on the maps in the back pocket of this volume, and also all features within the map area of Deception Island that have been named by the relevant authorities of Argentina, Chile, Poland, Spain and the UK. The place names of Deception Island listed in Appendix 2 are as published in the *Composite Gazetteer of Antarctica* (Scientific Committee on Antarctic Research, 1998, 2000, 2002; www.pnra.it/SCAR_GAZE); entries in the SCAR gazetteer were derived from the current national gazetteers and have been approved by the relevant naming authorities. Definitions and co-ordinates of all names other than those on Deception Island have been taken from Hattersley-Smith and Roberts (1993) and Alberts (1995).

Airstrip Crater (*POL*)		62°58'S 60°34'W
Andressen, Punta (*CHL*)		62°56'S 60°36'W
Antarctic Peninsula	Mainland peninsula north of a line joining Cape Adams and a point at 73°24'S 72°00'W, on English Coast	
Antarctic, The	The continent of Antarctica together with off-lying and oceanic islands, ice shelves, sea ice and ocean.	
Atrevida, Punta de la (*ESP*)		63°00'S 60°40'W
Baily Head (*GBR*; also Rancho, punta)		62°58'S 60°30'W
Baja, punta (*ARG*; also Penfold Point and Penfold, Punta)		63°00'S 63°33'W
Balcarce, punta (*ARG*; also Fildes Point and Fildes, Punta)		63°00'S 60°34'W
Baliza (*ESP*)		62°58'S 60°39'W
Balleneros, caleta (*ARG*; also Balleneros, Caleta and Whalers Bay)		62°59'S 60°34'W
Balleneros, Caleta (*CHL*; also Balleneros, caleta and Whalers Bay)		62°59'S 60°34'W
Barros, Punta (*CHL*)		62°56'S 60°36'W
Beazley, monte (*ARG*; also Stonethrow Ridge)		62°58'S 60°44'W
Bransfield Strait	Separates South Shetland Islands from Graham Land	
Bridgeman Island		62°03'S 56°45'W
Buen Tiempo, Ensenada (*CHL*)		62°57'S 60°36'W
Byers Peninsula		62°38'S 61°04'W
Bynon, monte (*ARG*; also Goddard Hill)		62°55'S 60°35'W
Campbell, monte (*ARG*; also Pond, Monte and Pond, Mount)		62°57'S 60°33'W
Cathedral Crags (*GBR*)		63°00'S 60°34'W
Caupolican, Punta (*CHL*; also Entrada, punta and Entrance Point)		63°01'S 60°33'W
Chacao, Punta (*CHL*)		62°56'S 60°41'W
Chaco, islote (*ARG*; also Lautaro, Islote and Låvebrua Island)		63°02'S 60°35'W
Chilota Laguna (*CHL*)		62°58'S 60°42'W
Ciego, Valle (*ESP*)		62°55'S 60°42'W
Collins Point (*GBR*; also Collins, Punta andFontana, punta)		63°00'S 60°35'W
Collins, Punta (*CHL*; also Collins Point and Fontana, punta)		62°59'S 60°35'W
Crater Lake (*GBR*; also Jade Crater Lake)		62°59'S 60°40'W
Crimson Hill (*GBR*; also Varela, Morro)		62°57'S 60°36'W
Cross Hill (*GBR*)		62°56'S 60°42'W
David, Monte (*CHL*; also Goyena, monte and Kirdwood, Mount)		63°00'S 60°37'W
Decepcion, isla (*ARG*)		62°59'S 60°43'W
Decepcion, Isla (*CHL*)		62°58'S 60°39'W
Deception Island(*GBR*)		62°57'S 60°38'W
Descubierta, Punta de la (*ESP*)		62°59'S 60°43'W
Drake Passage	Separates Cape Horn from South Shetlands Islands	
Dundee Island		63°29'S 55°58'W
Eastern Claw (*POL*)		62°54'S 60°33'W
Emerald Lake (*POL*)		62°59'S 60°42'W
Entrada, punta (*ARG*; also Caupolican, Punta and Entrance Point)		63°01'S 60°33'W
Entrance Point (*GBR*; also Caupolican, Punta and Entrada, punta)		63°00'S 60°33'W
Falkland Islands		51°45'S 59°37'W
Falsa Punta Rancho, punta (*ARG*)		63°01'S 60°34'W
Fildes Point (*GBR*; also Balcarce, punta and Fildes, Punta)		63°00'S 60°34'W
Fildes, Punta (*CHL*; also Balcarce, punta and Fildes Point)		63°00'S 60°34'W
Fontana, punta (*ARG*; also Collins Point and Collins, Punta)		63°00'S 60°35'W
Foster, puerto (*ARG*)		62°58'S 60°39'W
Foster, Puerto (*CHL*)		62°58'S 60°42'W
Foster, Port (*GBR*)		62°57'S 60°39'W
Fuelles de Neptuno, pasaje (*ARG*; also Neptunes Bellows and Fuelles de Neptuno)		63°00'S 60°34'W
Fuelles de Neptuno (*CHL*; also Fueles de Neptuno, pasaje and Neptunes Bellows)		63°00'S 60°34'W
Fumarolas (*ESP*)		62°57'S 60°43'W
Fumarole Bay (*GBR*; also Iquique, Surgidero and Primero de Mayo, bahía)		62°58'S 60°42'W
Gabriel de Castilla, Refugio (*ESP*)		62°58'S 60°40'W
Goddard Hill (*GBR*; also Bynon, monte)		62°55'S 60°35'W
Gonzalez Harbour (*POL*)		62°55'S 60°41'W
Goyena, monte (*ARG*; also David, Monte and Kirkwood, Mount)		63°00'S 60°39'W
Graham Land	That part of the Antarctic Peninsula north of a line joining Cape Jeremy and Cape Agassiz	
Green Crag (*POL*)		62°59'S 60°33'W
Gutierrez, Morro (*CHL*)		62°56'S 60°34'W
Hawkes Glacier (*POL*)		62°56'S 60°31'W
High Window (*POL*)		62°59'S 60°33'W
Holtedahl Hill (*POL*)		62°59'S 60°32'W
Iquique, Surgidero (*CHL*, also Fumarole Bay and Primero de Mayo, bahía)		62°58'S 60°44'W
Irizar Crater (*POL*)		62°58'S 60°42'W
Irizar Lagoon (*POL*)		62°58'S 60°42'W
Jade Crater Lake (*POL*; also Crater Lake)		62°59'S 60°40'W
Kendall Crater (*POL*)		62°58'S 60°35'W
Kendall Point (*POL*)		62°55'S 60°44'W

Kendall Terrace (*GBR*) 62°54'S 60°42'W
King George Island 62°05'S 58°15'W
Kirkwood, Mount (*GBR*; also David, Monte and Goyena, monte) 63°00'S 60°39'W
Kroner Lake (*GBR*; also Pennilea, Laguna and Verde, laguna) 62°59'S 60°35'W
Lautaro, Islote (*CHL*; also Chaco, islote and Låvebrua Island) 63°03'S 60°35'W
Lava Point (*POL*) 62°59'S 60°37'W
Låvebrua Island (*GBR*; also Chaco, islote and Lautaro, Islote) 63°01'S 60°35'W
Livingston Island 62°36'S 60°30'W
Macaroni Point (*GBR*) 62°54'S 60°32'W
Mohai, Rocas (*CHL*; also Sewing-Machine Needles) 62°58'S 60°28'W
Murature, punta (*ARG*; also Wensley, Punta) 62°58'S 60°43'W
Neptunes Bellows (*GBR*; also Fuelles de Neptuno and Fuelles de Neptuno, pasaje) 63°00'S 60°34'W
Neptunes Window (*GBR*; also Ventana de Neptuno, caleta) 62°59'S 60°33'W
New Rock (*GBR*; also Nueva, roca and Nueva, Roca) 63°01'S 60°44'W
North Point (*POL*) 62°53'S 60°38'W
Nueva, roca(*ARG*, also New Rock and Nueva, Roca) 63°01'S 60°44'W
Nueva, Roca (*CHL*; also New Rock and Nueva, roca) 63°01'S 60°45'W
Obsidianas, Collado de las (*ESP*) 62°56'S 60°42'W
Oscar Lakes (*POL*) 62°55'S 60°40'W
Pendulo (*ESP*) 62°56'S 60°35'W
Pendulo, caleta (*ARG*; also Pendulo, Caleta and Pendulum Cove) 62°56'S 60°36'W
Pendulo, Caleta (*CHL*; also Pendulo, caleta and Pendulum Cove) 62°56'S 60°35'W
Pendulum Cove (*GBR*; also Pendulo, caleta and Pendulo, Caleta) 62°56'S 60°36'W
Penfold Point (*GBR*; also Baja, punta and Penfold, Punta) 62°59'S 60°35'W
Penfold, Punta (*CHL*; also Baja, punta and Penfold Point) 62°59'S 60°33'W
Pennilea, Laguna (*CHL*; also Kroner Lake and Verge, laguna) 62°58'S 60°33'W
Perchuc Cone (*POL*) 62°57'S 60°33'W
Petes Pillar (*GBR*) 63°00'S 60°33'W
Pinguinera, rada (*ARG*) 63°00'S 60°43'W
Pond, Monte (*CHL*; also Campbell, monte and Pond, Mount) 62°56'S 60°32'W
Pond, Mount (*GBR*; also Campbell, monte and Pond, Monte) 62°57'S 60°33'W
Primero de Mayo, bahía (*ARG*; also Fumarole Bay and Iquique, Surgidero) 62°58'S 60°42'W
Protector Shoal 55°55'S 28°05'W
Rancho, punta (*ARG*; also Baily Head) 62°58'S 60°30'W
Ravn Rock (*GBR*) 63°00'S 60°34'W
Ravn, roca (*ARG*) 63°00'S 60°34'W
Ravn, Roca (*CHL*) 62°59'S 60°32'W
Recta, Costa (*ESP*) 62°55'S 60°30'W
Red Crag (*POL*) 62°59'S 60°32'W
Red Spur (*POL*) 62°56'S 60°35'W
Relict Lake (*GBR*) 62°57'S 60°36'W
Ronald Hill (*GBR*) 62°58'S 60°34'W
Sail Rock (*GBR*; also Vela, roca and Vela, Roca) 63°02'S 60°57'W
Scotia Sea Bounded by South Georgia, South Sandwich Islands, South Orkney Islands and long. 55°00'S
Sewing-Machine Needles (*GBR*; also Mohai, Rocas) 62°58'S 60°30'W
South East Point (*GBR*; also Sudeste, punta and Sur Este, Punta) 62°59'S 60°31'W
South Georgia 54°20'S 36°40'W
South Point (*GBR*; also Sur, Punta) 63°02'S 60°37'W
South Sandwich Islands Group extending from 56°18'S 27°34'W to 59°27'S 27°15'W
South Shetland Islands Between 61°00'S and 63°20'S, 54°00'W and 62°45'W
South-west Point (*POL*) 63°01'S 60°40'W
Stacy, banco (*ARG*; also Stanley Patch) 62°59'S 60°38'W
Stancomb Cove (*GBR*) 62°56'S 60°41'W
Stanley Patch (*GBR*; also Stacy, banco) 62°59'S 60°38'W
Stonethrow Ridge (*GBR*; also Beazley, monte) 62°58'S 60°44'W
Stonington Island 68°11'S 67°00'W
Sudeste, punta (*ARG*; also South East Point and Sur Este, Punta) 62°59'S 60°31'W
Sur, Punta (*CHL*; also South Point) 63°01'S 60°37'W
Sur Este, Punta (*CHL*; also South East Point and Sudeste, punta) 62°59'S 60°31'W
Telefon, bahía (*ARG*; also Telefon, Bahía and Telefon Bay) 62°56'S 60°41'W
Telefon, Bahía (*CHL*; also Telefon, bahía and Telefon Bay) 62°55'S 60°40'W
Telefon Bay (*GBR*; also Telefon, bahía and Telefon, Bahía) 62°56'S 60°41'W
Telefon Pass (*POL*) 62°56'S 60°43'W
Telefon Ridge (*GBR*) 62°56'S 60°43'W
Vapour Col (*GBR*) 62°59'S 60°44'W
Vapour Point (*POL*) 62°58'S 60°44'W
Varela, Morro (*CHL*; see also Crimson Hill) 62°56'S 60°34'W
Vela, roca (*ARG*; also Sail Rock and Vela, Roca) 63°02'S 60°57'W
Vela, Roca (*CHL*; also Sail Rock and Vela, roca) 63°04'S 60°59'W
Ventana de Neptuno, caleta (*ARG*; also Neptunes Window) 62°59'S 60°33'W
Verde, laguna (*ARG*; also Kroner Lake and Pennilea, Laguna) 62°59'S 60°35'W
Wensley, Monte (*CHL*; also Wensleydale Beacon and Wensleydale, colina) 62°57'S 60°41'W
Wensley, Punta (*CHL*; also Murature, punta) 62°57'S 60°40'W
Wensleydale Beacon (*GBR*; also Wensley, Monte and Wensleydale, colina) 62°57'S 60°42'W
Wensleydale, colina (*ARG*; also Wensleydale Beacon and Wensley, Monte) 62°57'S 60°42'W
62°56'S 60°42'W
Wensleydale Valley (*POL*) The minor region of Antarctica lying on the Pacific Ocean side of the Transantarctic Mountains 62°57'S 60°45'W
West Antarctica 62°54'S 60°35'W
West Point (*POL*) 62°59'S 60°34'W
Western Claw (*POL*) 78°30'S 164°20'W
Whalers Bay (*GBR*; also Balleneros, caleta and balleneros, Caleta) 62°55'S 60°41'W
Whales, Bay of
Yelcho Hill (*POL*)

REFERENCES

ALBERTS, F.G., compiler. 1995. *Geographic names of the Antarctic.* Second edition. Arlington, National Science Foundation, 834 pp.
HATTERSLEY-SMITH, G. *and* ROBERTS, A., compilers. 1993. *Gazetteer of the British Antarctic Territory.* Second edition. London, Her Majesty's Stationery Office, 45 pp.

Appendix 3 Chronology of eruptions of Deception Island

by J.L. Smellie

Table A3.1. Chronological list of historical eruptions on Deception Island with known or inferred vent locations

Dates of eruption (A.D.)	*Vent location*	*Dating criteria*	*References*
1970 (*c.* 13 August)	Telefon Bay, between Cross Hill and Goddard Hill	Contemporary eruption with field evidence	González-Ferrán and others, 1971 Baker and others, 1975
1969 (21 February)	Fissure extending from north of Pendulum Cove, across Mt Pond ice cap to near Whalers Bay	Eruption observed; field evidence	Baker and others, 1975
1967 (4–7 December)	Telefon Bay (new island); west of Goddard Hill (land centre)	Eruption observed; field evidence	Valenzuela and others, 1968 Baker and others, 1975
Between 1931 and 1955	West upper slopes of Mount Pond ice cap	Scoria tephra on Mount Pond ice cap	Roobol 1973 Pallas and others, 2001
Between 1830 and 1927; probably pre-1912	Uncertain but Mt Pond fissure likely. Winter eruption? (no contemporary record from summer whaling station personnel; station established 1912)	Grey scoria lapilli strewn on "Airstrip" and Kroner Lake craters (mapped by Holtedahl (1929) and Hawkes (1961) as 'lava')	This paper
Between 1830 and 1908	North of Whalers Bay (Kroner Lake, airstrip crater)	Topographical changes	Roobol 1973, 1980 Pallas and others, 2001
1842	Fissure north-east of Mt Kirkwood	Eruption observed; field evidence	Smiley in Wilkes, 1845 Hawkes, 1961
1838–39	Fissure north-west of Mt Kirkwood	Steam observed at lava front, southern margin of Crater Lake; lichenometric dating	Whittle in Wilkes, 1845 Roobol, 1980 Birkenmajer, 1991 Pallas and others, 2001
Between 1800 and 1828	Pendulum Cove (Crimson Hill crater)	Topographical evidence	Map by Kendall, 1829 Roobol 1973, 1980 Pallas and others, 2001
Between 1790 and 1800	"Sealers harbour" (south-west of Goddard Hill; same site as 1967 land centre eruption)	Topographical evidence	Map by Kendall, 1829 (in Roobol, 1973) Roobol 1973, 1980 Pallas and others, 2001
Likely 18th century?	Crater Lake and associated craters	Crater morphology and field evidence	Pallas and others, 2001

Table A3.2. Chronological list of eruptions of Deception Island from dated marine, lacustrine and moss bank tephra layers. All ages as years before present (B.P.)

TEPHRA SOURCE	
lakes and moss banks	*marine sediments*
250	
450	
750	
1050	
1350	
1850	
2100	
2250	
2500	
2650-2750	
3500	
	3900-3100
	4000-4500
4100?	
4700	
5000?	
	5200
	8700
	10670
	21660
	26400
	35400

Ages derived by:
a) ice layer counting or
b) C^{14} dating of associated organic material.
Data sources: Moreton, 1999, and summary by Smellie, 1999.
Note: marine tephra ages in italics are disputed.

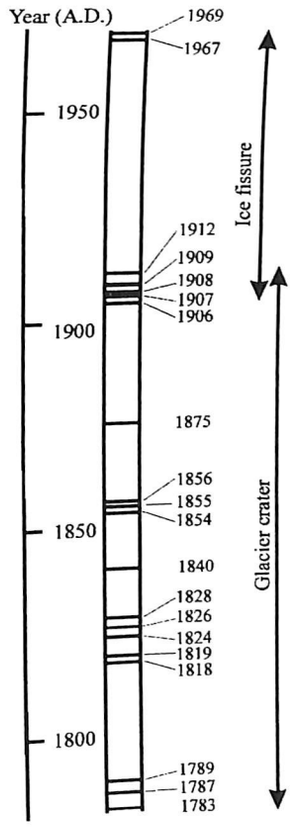

Fig. A3.1. Composite stratigraphy for ash layers preserved in ice on Deception Island (after Orheim, 1972b). The record probably represents less than half the total number of eruptions that occurred during the period depicted. All ages in calendar years (A.D.). There is a nine-year overlap between the two sections. Due to cumulative errors, the ages of the lowest layers should probably be increased by about six years. In addition to this record, Aristarain and Delmas (1998) have dated a single Deception Island ash layer in an ice core on James Ross Island as 1641 ± 3 A.D.]

Appendix 4 Geochemical and isotopic analyses of selected rocks from Deception Island

by J.L. Smellie and I.L. Millar

Table A4.1 Chemical analyses of selected lavas and bombs from the pre-caldera Port Foster Group, Deception Island Volcanic Complex

Formation	***Fumarole Bay***					***Basaltic Shield***					
Sample	*B.753.13*	*B.760.38*	*B.786.6*	*B.793.9*	*B.867.3*	*B.751.5A*	*B.751.6B*	*B.791.2*	*B.791.5*	*B.791.7*	*B.791.10*
Lithology	*bomb*	*bomb*	*bomb*	*bomb*	*bomb*	*lava*	*lava*	*lava*	*bomb*	*lava*	*agglutinate*
SiO_2	52.11	50.92	51.56	53.12	51.62	51.95	52.72	53.46	53.75	52.57	54.67
TiO_2	2.3	1.92	2.23	2.42	2.4	1.52	2.05	2.3	2.34	2.24	2.05
Al_2O_3	15.66	16.17	15.85	15.67	15.73	16.84	15.56	15.17	14.98	15.42	16
Fe_2O_3T	11.26	10.28	11.13	11.55	12.13	9.46	10.83	11.84	11.91	11.9	10.33
MnO	0.18	0.17	0.18	0.18	0.19	0.16	0.18	0.19	0.2	0.19	0.18
MgO	4.65	5.58	4.83	3.86	4.39	6.07	4.97	3.88	3.64	4.49	3.53
CaO	8.49	9.54	9.03	7.22	8.62	9.82	8.81	7.53	7.16	8.2	7.03
Na_2O	4.3	4.31	4.4	5.09	4.63	3.92	4.63	4.96	5	4.72	5.12
K_2O	0.62	0.47	0.59	0.57	0.45	0.35	0.5	0.62	0.69	0.54	0.74
P_2O_5	0.35	0.26	0.35	0.38	0.3	0.2	0.28	0.37	0.39	0.33	0.33
LOI	0	0.38	0.09	-0.03	-0.11	-0.16	-0.52	-0.1	-0.14	-0.29	0.06
TOTAL	99.92	100.01	100.24	100.04	100.34	100.13	100.02	100.23	99.92	100.31	100.04
Cr	17	66	45	14	24	131	18	0	0	9	0
Ni	22	28	28	20	12	46	26	15	11	18	12
Cu	48	67	52	49	37	53	60	101	103	91	41
Zn	94	82	94	94	96	69	78	98	103	94	90
Ga	23	18	20	21	20	15	23	25	21	21	20
Rb	8	4	5	9	7	7	8	7	7	6	12
Sr	391	346	365	334	321	350	331	390	375	400	375
Y	40	33	39	41	43	30	41	39	42	37	40
Zr	207	176	197	232	198	143	200	204	217	184	242
Nb	10	8	9	8	7	6	8	9	9	8	10
Ba	123	69	107	107	54	88	99	109	124	95	127
La	2	0	0	5	3	0	2	4	2	2	6
Ce	31	31	33	36	33	14	29	32	29	34	16
Nd	32	29	20	29	29	13	16	24	20	30	15
Pb	10	9	11	9	11	8	7	11	10	9	13
Th	1	1	1	4	2	2	1	6	5	6	5
V	373	285	349	329	324	219	278	386	376	388	268

Oxides in Wt %, trace elements in ppm. Fe_2O_3T = total iron as Fe_2O_3. LOI = loss on ignition.
Major and trace elements determined by XRF at the University of Keele, England, using methods described by Floyd (1986).

Table A4.1 (cont.)

Formation	Outer Coast Tuff													
Sample	B.751.2	B.751.3	B.789.9	B.789.11	B.793.3	B.822.7	B.823.2	B.837.5	B.839.1	B.848.6	B.858.4	B.859.3	B.863.1	B.868.1
lithology	bomb	bomb	bomb	bomb	bomb	bomb	bomb	bomb	pumice	pumice	bomb	bomb	bomb	bomb
SiO_2	51.69	51.75	56.05	53.93	56.17	54.41	56.68	48.76	66.07	66.12	53.25	49.98	54.67	55.16
TiO_2	1.73	2.51	1.46	1.26	1.46	1.47	1.37	0.7	0.52	0.52	1.71	1.72	1.48	1.43
Al_2O_3	17.04	15.27	16.42	18.32	16.82	17.42	16.82	21.57	13.94	14.32	16.88	18.17	17.08	16.92
Fe_2O_3T	9.7	12.39	8.21	7.41	8.44	8.65	7.89	6.09	4.26	4.32	9.58	9.65	8.66	8.42
MnO	0.16	0.19	0.16	0.13	0.16	0.15	0.15	0.09	0.16	0.16	0.16	0.16	0.15	0.16
MgO	5.74	4.21	4.06	5.09	4.04	4.41	3.62	8.19	0.34	0.35	4.36	6.34	4.34	4.03
CaO	9.65	8.07	6.99	9.19	7.52	8.53	7.15	12.43	1.17	1.54	8.09	10.01	8.25	7.85
Na_2O	4.1	4.92	5.12	4.18	4.97	4.7	5.26	2.37	7.08	7.12	4.47	3.83	4.86	4.86
K_2O	0.44	0.51	0.88	0.61	0.78	0.61	0.86	0.22	2.23	2.15	0.55	0.47	0.58	0.72
P_2O_5	0.25	0.35	0.25	0.2	0.25	0.21	0.22	0.08	0.06	0.07	0.22	0.25	0.22	0.22
LOI	-0.05	-0.33	0.72	-0.15	-0.17	-0.25	-0.02	0.02	4.16	3.71	0.74	-0.3	-0.22	0.12
TOTAL	100.46	99.86	100.33	100.18	100.45	100.31	100.01	100.53	100	100.39	100	100.27	100.08	99.87
Cr	101	0	13	99	15	37	19	279	4	3	32	109	28	26
Ni	32	11	20	48	23	26	15	127	2	1	20	39	22	19
Cu	56	34	51	47	53	57	47	61	3	2	58	46	57	55
Zn	75	95	81	65	81	78	83	45	113	112	84	72	80	81
Ga	20	19	20	19	19	18	20	14	24	23	19	17	20	19
Rb	6	8	13	7	10	11	13	5	32	30	8	7	9	12
Sr	429	325	330	374	343	391	343	444	53	68	372	422	383	369
Y	33	44	40	30	36	35	41	14	82	79	36	30	39	39
Zr	158	217	260	184	240	197	260	74	685	647	193	158	213	225
Nb	7	9	9	7	9	7	8	2	18	17	7	9	7	7
Ba	88	72	112	87	102	78	118	19	219	243	76	48	79	97
LaXRF	6	3	8	3	14	8	13	2	33	27	8	3	5	14
CeXRF	2	30	60	30	32	29	41	17	105	85	36	33	25	29
NdXRF	8	20	47	30	20	18	27	19	50	48	23	25	21	31
Pb	9	9	6	5	6	14	11	12	15	15	10	12	13	12
Th	2	5	1	0	0	1	0	0	1	1	0	1	0	0
V	254	343	186	165	202	207	177	114	2	10	247	226	209	203

Oxides in Wt %, trace elements in ppm. Fe_2O_3T = total iron as Fe_2O_3. LOI = loss on ignition.
Major and trace elements determined by XRF at the University of Keele, England, using methods described by Floyd (1986).

Table A4.2. Chemical analyses of selected lavas and bombs from the post-caldera Mount Pond Group, Deception Island Volcanic Complex

Formation	***Stonethrow Ridge Fmn***										***Baily Head***				
Sub-unit	*Mount Kirkwood Member*				*Kendall Terrace Member*										
Sample	*B.775.4B*	*B.797.1*	*B.797.4*	*B.799.9*	*B.753.4*	*B.753.6*	*B.753.9*	*B.791.14*	*B.773.1*	*B.773.2*	*B.783.2*	*B.792.1*	*B.793.6*	*B.855.2*	*B.843.3*
Lithology	*bomb*	*bomb*	*bomb*	*lava*	*bomb*	*lava*	*agglu-tinate*	*bomb*	*lava*	*lava*	*bomb*	*bomb*	*bomb*	*bomb*	*bomb*
SiO_2	55.13	55.59	58.69	54.85	50.17	54.9	53.39	50.34	52.82	55.33	54.57	52.83	52	53.33	50.77
TiO_2	2.06	1.99	1.69	2.04	1.61	1.95	2.26	1.65	1.99	2.33	2.17	1.82	1.62	1.6	2.32
Al_2O_3	15.91	16.02	15.97	15.93	17.73	16.18	16.06	17.54	16.47	15.43	15.92	16.56	16.59	17.19	15.31
Fe_2O_3T	10.73	10.28	8.54	10.61	9.42	10.04	10.97	9.41	10.58	10.9	10.75	10	9.41	9.31	11.74
MnO	0.18	0.17	0.17	0.18	0.15	0.18	0.19	0.15	0.17	0.17	0.18	0.17	0.16	0.15	0.19
MgO	3.56	3.44	2.48	3.61	6.47	3.54	3.82	6.3	4.48	3.33	3.83	4.95	4.64	4.46	4.41
CaO	7	7.09	5.39	7.27	10.26	7.06	7.44	10.12	8.63	6.85	7.43	8.83	8.53	8.81	8.19
Na_2O	5.17	5.23	5.86	5.23	3.73	5.2	5.19	3.92	4.73	5.24	5.02	4.44	4.41	4.57	4.81
K_2O	0.77	0.77	1.05	0.78	0.44	0.79	0.69	0.46	0.6	0.84	0.71	0.54	0.54	0.5	0.64
P_2O_5	0.31	0.32	0.43	0.3	0.25	0.34	0.36	0.27	0.32	0.43	0.37	0.28	0.3	0.24	0.35
LOI	-0.48	-0.41	-0.19	-0.33	-0.33	-0.46	-0.37	-0.22	-0.39	-0.39	-0.5	-0.11	1.53	0.08	1
TOTAL	100.34	100.48	100.09	100.46	99.89	99.71	100	99.93	100.4	100.46	100.46	100.31	99.73	100.24	99.73
Cr	1	0	0	5	112	0	1	111	0	0	2	47	17	32	14
Ni	9	9	6	10	32	8	9	31	9	10	13	19	23	21	13
Cu	79	62	20	65	45	36	24	43	30	65	83	53	64	49	40
Zn	91	88	92	86	72	87	92	74	81	92	88	79	74	79	98
Ga	20	19	20	19	18	19	20	19	20	22	19	15	17	19	20
Rb	10	9	14	10	4	10	9	7	5	11	8	6	5	7	10
Sr	346	350	318	338	458	358	370	468	389	367	374	367	388	414	360
Y	39	40	48	38	27	41	41	28	35	41	37	33	30	33	42
Zr	237	243	318	232	138	246	217	147	191	241	206	172	167	167	194
Nb	11	9	12	10	9	11	10	8	8	10	10	9	7	6	8
Ba	135	141	184	128	73	135	113	69	116	141	122	91	83	74	72
LaXRF	7	6	7	7	0	13	4	0	0	10	6	2	5	3	9
CeXRF	17	42	37	32	27	35	35	21	13	40	31	18	30	29	27
NdXRF	17	29	29	17	21	27	31	16	17	24	24	26	26	21	20
Pb	12	12	11	8	10	9	9	10	12	11	9	10	7	11	11
Th	2	1	2	1	0	4	2	6	0	1	0	2	2	1	0
V	318	276	137	311	235	265	302	243	276	320	325	268	248	247	306

Formation	***Pendulum Cove***		*[data divided into geographical clusters of cones; no relative ages implied]*									
Sub-unit	*Telefon Bay cluster*							*Cross Hill cluster*				
Sample	*B.767.1*	*B.770.2*	*B.856.1*	*B.856.4*	*B.768.2B*	*B.782.2*	*B.856.3*	*B.766.1*	*B.780.13*	*B.764.1*	*B.763.2*	*B.763.4*
Lithology	*bomb*	*bomb*	*bomb*	*bomb*	*bomb*	*bomb*	*bomb*	*bomb*	*bomb*	*bomb*	*bomb*	*bomb*
SiO_2	59.59	58.75	57.85	57.7	61.13	56.17	57.55	55.98	52.18	53	54.8	54.31
TiO_2	1.6	1.76	1.89	1.92	1.36	2.04	1.91	1.86	1.83	2.3	1.99	1.95
Al_2O_3	16.07	16.01	16.13	16.09	16.02	15.84	16.08	15.83	16.51	15	16.04	15.97
Fe_2O_3T	8.27	8.73	9.06	8.67	7.65	10.07	9.1	9.72	10.11	12	10.26	10.1
MnO	0.17	0.17	0.17	0.16	0.17	0.17	0.17	0.17	0.16	0.2	0.17	0.17
MgO	2.34	2.47	2.67	2.68	1.91	3.23	2.74	3.25	5.2	4.1	3.91	3.98
CaO	5.13	5.44	5.73	5.68	4.44	6.61	5.78	6.6	9.35	7.8	7.64	7.71
Na_2O	6.02	5.98	5.86	5.66	6.38	5.47	5.75	5.46	4.49	5.1	4.9	4.81
K_2O	1.07	1.02	0.97	0.93	1.19	0.84	0.94	0.91	0.48	0.6	0.74	0.73
P_2O_5	0.44	0.42	0.36	0.37	0.47	0.35	0.36	0.33	0.28	0.4	0.35	0.34
LOI	-0.32	-0.36	-0.28	-0.35	-0.21	-0.38	-0.38	-0.4	-0.41	0	-0.31	0.14
TOTAL	100.36	100.39	100.42	99.52	100.5	100.4	99.99	99.69	100.19	100	100.49	100.2
Cr	0	0	1	2	0	0	5	0	48	3	34	28
Ni	7	6	4	4	5	8	3	11	25	13	18	18
Cu	21	22	24	26	17	50	29	55	53	44	81	82
Zn	94	96	95	93	93	93	97	91	82	93	89	90
Ga	20	19	20	22	20	21	21	20	20	20	16	20
Rb	14	13	16	15	15	10	15	11	3	7	8	8
Sr	312	319	332	332	291	335	332	317	361	336	366	365
Y	51	49	49	49	54	42	48	42	33	42	39	39
Zr	324	308	287	290	356	259	286	266	170	212	219	215
Nb	11	11	10	9	12	11	10	10	8	9	9	9
Ba	174	174	144	154	206	146	161	146	97	106	128	124
LaXRF	12	6	6	17	8	6	16	10	4	4	6	11
CeXRF	48	50	43	52	54	32	52	44	6	19	45	27
NdXRF	16	32	38	34	26	16	31	26	7	10	29	23
Pb	12	9	13	12	10	12	13	12	12	14	15	10
Th	4	1	0	0	1	0	0	2	1	1	2	1
V	119	136	168	166	83	250	163	262	268	319	313	295

Table A4.2 (cont.)

Formation	***Pendulum Cove***											
Sub-unit	*Vapour Col cluster*			*Crater Lake cluster*				*Collins Point cluster*			*Kroner Lake cluster*	
Sample	*B.785.2*	*B.789.17*	*B.799.3*	*B.799.5*	*B.799.10*	*B.800.7*	*B.801.1*	*B.795.8*	*B.795.10*	*B.795.12*	*B.809.5*	*B.841.2*
Lithology	*bomb*	*bomb*	*bomb*	*bomb*	*bomb*	*bomb*	*bomb*	*bomb*	*bomb*	*bomb*	*bomb*	*bomb*
SiO_2	52.58	52.53	53.75	55.75	56.23	56.13	55.82	61.61	53	53.71	57.9	57.29
TiO_2	1.79	1.8	2.48	1.86	1.93	1.93	1.91	1.27	2	2.34	1.83	1.91
Al_2O_3	16.67	16.48	15.39	15.83	15.95	15.75	15.66	15.49	16	15.28	15.77	15.99
Fe_2O_3T	9.9	9.96	11.28	9.81	9.96	9.91	9.95	7.77	11	11.6	9.19	9.46
MnO	0.16	0.16	0.19	0.17	0.17	0.17	0.17	0.18	0.2	0.19	0.17	0.17
MgO	5.05	4.88	3.54	3.33	3.3	3.22	3.25	1.71	4.3	3.68	2.65	2.83
CaO	9.26	9.08	7.18	6.76	6.66	6.5	6.43	4.13	8.3	7.37	5.54	5.97
Na_2O	4.41	4.49	5.5	5.37	5.37	5.52	5.36	6.37	4.8	5.18	5.78	5.45
K_2O	0.5	0.53	0.68	0.87	0.87	0.93	0.94	1.35	0.6	0.67	1.03	0.92
P_2O_5	0.27	0.27	0.45	0.33	0.34	0.33	0.33	0.41	0.3	0.41	0.38	0.34
LOI	-0.46	-0.43	-0.47	-0.48	-0.46	-0.36	-0.3	-0.25	0	-0.18	-0.4	-0.34
TOTAL	100.15	99.75	99.95	99.61	100.32	100.02	99.51	100.05	100	100.26	99.85	99.99
Cr	57	35	0	0	0	0	0	0	16	0	0	4
Ni	24	24	6	11	12	11	10	4	13	8	8	6
Cu	55	62	30	58	55	55	59	30	44	33	44	54
Zn	78	75	99	90	90	94	92	99	88	96	95	95
Ga	19	18	19	21	21	21	19	20	21	22	20	20
Rb	5	6	7	10	11	12	12	18	7	7	14	16
Sr	372	379	355	331	331	329	330	274	373	335	310	327
Y	31	33	43	41	42	43	43	57	36	43	46	46
Zr	169	173	226	262	266	276	275	398	200	226	308	285
Nb	9	9	9	10	10	10	11	14	8	10	11	10
Ba	94	97	118	146	157	143	147	202	114	118	169	150
LaXRF	0	5	2	8	3	14	2	16	3	4	9	11
CeXRF	16	13	31	34	30	41	48	66	29	13	46	52
NdXRF	20	9	23	29	20	20	32	37	34	11	24	33
Pb	9	10	11	9	12	11	11	11	13	10	10	13
Th	0	0	1	0	1	1	0	2	0	0	1	0
V	264	255	283	270	278	273	278	66	279	310	196	217

Oxides in Wt %, trace elements in ppm. Fe_2O_3T = total iron as Fe_2O_3. LOI = loss on ignition.
Major and trace elements determined by XRF at the University of Keele, England, using methods described by Floyd (1986).

Table A4.3. Isotopic analyses of selected rocks from Deception Island

Formation	*Sample*	$^{87}Sr/^{86}Sr$	$^{143}Nd/^{144}Nd$
Fumarole Bay	B.754.10	0.703606	0.512912
Fumarole Bay	B.760.38	0.703299	0.513013
Fumarole Bay	B.793.19	0.703478	0.512965
Basaltic Shield	B.751.50	0.703358	0.512987
Basaltic Shield	B.751.10	0.703243	0.512945
Outer Coast Tuff	B.760.32	0.703416	0.512985
Baily Head	B.752.90	0.703401	0.513089
Baily Head	B.753.20	0.703177	0.512938
Baily Head	B.783.20	0.703450	0.512996
Pendulum Cove	B.785.20	0.703307	0.512974
Pendulum Cove	B.757.22	0.703455	0.513080
Stonethrow Ridge	B.775.4b	0.703381	0.513016
Stonethrow Ridge	B.799.80	0.703324	0.512955
Stonethrow Ridge	B.799.90	0.703366	0.512975
Stonethrow Ridge	B.806.60	0.703292	0.512984

Sr and Nd isotope analyses were carried out at the NERC Isotope Geosciences laboratories, in London and latterly at Keyworth, using techniques summarised in Pankhurst and others (1993) and Pankhurst and Rapela (1995). $^{87}Sr/^{86}Sr$ ratios are normalized to $^{86}Sr/^{88}Sr = 0.1194$, and $^{143}Nd/^{144}Nd$ ratios are normalized to $^{146}Nd/^{144}Nd = 0.7219$. Long-term reproducibility of Sr and Nd isotope ratios in standard solutions is 15–20 ppm (1), but on rock standards this rises to 30–40 ppm. Sr results are normalized to a value of 0.710250 for NBS987.

Appendix 5 Acronyms and abbreviations

AD	*anno Domini*
a.s.l.	Above sea level
ASMA	Antarctic Specially Managed Area
ATV	All-terrain vehicle
BAB	Back-arc basin
BABB	Back-arc basin basalt
BAS	British Antarctic Survey
BP	Before Present
CEP	Committee for Environmental Protection
CGA	Composite Gazetteer of Antarctica
EDM	Electronic distance meter
FIDS	Falkland Islands Dependencies Survey
FIDASE	Falkland Islands and Dependencies Aerial Survey Expedition
GPS	Global positioning system
IAT	Island arch tholeiites
IEO	Instituto Español de Oceanografía
IHM	Instituto Hidrográfico de la Marina
Ka	Thousand years
MORB	Mid-ocean ridge basalt
OIB	Ocean island basalt
OTF	Outer Coast Tuff Formation
REE	Rare earth element
rms	Root mean square value
ROA	Real Observatorio de la Armada
SCAR	Scientific Committee on Antarctic Research
SGE	Servicio Geográfico del Ejército
TAS	Total alkalis-silica
TOPAS	Topographic Parametric Sound
UAM	Universidad Autónoma de Madrid
USA	United States of America
WGS	World Geodetic System
XRF	X-ray fluorescence